# Numerical Study on the Hydraulics of Stormwater Catch Basin Grate Inlets under Clean and Clogging Conditions

By

**Xiangdong Li**

A thesis submitted in partial fulfillment of the requirements for the degree of

Master of Science

in

Water Resources Engineering

Department of Civil and Environmental Engineering

University of Alberta

**Abstract**

Accurate assessment of urban drainage system is vital for municipalities. Stormwater catch basin (CB) inlets are critical linkages between the two dimensional (2-D) urban street flow and the 1-D underground sewer network flow. So far, extensive studies have been conducted to quantify the performance of various types of CB inlets, focusing mainly on CB inlet capacity and efficiency under clean conditions. However, in reality, CB inlets can be easily clogged by debris, garbage, leaves and others, largely reducing their capacity and efficiency. There has been no numerical study that investigates the clogging effect, despite there are a few limited experimental studies.

This thesis was written as paper-based, including two pieces of work. The first piece of work (Chapter 2) is a comprehensive literature review on each of the three major types of CB inlets: grate inlets, curb-opening inlets and combination inlets. The second piece of work is a 3-D numerical modeling study using a commercial computational fluid dynamic (CFD) package, FLUENT, to assess hydraulics of CB grate inlets under different conditions: clean and clogging conditions, large water depth on street, vertical depression of grate inlets compared to street surface, and outflow through grate inlets due to surcharging of underground sewers.

The CFD model was first calibrated with the physical experiments of CB grate inlets under both clean and clogging conditions, and the results showed that the model built with the RANS and RNG k- $\epsilon$ equations and the VOF approach can simulate grate inlet hydraulics satisfactorily. Based on the calibrated model, the clogging factor for the grate inlets was calculated to be 0 - 0.7, depending on the clogging area, approaching flow and road slopes. Generalized clogging patterns tend to overestimate grate inlet intercepted flow rate, compared to the real clogging patterns. During urban flooding, large water depth on streets generate near-constant clogging factor, independent of approaching flow rate; and a discharge coefficient of 0.6 can be used with the

orifice flow equation to predict the inlet intercepted flow rate. If the grate inlet has a vertical depression of 2 cm (i.e., 2 cm lower than road surface), it will increase the inlet intercepted flow rate and efficiency and decrease the clogging factor, compared to the non-depressed case. When underground sewers are surcharging via CBs to road surface, it was found that road slopes (longitudinal and transverse slopes) have no impact on the discharge coefficient $C_{do}$, but the approaching flow on road will decrease $C_{do}$. The suggested value of the discharge coefficient, 0.6, would overestimate the outflow via the grate inlet. Moreover, based on the simulation results, new formulas were proposed in this study for CB grate inlet efficiency, clogging factor, and orifice discharge coefficient. The predicted results of the formulas agreed well with the simulated results.

General conclusions and future research directions were provided at the end of the thesis.

## Preface

This dissertation is original work of Xiangdong Li. The literature review and CFD study are my original work with the assistance of Dr. Wenming Zhang. Xinzai Peng helped in developing the CFD model.

**Acknowledgments**

This M. Sc. experience has been pretty valuable for my life.

I would like to express my sincere thanks to my supervisor, my friend, Dr. Wenming (William) Zhang, for all the kindness, help, guidance, and inspiration during this truly meaningful journey.

This work would not have been completed without the corporation and support from Xinzai Peng, Huan Zhang, and other students in our research team.

I would also like to say a big thanks to my parents and elder sister for supporting me all the time.

Thank my lover, Qiaoqiao, for all the love, warmth, and support.

Finally, I gratefully acknowledge donation of catch basins from the Trojan Industries in Edmonton.

**Table of contents**

**Lists of Tables**

**Lists of Figures**

**List of Major Symbols**

A = the specific coefficient for certain inlet.

$A_g$ = the minimum rectangular area of the inlet including all the holes.

$A_h$ = the area of holes in the grate inlet.

$A_o$ = the orifice cross section area.

B = the specific coefficient for certain grate inlet.

$c_0$ = the single-grate clogging factor.

$C_{do}$ = the discharge coefficient for type of orifice flow through the grate inlet.

$C_{dw}$ = the discharge coefficient for type of weir flow through the grate inlet.

d = the flow depth immediately upstream the grate inlet.

$d_{max}$ = maximum gutter water depth.

$d_i$ = the effective head on the center of the orifice throat,

e = decay factor.

E = efficiency of inlet.

$E_0$ = the ratio of a frontal (gutter) flow to the street flow (design discharge).

$Fr_G$ = the Froude number concerning the front flow.

$F_W$ = the flow Froude number at the flow spread edge.

g = the gravity acceleration.

G = non-dimensional parameter relating to the Froude number, characteristics of flow and grate inlets.

$G_d$ = the grating parameter relating to the hydraulic capacity of different types of grate inlets; design value of G.

$h_G$ = the water height upstream of grate inlet.

$h_{grate}$ = the water level above the grate inlet (difference of the pressure height at the sewer and the atmospheric pressure height over the grate).

$h_{gu}$ = the water depth in the gutter.

$h_s$ = the hydraulic parameter of inlet.

H = water depth at the curb.

k = the local loss coefficient.

*K* = a coefficient and varies with the depression configurations.

$L_G$ = the length of grate inlet.

$L_w$ = the effective length of the weir.

*n* = Manning's roughness coefficient.

$n_t$ = the number of transversal bars of the inlet.

$n_l$ = the number of longitudinal bars of the inlet.

$n_d$ = the number of diagonal bars of the inlet.

N = number of grates.

$N_o$ = the orifice area opening ratio.

$N_w$ = the weir length opening ratio after subtracting steel bars.

p = the ratio in % between the total area of hole and $A_g$.

P = wetted perimeter of grate inlet.

$P_v$ = the effective perimeter of the voids specific for each manhole design.

$Q_{int}$ = the intercepted flow by inlet.

$Q_a$ = the total flow approaching inlet.

$Q_f$ = the front flow approaching inlet.

$Q_0$ = is the largest approaching flow that can be completely captured.

$Q_t$ = represents the upper limit on the captured discharge

$Q_s$ = flow on street.

$Q_w$ = frontal flow carried by the gutter width.

$Q_x$ = side flow carried by street width.

$R_f$ = the interception percentage of the frontal flow.

$R_s$ = the interception percentage of side flow.

$S_T$ = street transverse slope.

$S_x$ = street longitudinal slope.

$S_w$ = gutter cross slope.

$T_1$ = water spread width of the gutter flow defined by Guo (1997).

$T_x$ = water spread width of the side flow

V = the average velocity.

$V_0$ = the flow velocity on the street.

$V_s$ = the street velocity under the grate interference.

W = the width of gutter.

$W_G$ = the width of grate inlet.

Y = flow depth at the gutter.

$Y_s$ = the sump depth.

$\alpha, \beta$ = constants representing the geometric characteristics of the grate inlets.

$\Delta h_k$ = the local loss.

p, g, r, s = empirical constants for various grate inlets (Guo, 1997).

η = efficiency of inlets, in %.

# Chapter 1 Introduction

## 1.1 Problem Statement

Urban areas are characterized by increasing population densities and impervious surfaces such as roadways and buildings. The principle in urban drainage is to remove stormwater from streets as quickly and economically as possible (Butler et al., 2004). However, rapid urbanization and climate change can lead to inefficient operation of urban drainage infrastructures. Larger peaks of surface runoff and more rapid hydrological response require larger capacity of storm sewer system (Orta-Ortiz et al., 2022; Zhou et al., 2021). Catch basins (CB), the critical linkage between storm sewers and street flow, is vital for urban flooding mitigation and prevention. The interception of street flow by a CB is a complex hydraulic process and involves various elements, including CB inlet itself and internal components such as CB barrel, CB sump and CB lead that connects the CB with storm sewers.

There are various designs of CB inlets in different regions of the world, and extensive physical experiments, numerical simulations and theoretical analyses on CB inlet capacity and efficiency have been conducted. Early studies in 1940s to 1980s mainly explored the influential variables for CB inlet hydraulics and provided prediction equations and charts for their engineering applications (Yucel et al., 1969; Woo et al., 1974; Burgi et al., 1978). In recent decades, researchers have been trying to further understand and improve the hydraulic performance of CB inlets considering specific designs or malfunctions such as clogging of grate inlets, vertical depression of grate inlets, continuous transverse inlets (Gómez et al., 2013, 2018; Russo et al., 2013; Leitao et al., 2016; Guo et al., 2021). Moreover, a few studies focused on the flow field analysis (Martins et al., 2018; Tellez et al., 2020) and interaction role of CB inlets between surface flow and underground sewer system (Djordjević et al., 2005; Galambos et al., 2012; Rubinato et al., 2017).

Accurate assessment of catch basin inlet capacity and efficiency is essential for urban drainage operation and flood mitigation. Inappropriate estimate of the actual interception of CB inlets during design storm events may lead to overloading, surcharging of storm sewer system, and unanticipated flooding. Based on the studies in the literature, the capacity of CB inlets varies substantially with inlet designs (shapes, dimensions and grate spacing), road conditions (slopes and depression), climate (e.g., rainfall intensities and durations), clogging conditions (patterns and materials), and capacities of underground sewers. However, there is no systematic study of CB inlet capacity under these conditions, and the state-of-the-art and widely-used urban drainage models such as SWMM and Mike Urban do not consider impacts of these factors, therefore affecting the effectiveness of strategies and measures for urban flood mitigation.

### 1.2 Knowledge Gaps and Research Objectives

Specific knowledge gaps have been identified as follows, based on the comprehensive literature review presented in Chapter 2 of the thesis:

1. There is a lack of comprehensive literature review on stormwater CB inlets.
2. There have been no studies on modelling CB grate inlets under the following specific conditions, which are however commonly seen in daily life:
    1) under clogging conditions;
    2) with a vertical depression (i.e., the inlet is lower than the ambient road surface);
    3) with outflow from grate inlets to road surface due to surcharging of sewers;
    4) with large water depth on roads during flooding.
3. No prediction formulas are available for CB grate inlet efficiency and clogging factor, considering clogging effects.

To address these knowledge gaps, three research objectives are proposed:

1. To conduct a critical, comprehensive literature review that covers over 100 studies on this topic over the past 70 years.
2. To build a three-dimensional (3D) numerical model for CB grate inlets under both clean and clogging conditions, using the commercial computational fluid dynamics (CFD) package, ANSYS FLUENT, to explore the grate inlet hydraulics (performances) under the four specific conditions listed above that have not been numerically studied.
3. To develop formulas for predicting for CB grate inlet efficiency and clogging factor under clogging conditions.

### 1.3 Thesis Structure

Following the introduction of this research in Chapter 1, Chapter 2 presents a critical, comprehensive literature review on a total of 104 numerical and experimental studies on CB inlet hydraulics (focusing on capacity and efficiency) over the past 70 years. Chapter 3 describes a CFD modeling study on CB grate inlets, which were calibrated under both clean and clogging conditions. Based on the calibrated model, a few new scenarios were examined, including real clogging condition, more clogging patterns, large water depth on street, vertical depression of CB inlets compared to road surface, outflow through CB inlets due to surcharging of underground sewers.

Conclusions are drawn in Chapter 4, and future research directions are provided.

# Chapter 2 A Comprehensive Literature Review on the Hydraulics of Stormwater Catch Basin Inlets

## 2.1 Introduction

Despite extensive studies on CB inlet, comprehensive reviews are still lacking. To summarize the current progress and guide future research, this study presented a critical review on 104 CB inlet studies over the past 70 years (1945- 2022). First, analysis of global CB inlets research trend and the types of CB inlets were introduced. Then, the experimental investigations of hydraulics of the three primary CB inlets, grate inlet, curb opening inlet, and combination inlet, were reviewed, followed by numerical studies. Next, the performance of CB inlets in extreme weathers was discussed. Finally, the research gaps on CB inlet hydraulics were summarized and future research directions were suggested.

## 2.2 Major Types of CB Inlets and Their Characteristics

Different types of CB inlets have different shapes, dimensions and grate spacing, which determine their hydraulic performances. There are four major types (Guo, 1997; Brown et al., 2013): grate inlets, curb opening inlets, combination inlets and slotted drain inlets (see in Fig. 2.1). Considerations for different types of CB inlet selections were summarized in **Table 2.1**. Grate inlets generally use metal bars placed on roadway surface. Based on variations of spacing and layout of metal bars, grate inlets can be further divided into many sub-types, e.g. Guo (1997) summarized nine types of grate inlets including parallel bar p-1-7/8 grate, parallel bar p-1-1/8 grate, curved vane grate, tilt bar-45° grate, parallel safety bar p-1-7/8 grate, tile bar-30° grate, reticuline grate, type 16 grate and nonstandard grate. The advantage of grate inlets is that they perform well over a wide range of roadway longitudinal slopes, while the main disadvantage is they may be clogged easily by floating trash or debris (Larson 1947; Guo et al., 2000). A curb opening inlet is

a vertical opening in road curb through which the runoff flow passes. Curb opening inlets are preferred on flatter slopes, in sags, and with flow carrying signification amount of floating debris (Brown et al., 2013). Based on their throat geometry, curb opening inlet can be further divided into three categories: horizontal, vertical and inclined. A combination inlet is composed of a curb opening inlet and a grate inlet acting as one unit, providing the advantages of both inlet types. A special case of the combination inlets is sweeper inlets, where the curb opening extends upstream of the grated section and plays a role of intercepting trash during the initial phase of storms. The sweeper inlets can have curb openings on both (upstream and downstream) sides of the grates when they are used in a sag area. A slotted drain inlet comprises a pipe cut along the longitudinal axis with a grate of space bars to form slot drainage. Slotted drain inlets can intercept flow over a wide road. Similar to grate inlets, slotted drain inlets can be easily clogged by sediments and debris (Brown et al., 2013).

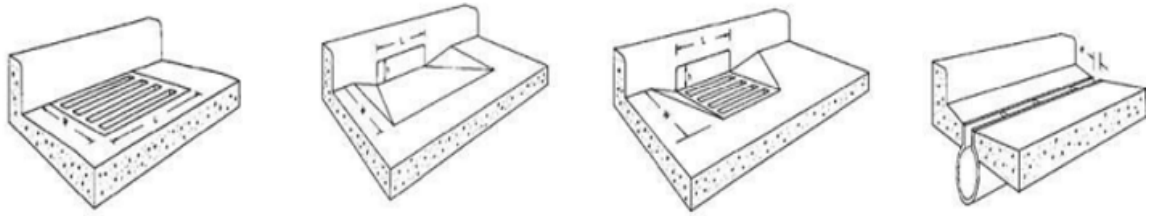

(1). Grate inlet (2). Curb opening inlet (3). Combination inlet (4). Slotted inlet

Figure 2.1 CB inlet types (Kemper et al. 2016).

Grate inlets as well as curb-opening inlets can be also classified as depressed and undepressed inlets in terms of its elevation relative to road surfaces. For curb-opening inlets, they can be further divided into three types: the undepressed, the continuously depressed, and the locally depressed curb inlets (Li et al., 2019). For streets where space is available and subsurface utility lines could be accommodated, depressed CB inlets are recommended to place some distance behind the gutter

line to minimize the dip in the travel lane (Holley, 1992). In addition to depressed or undepressed inlets, CB grate inlets can be also curved to fit the inclined street curbs such as the K-7 grate inlet used in the City of Edmonton, Canada (Rajaratnam, 1997), or conform to the configuration of the gutter such as the Type S gutter inlet used in Florida, USA (Cromwell et al., 2001).

Apart from inlet configuration, CB inlets can be also classified as per specific design aims. For example, CB inlets could be classified as being on a "continuous grade" or in a "sump/sag". "Continuous grade" refers to an inlet placed in curb and gutter such that the street has the same longitudinal slope as the inlet, and therefore water ponding does not occur at the inlet. The "sump/sag" condition exists whenever an inlet is purposely located at a low point of a road (e.g., where a positive grade of a road joins with a negative grade) or at a street corner that is confined by street curbs and crowns (Brandson et al., 1972; Adam et al., 1974; Guo, 2000). For some areas where there is need to discharge large volumes of surface flow as soon as possible, multiple CB inlets and macro-inlets can be used. Compared to single inlet, multiple CB inlets have two or more closely spaced inlets working as a unit (Mustaffa, 2001) such as inlets in series and continuous transverse inlets (Gómez et al., 2009; Russo et al., 2013; Guo et al., 2021). Macro-inlets are a type of special grate inlets with large dimensions (e.g., 50 cm × 100 cm) and elevated void area and thus generally high hydraulic efficiency (Gómez et al., 2007).

**Table 2.1 Major types of CB inlets and selection consideration**

| Inlet Type | Main subtype | Definition | Applicable Setting | Advantages | Disadvantages |
|---|---|---|---|---|---|
| Grate inlets | ● Parallel bar P-1-7/8 grate;<br>● Parallel bar P-1-1/8 grate;<br>● Curved vane grate;<br>● Tilt bar-45 ° grate;<br>● Parallel safety bar P-1-7/8 grate;<br>● Tilt bar-30 ° grate;<br>● Reticuline grate;<br>● Type 16 grate;<br>● Nonstandard grate.<br>● On grade<br>● In sump | A grate inlet uses metal bars placed in the roadway surface with the bars parallel and/or perpendicular to the flow of water. | Sumps and continuous grades (should be made bicycle safe). | Perform well over wide range of grades. | Can become clogged;<br>lose some capacity with increasing grade;<br>Interference with traffic, especially bicycles. |
| Curb opening inlets | ● Horizontal;<br>● vertical;<br>● Inclined. | A curb inlet is a vertical opening in the curb through which the runoff flow passes. | Sumps and continuous grades (but not steep grades, less than 3%). | Relatively low construction and maintenance costs;<br>Do not clog easily;<br>Bicycle safe. | Lose capacity with increasing grade. |
| Combination inlets | ● Sweeper.<br>● Equal length | A combination inlet is composed of a curb and grate inlet acting as a unit. | Sumps and continuous grades (Should be made bicycle safe). | High capacity;<br>Do not clog easily. | More expensive than grate or curb-opening acting alone. |
| Slotted inlets | | Slotted inlet comprises a pipe cut along the longitudinal axis with a grate of space bars to form slot drainage. | Locations where sheet flow must be intercepted. | Intercept flow over a wide section. | Susceptible to clogging. |
| Multiple inlets | ● Inlets in series;<br>● Continuous transverse inlets. | A multiple inlet is two or more closely spaced inlets acting as a unit. Two identical inlets end-to-end are double inlets. | Locations where much flow must be intercepted. | Intercept flow over large length or width. | Uneconomical. |

Source: Brown et al. (2009), Guo (1997), Mustaffa (2003) and UDFCD (2016).

### 2.3 Preliminary bibliometric analysis of global CB inlets research trends

First, global CB inlets research article number is censused. Totally 104 research campaigns were searched and summarized including 93 physical experiments studies and 11 numerical studies. Specifically, 61 experimental studies focused on grate inlets, of which 15 experimental studies considered clogging effects; 42 experimental studies evaluated the hydraulic performance of curb opening inlets; 9 experimental studies assessed the hydraulics of combination inlets. For 11 numerical studies, 8 studies assessed grate inlets while 4 studies focused on curb opening inlets.

Then, Fig. 2.2 shows the scientific articles number of CB inlets throughout the study period. According to Fig. 2.2 (a), research on CB inlets began to increase from 1945 to 1978. From 1978 to 1990, studies on CB inlets seemed to stop. After the year of 1990, research campaigns on CB inlets entered the 'fast lane', the number of articles increased rapidly. This large increasement can be ascribed to the intensive research on grate inlets after 1990 according to Fig. 2.2 (b). Moreover, it was clear that there the topic on grate inlets was much hotter than that of curb opening inlets after 1990 (see Fig 2.2 (b) and (c)).

According to the results, 13 countries have engaged in CB inlets research. In detail, the country with largest number of publications were the USA (65), then followed by Spain (9), China (5), Canada (4), Germany(4), Turkey (4), the UK (4), Malaysia (2), Australia (1), Egypt (1), Italy (1), Japan (1), Portugal (1), the South Korea (1), Singapore (1).

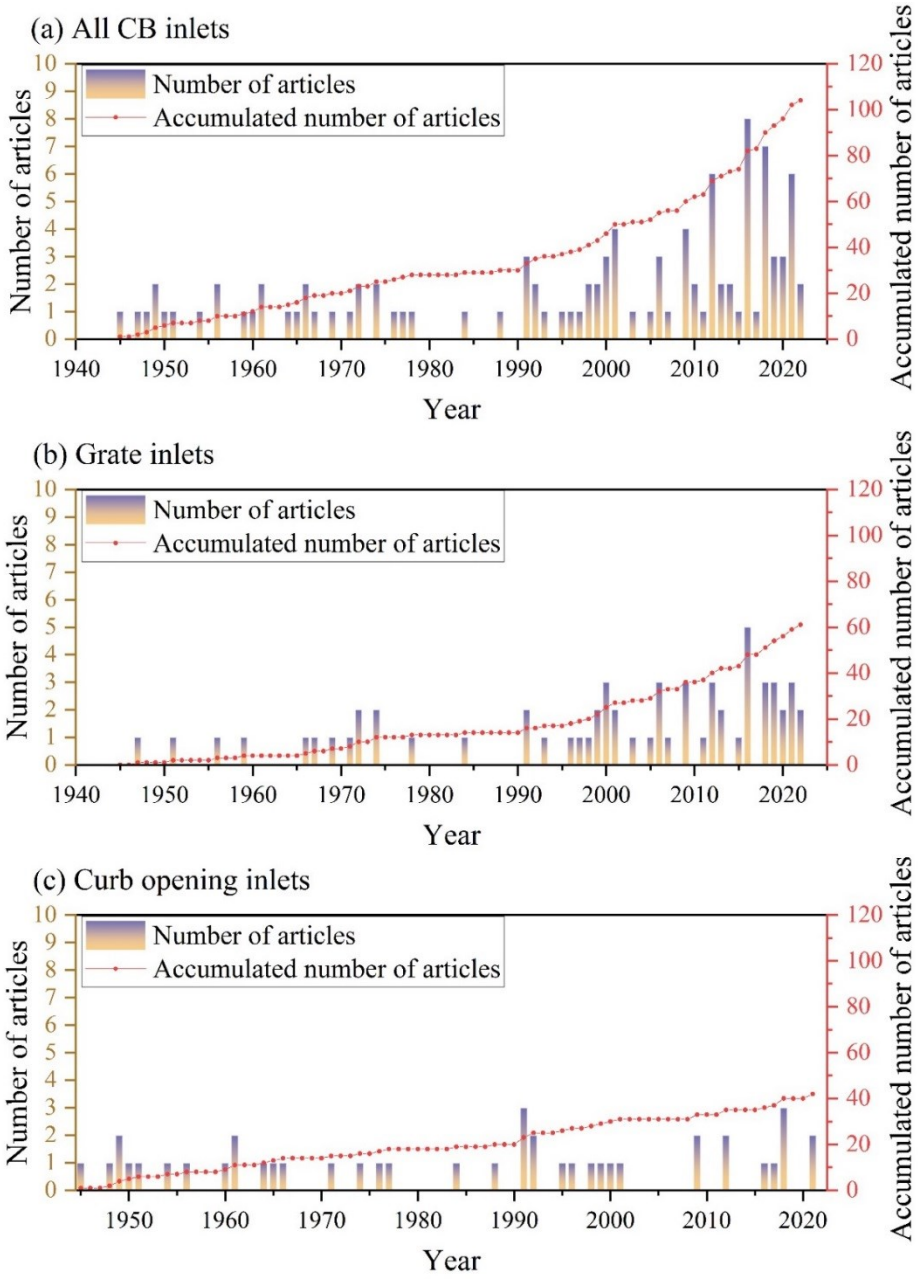


Figure 2.2 Scientific articles of CB inlets related literatures for all CB inlets (a), grate inlets(b) and curb opening inlets (c).

## 2.4 Grate inlets

### 2.4.1 Under clean conditions

#### 2.4.1.1 Influencing parameters for CB grate inlets

In early studies from 1948 to 1999, hydraulic tests mainly explored the factors that affect hydraulic performance of CB grate inlets under clean (without clogging) conditions. The results indicated that intercepted capacity of a CB grate inlet is dependent upon the length and width of the grate, bar spacing, gap width between the curb and the grate, and transverse and longitudinal slopes of the street (Larson et al., 1948; USACOE, 1949; Cassidy, 1966; Yucel et al., 1969; Woo et al., 1974; Burgi et al., 1978; McEnroe et al., 1999). The results were generally presented in the forms of graphs and tables.

Most of recent studies derived empirical formulas for the capacity and efficiency of CB grate inlets based on approaching flow parameters (e.g., velocity, water depth, Froude number), road slopes and geometries of grate inlet (Spaliviero et al., 2000; Gómez et al., 2011; Wu et al., 2015; Kim et al., 2016; Kemper et al., 2019, Dai et al. 2021). Besides the empirical formulas, a few of recent studies proposed semi-empirical formulas based on weir and orifice equations to describe capacity of grate inlets.

The influencing factors on capacity and efficiency of grate inlets are listed below:

- Inlet width. Larson (1947) found the inlet width (normal to the flow direction) and the effective length of individual inlet opening were most influential for grate inlets. Yucel et al. (1969) explained that the efficiency of grates would decrease very rapidly for a short grate inlet due to carry-over flow.

- Inlet length. Li et al. (1956), Cassidy (1966) and Yucel (1969) reported that a longer grate inlet has a larger capacity, although Li et al. (1956) pointed out that the increase in capacity was quite small unless the grate inlet was depressed. Cassidy (1966) stated that the length of the grate inlet has only a minor effect on the inlet efficiency as long as the flow does not pass over the grate inlet.
- Grate bars. Cassidy (1966) tested six types of grate bars and found that the curved-vane type bars were the most efficient and the closely-spaced, relatively wide and flat bars were most inefficient among the six types of grate inlets tested. Black (1967) found that straight bars or vanes running parallel to the flow would allow more water to pass over at higher velocities than the vanes in such positions that any flow across the face of the grate inlet was broken. Bouchard and Townsend (1984) investigated bar orientations of grate inlets from 0° to 180°at a 15° interval, where 90° represented the bars perpendicular to the road/flow direction. They recommended the use of 135° bars, which showed optimal capacity for small discharges, only slightly inefficiency for high discharges, and safety to bicyclists. In terms of bar widths, Wilson (1983) reported that the allowable bar widths shall be in the range of 10 mm to 38 mm, while Stephenson (1981) recommended 25 mm or less for the safety of bicyclists.
- Approaching flow. As approaching flow increased, the capacities of grate inlets increased (Guillou 1959), but the efficiencies of grate inlets decreased (Cassidy 1966, Dai et al., 2021). The efficiency of grate inlet would decrease with increasing velocity (Black 1967) or flow (Black 1969; Appel 1972; McEnroe et al., 1999) of the approaching flow.
- Road slopes. McEnroe et al. (1999) found that the longitudinal slope ($S_L$) did not have a significant effect on capacity of the grate inlet, but the steeper transverse slope ($S_x$)

increased the inlet capacity. A steeper transverse slope also increases the efficiency of grate inlet (Black 1969). Dai et al. (2021) also noticed the similar trends as McEnroe et al. (1999) and Black (1969).

- Other factors. Numerous studies have investigated hydraulic performance of various types of CB grate inlets in different areas and under different conditions, including on grade and in road sags (Brandson et al., 1971; Adam et al., 1974), in the forms of single and multiple-unit (McEnroe et al., 1999), with road resurfacing (McEnroe et al., 1999), with and without clogging (Guo et al., 2000; Spaliviro et al., 2000; Gómez et al., 2013; Gómez et al., 2018), with sub- and super-critical approaching flow (Cromwell et al., 2001; Kemper et al., 2019), with large longitudinal slope of road (Wu et al., 2015), with and without pressure (backwater effect) from sewers (Gómez et al., 2019; Gómez et al., 2020), with and without inclination of grate inlet towards road surface (Guo et al., 2016), as well as with and without vertical depression (Wakif et al., 2019), different relative grate inlet areas( Fathy et al., 2022).

#### 2.4.1.2 Empirical equations for CB grate inlets on continuous grade

Due to so many factors involved, it is not practical to predict their influences on the hydraulic performance for a given CB grate inlet without an extensive testing. And as a result of the complex flow through the grate inlets of various configurations, an analytical solution to the hydraulic capacity or efficiency is currently not available.

The guideline HEC-12 (Johnson et al., 1984) and HEC-22 (Brown et al., 1996) both provided a semi-theoretical method for estimating captured discharge and efficiency of grate inlets on grade. The flow captured by grate inlets can be divided into two parts and calculated separately: 1) the frontal flow($Q_f$), defined as the portion of the flow within the width of the grate; 2) the side

flow ($Q_s$), defined as the portion of the flow outside the grate width. Capacity and capture efficiency ($E$) of grate inlets are determined based on $Q_f$ and $Q_s$.

NFCO (1998), a manufacturer in Wisconsin, USA, proposed the captured discharge of grate inlets as a function of the water depth. Based on the tests conducted at the Technical University of Catalonia (UPC) in 1997 and the studies of Wallingford (1998), Spaliviero et al. (1998) proposed an expression for $E$:

$$E = A(\frac{Q_a}{d})^{-B} \tag{2.1}$$

where $d$ is the flow depth (m) immediately upstream the grate inlet, and $A$ and $B$ are two characteristics coefficients of the grate specifically.

Gómez et al. (2011) experimentally tested eleven types of grate inlet and found a similar empirical formula as Eq. 2.1, except for the different definitions of $A$ and $B$.

Besides Eq. 2.1, there were other forms of empirical equations for determining $E$. McEnroe et al. (1999) explored the performance characteristics of grate inlets through hydraulic model tests and theoretical calculations. They found that the captured discharge and total discharge for each set-up can be approximated satisfactorily by a set of equations (seen in **Table 2.2**). Spaliviero et al. (2000) tested 21 types of grate inlets and stated that efficiency is a characteristic length related to the flow conditions upstream of grate inlets. Moreover, they found that, except at low values of efficiency, the discharge efficiency of grate inlet linearly increased with the ratio between approaching flow and water depth.

Recently, discharge efficiency using equations was determined considering the Froude number of approaching flow (Wu et al., 2015; Kemper et al. 2018&2019; Dai et al., 2021). Wu et al. (2015) conducted half scaled experiments on four types of grate inlets with varying longitudinal slopes of

up to 20%. Kemper et al. (2018, 2019) proposed an empirical formula with supercritical approaching flow conditions based on physical model tests and numerical simulations. Kemper et al. also considered the influence of grate bar orientation on the efficiency. Dai et al. (2021) tested six types of grate inlets and related efficiency to several geometrical parameters, local topographical parameters and hydraulic parameters. The average errors for six sets of efficiency prediction formulas used for calibration and validation were in the range of -0.82% - -0.23% and -1.26 %– 8.2%, respectively. Dai et al. (2021) also compared their method to the method of Gómez et al. (2011). It was found Gómez et al. (2011)'s method replicates the change trend of experimental dataset correctly but with larger errors than their method. The possible reasons they mentioned were that Gómez's formula is with non-homogeneous dimension and the types of grate inlets.

Fathy et al. (2022) tested five types of grate inlets for assessing the effect of changing the shape and size of grate inlets on CB inlets efficiency. The results indicated that changing the relative area of grate inlets from 26% to 64% has a significant impact on CB inlets efficiency which deceases by 4%. They developed an empirical equation relating relatives grate inlets area and inlet efficiency.

Note that the equations mentioned above are empirical or semi-empirical and the experiments conditions were specific to certain scales, configurations of grate inlets, approaching flow conditions, and street slopes and roughness. Consequently, they should be used with caution.

#### 2.4.1.3 Theoretical equations for CB grate inlets

Besides these semi-empirical and empirical equations, discharge through CB inlets is commonly computed using the weir or orifice formula depending on the inlets are submerged or not (Mustaffa et al., 2006; Guo et al., 2009; Lee et al., 2012; Guo et al., 2016; Rubinato et al., 2017; Cosco et al.,

2020). This method is also adopted by most of the commercial software on urban drainage such as SWMM and MIKE URBAN.

If CB grate inlets are not submerged, the weir equation can be used (Lee et al., 2012):

$$Q_{int} = \frac{2}{3} C_{dw} L_w \sqrt{2g} (H_t)^{\frac{3}{2}} \tag{2.2}$$

where the total head $H_t = h + \frac{V_{grate}^2}{2g}$, $C_{dw}$ is the discharge coefficient for weir, $L_w$ is the effective length of the weir, $h$ is the piezometric head over the weir, $V_{grate}$ is the average velocity of the flow over the inlet and $g$ is the acceleration of gravity. Generally, the velocity head term, $\frac{V_{grate}^2}{2g}$, is assumed to be 0. For subcritical conditions, the effective length is estimated as the sum of the grate inlet length plus twice its width; and for supercritical conditions, it is the sum of the length and width of grate inlets (Cosco et al., 2020).

If grate inlets are submerged, an orifice equation is generally used (Lee et al., 2012):

$$Q_{int} = C_{do} A_o \sqrt{2gh} \tag{2.3}$$

where $A_o$ is the orifice cross section area, $h$ is the piezometric head over the orifice, and $C_{do}$ is the orifice discharge coefficient.

The actual discharge coefficients depend on grate inlet geometry, clogging condition and approaching flow condition. Research on discharge coefficient is insufficient, which can be a source of uncertainty for grate inlet discharge calculation (Djordjević et al., 2005). Mustaffa et al. (2006) investigated three types of grate inlets, and the orifice coefficients were calculated with Eq. (2-3) with using the specific energy instead of the piezometric head over the orifice. The results revealed that values of $C_{do}$ of the two of three grate inlets kept approximately constant as the $Fr$ of approaching flow increased. While for the third type of grate inlet, $C_{do}$ decreased slightly from

about 1.2 to 0.9 as the $Fr$ increased. Chanson et al. (2002) suggested the relations of $H_t/b_0$ as a criteria to distinguish the weir and orifice flows, where $b_0$ is the orifice thickness for orifice flow (or grate width for weir flow), and that observation of the experiments suggested that the orifice flow became a weir flow for $H_t/b_0$ = 0.43 to 0.51. Lee et al. (2012) conducted 1:10 scaled experiments on grate inlets, adopting the relationship of $H_t/b_0$ = 0.5 as a criteria and concluded that $C_{dw}$= 0.48 and $C_{do}$= 0.57 using Eqs. (2-2) and (2-3). Furthermore, Lee et al. (2012) stated that there was no significant difference for discharge coefficients between the square type and grid type inlets, as each grid space was too large to represent the shape of grate inlets properly.

Rubinato et al. (2017) tested ten types of grate inlets using a physical model and found $C_{dw}$ = 0.115-0.372 and $C_{do}$ = 0.349-2.038 for the weir and orifice flows, respectively. Moreover, the results indicated that discharge coefficients were a function of the perimeter and effective area of the grate grooves, and the coefficients approached approximately constants ($C_{dw}\approx$ 0.115 and $C_{do}\approx$ 0.35) as the perimeter or effective area of the grate grooves increased.

Cosco et al. (2020) conducted a prototype experiment to investigate the influence of the Froude number of the approaching flow on discharge coefficients of three grate inlets. The orifice discharge coefficient $C_{do}$ranged 0.055-0.294, 0.033-0.431, and 0.054-0.423 for the three tested grate inlets, while weir discharge coefficient $C_{dw}$ for these three grate inlets ranged 0.009-0.244, 0.003-0.245, and 0.006-0.286, respectively. They found that both orifice and weir discharge coefficients decreased as the $Fr$ increased, which indicates that grate inlets perform worse in terms of flow interception with higher flow velocities. In addition to grate inlets under non-surcharged condition, Gómez et al. (2019) adopted Eq. 2.3 to estimate the discharge coefficients of a grate inlet under surcharged condition and found that the values of $C_{do}$ increased from 0.13 to 0.41 as the surcharge flow rate increased.

#### 2.4.1.4 Grate inlets in road sags and other special conditions

There are a few studies on special grate inlets, for example, grate inlets in sags, continuous transverse inlets, and grate inlets with vertical depression. The inflow to grate inlets in sags varies with water depth and can be still described using the weir and orifice formulas (Brandson, 1971; Adam et al., 1974; Johnson et al., 1984; Guo, 1997; Brown et al., 2009; Guo et al., 2009). Guo et al. (2009) proposed the formulas for grate inlets in sags under weir flow and orifice flow conditions:

$$\text{Weir flow} \qquad Q_{int} = N_w C_{dw} \sqrt{2g} (2W + L)(d)^{\frac{3}{2}} \tag{2.4}$$

$$\text{Orifice flow} \qquad Q_{int} = N_o C_{do} \sqrt{2g} WL(d)^{\frac{1}{2}} \tag{2.5}$$

where $W$ is the width of grate inlet, $L$ is the length of grate, $N_w$ is the weir length opening ratio after subtracting steel bars, and $N_o$ is the orifice area opening ratio. A set of equations for grate inlets in sump under weir and orifice conditions (Almedeij et al., 2006; Brown et al., 2009) were also developed as:

$$\text{Weir flow} \qquad Q_{int} = C_{dw} P(d)^{\frac{3}{2}} \tag{2.6}$$

$$\text{Orifice flow} \qquad Q_{int} = C_{do} A_g \sqrt{2gd} \tag{2.7}$$

where $P$ is the grate perimeter excluding the side along the curb, $C_{dw}$ = 1.66, $d$ is the average water depth across the grate, $C_{do}$ = 0.67, and $A_g$ is the void area of the grate inlet.

Brandson (1971) and Adam and Brandson (1974) investigated the capacities of grate inlets in sags for the City of Winnipeg, Canada, using a full-scale laboratory model. The results revealed that an increase in the longitudinal slopes of road caused a decrease in the capacity of the grate inlet in sags, and the capacity was related with the depth of water ponding.

The USWDCM (2001) recommended that the sump inlet capacity can be calculated as the smaller value of using the orifice and weir equations. CDOT (2004) and Guo (2006) indicated that some sump inlets were longer than necessary, while others were shorter than needed. Guo et al. (2009) presented a laboratory investigation of the interception capacities of several types of sump inlets, including bar grate inlets and vane grate inlets. The transition between weir and orifice flows was termed as mixing flow ($Q_m$) and the smallest among the mixing flow, orifice flow, and weir flow was recommended as the interception capacity of a grate inlet in sag for a given water depth. They also found that the Brown et al. (2009)'s method overestimated capacity of bar grate inlet for small water depths and overestimated the capacity of vane grate inlets until the water became significantly deep.

***Continuous transverse grate inlets***

Continuous transverse grate inlets are commonly used in urban area such as city squares, airport pavements, parks, and pedestrian areas, but only a few studies have been reported. Sipahi (2006) conducted a laboratory study and related efficiencies of continuous traverse grate inlets with the approaching flow rate and the Froude number of approaching flow. Gómez et al. (2009) analyzed four types of continuous transverse grate inlets experimentally, and linked hydraulic efficiency to approaching Froude number, flow depth, and effective length of the grate. Tiğrek et al. (2012) formulated the efficiency in terms of approaching flow rate, longitudinal road slope, and Froude number based on experiment on one type of continuous transverse grate inlets. Based on additional experiments, Russo et al. (2013) further complemented the results of Gómez et al. (2009) by developing two equations for estimating two parameters, $\alpha$ and $\beta$, which depend on geometric characteristics of the analyzed grate inlets. Ünver (2015) experimentally analyzed the influence of grate void ratio, grate configuration, and the distance between two consecutive grate inlets on

hydraulic efficiency. Guo et al. (2021) conducted full-scale experiments on the hydraulic performance of eight continuous transverse grates and evaluated the influencing factors of hydraulics efficiencies including the Froude number and the grate's geometry (grate length, effective length and width, effective length and width ratios, opening style, and opening rate). They proposed a theoretical formula for the efficiency of grates and found that the formula predicted well against the experiment results with a difference of < 15% overall.

The relationships between the efficiencies of continuous transverse grate inlets and the Froude number (*Fr*) are quite different in Gómez et al. (2009), Tiğrek et al. (2012), and Guo et al. (2021). According to Gómez et al. (2009), the efficiencies of the continuous transverse grate inlets decreased as *Fr* increased. But the experimental results of Tiğrek et al. (2012) indicated the efficiency increased as *Fr* increased. Guo et al. (2021) noticed these contradictory conclusions and found that the efficiency of different continuous transverse grate inlets did not have a consistent relationship with *Fr*.

Traffic loads, environmental factors, aging of infrastructure, erosion and settlement of road shoulders, and overlaid carriageways are causes of vertical depression of CB grate inlets. Wakif et al. (2019) was the first who examined the effects of vertical depression on the efficiency of grate inlets in Malaysia. They showed that vertical depression reduced the hydraulic efficiency by 6-10% for a 0.02 m depression of a grate inlet.

**Table 1.2 Research campaigns for hydraulic performance of grate inlets**

| Study Country/State | Major interests | Equation Components | Conditions |
|---|---|---|---|
| Dai et al. (2021) China | To evaluate the efficiencies of six types of grate inlets under different road slopes and approaching discharge | $E = c_1 + c_2\left(\frac{nb}{B}\right)^{c_3}\left(\frac{ml}{B}\right)^{c_4}(\varepsilon)^{c_5}(S)^{c_6}(i)^{c_7}(Fr)^{c_8}\left(\frac{h}{nb}\right)^{c_9}$ $c_i$ (i=0, 1 to 9) represents the undermined coefficient to be calculated using the experimental data. | Setup size: 7m x 2.33m Scale: full $S_L$: 2%, 5%&8% $S_T$: 0.7%-3% Flow: 10-81 L/s |
| Guo et al. (2021) China | Investigated the efficiencies of the continuous transverse grate inlets and its influencing factors. | $E = C_{d0}A_o\sqrt{2g}\left(\frac{n}{W}\right)^{0.3}Q_a^{-0.7}S_L^{-0.15}$ | Setup size: 12m x 3m Scale: full $S_L$: 1-4% $S_T$: 0% Flow: 2.778-22.22 L/s |
| Cosco et al. (2020) Spain | Investigated the influence of Froude number on discharge coefficients. | Weir and orifice equations (Lee et al. 2012) $C_{dw}$: 0.009-0.244, 0.003-0.245, and 0.006-0.286 $C_{do}$: 0.055-0.294, 0.033-0.431, and 0.054-0.423 | Setup size: 5.5m x 3m Scale: Full $S_L$: 0-10% $S_T$: 2% Flow: 10-50 L/s |
| Tellez-Alvarez et al. (2020) Barcelona, Spain | To quantify energy loss in two grate inlets under pressure. | $\Delta h_k = k\frac{v^2}{2g}$ 0.25-3.41 for k while overflows ranging 20-50 L/s $\Delta h_k$ is local energy loss, k is local energy loss coefficient, v is the water velocity through grate inlets. | Setup size: 5.5m x 3m Scale: Full Inlet types: 2 $S_L$: 0-10% $S_T$: 2% Flow: 20-50 L/s |
| Gómez *et al.* (2019) Barcelona, Spain | To estimate the discharge coefficient of a grate inlet under surcharge conditions. | Weir and orifice equations (Lee et al., 2012) $C_{do}: 0.3 - 0.41$ for flow from $10 - 50$ $\mathrm{L}\frac{}{\mathrm{s}}$. | Setup size: 5.5m x 3m Scale: Full $S_L$: 0-10% $S_T$: 2% Flow: 10-50 L/s |
| Kemper *et al.* (2018; 2019) Germany | Investigated the hydraulic capacity of six types of grate inlets with supercritical surface flow conditions. | $E = 1 - Fr^{9.5}\left(\frac{d^{1.5}W}{LA_0}\right)^S$ $S$ is the parameter for the orientations of grate bars | Setup size:10m x 1.5m Scale: full $S_L$: 2.5-10% $S_T$: 2.5% Flow: 3-21 L/s n: 0.0128 (Roofing paper) |
| Wakif *et al.* (2019) Malaysia | Study on the effects of vertical depression on the efficiency of grate inlets. | Graphics of: $Q_a$ *vs.* $E$ $E$ *vs.* $S_L$ $E$ *vs.* $S_T$ $E$ *vs.* $q/y$ $Q_a$ *vs.* $Fr$ | Setup size: 2.44m x 1.83m Scale: Full $S_L$: 1.25–2.5% $S_T$: 1– 2% Flow: 4-12 L/s |

| | | | |
|---|---|---|---|
| | | q is the unit with approaching flow. | |
| Gómez *et al.* (2018)<br>Barcelona, Spain | Presented a methodology to consider the hydraulic effects of clogging phenomena. | $E = A\left(\frac{Q}{d}\right)^{-B}$ | Setup size: 5.5m x 3m<br>Scale: Full<br>$S_L$: 0-10% $S_T$: 0-4%<br>Flow:20-200 L/s |
| Rubinato *et al.* (2017)<br>Sheffield, UK | Conducted experiments to investigate the hydraulics of circular grates. | Weir and orifice equations (Lee et al., 2012)<br>$C_{dw}$= 0.115-0.372 and $C_{do}$= 0.349-2.038 | Setup size: 8.2m x 4m<br>Scale: 1:6<br>$S_L$: 0.1% $S_T$: 0%<br>Flow:4-10 L/s |
| Guo *et al.* (2016)<br>Colorado, US | Investigated flow interception capacity of inclined grate inlet. | Modified form of weir & orifice equations | Setup size: 12.3m x 0.6m<br>Scale: 1:3 |
| Kim *et al.* (2016)<br>South Korea | To investigate the hydraulics of grate inlets | Empirical equation:<br>$Q_{int} = f(Q_a, S_L, S_T)$ | Setup size: 11m x 1.2m<br>Scale: 1:2<br>$S_L$: 0-10% $S_T$: 2-10%<br>Flow: 0.5-6 L/s |
| Wu *et al.* (2015)<br>Hong Kong, China | Investigated hydraulic interception efficiency of four types of grate inlets on steep roads. | $E = aG + b$<br>$G = \frac{Q_a}{H}\frac{2}{\sqrt{g}}\frac{h^{0.3}}{L^{0.8}\,W}$<br>a and b vary for each inlet | Setup size: 1.4x1<br>Scale: 1:2<br>$S_L$: 5-20% $S_T$: 2.5%<br>Flow: 3.8-7.6 L/s |
| Gómez *et al.* (2013)<br>Barcelona, Spain | To determine clogging factors of two types of grate inlets. | $E = A\left(\frac{Q_a}{y}\right)^{-B}$ | Setup size: 3x5m<br>Scale: full<br>Inlet types: 2<br>$S_L$: 0-10% $S_T$: 0-4%<br>Flow: 0-200 L/s |
| Russo *et al.* (2013)<br>Zaragoza, Spain | To develop a methodology to estimate the hydraulic performance of seven types of non-tested continuous transverse grate inlets. | Complemented the equation proposed by Gómez et al. (2009) and developed:<br>$\alpha = -1.924\,\frac{L^{0.631}}{A_H^{0.279}}\,(n_d+1)^{-0.089}(n_l+1)^{-0.238}\,(n_t+1)^{-0.045}$<br>$\beta = -26803\,L^{-4.953} + 1.213$ | Setup size: 5x1.5m<br>Scale: Full<br>$S_L$: 0 - 10% $S_T$: 0%<br>Flow: 6.7-100 L/s/m |

| | | | |
|---|---|---|---|
| Sabtu *et al.* (2012, 2016)<br>Sheffield, UK | Hydraulic interaction between the above and below ground drainage systems via gully inlets. | Graphics of:<br>$Q_a$ *vs. y;*<br>$Q_a$ *vs. E;*<br>$C_{do}$*vs. E;*<br>$C_{do}$*vs.* $Q_a$ | Setup size: 1.83x4.27m<br>Scale: 1:1<br>$S_L$: 0-3.3%<br>Flow: 0-50 L/s |
| Tiğrek *et al.* (2012)<br>Turkey | Investigated hydraulic efficiency of one type of continuous transverse grate inlets. | $E = A(Q_a)^B$<br>A and B are coefficients that depending on longitudinal slopes and approaching flow rates. | Setup size: 12x1<br>$S_L$: 0-4% $S_T$: 0%<br>Flow: 0.25 – 4.74 L/s |
| Lee *et al.* (2012)<br>Kyoto, Japan | Study on grate inlet discharge coefficients using the formulas of weir and orifice flow. | Weir flow:<br>$Q_{int} = \frac{2}{3} C_{dw} L \sqrt{2g} (H_t)^{\frac{3}{2}}$<br>$H_t = h + \frac{V_{grate}^2}{2g}$<br>Orifice flow:<br>$Q_{int} = C_{do} A_o \sqrt{2gh}$<br>$h$ is the piezometric head over the weir or the orifice.<br>$A_o$ is the orifice cross section area.<br>$V_{grate}$ is the average velocity of the flow over the inlet, and $\frac{V_{grate}^2}{2g}$ is generally ignored.<br>$L$ is the effective length of the weir, $H_t$ is the total head.<br>$C_{dw}$= 0.48 and $C_{do}$= 0.57. | Setup size: 6x0.5<br>Scale: 1:10<br>$S_L$: 0% $S_T$: 0%<br>Flow: 0.8 – 5.0 L/s |
| Gómez *et al.* (2011)<br>Barcelona, Spain | Assessed efficiency of 11 types of grate inlets efficiency. | $E = A\left(\frac{Q_a}{y}\right)^{-B}$<br>$E' = A\left(f\frac{Q_{roadway}}{d}\right)^{-B}$ | Setup size: 5.5x3<br>Scale: Full<br>$S_L$: 0-10% $S_T$: 0-4%<br>Flow: 20-200 L/s |

| | | | |
|---|---|---|---|
| | | $A = \frac{1.988\, A_g^{0.403}}{P^{0.19}\,(n_t+1)^{0.088}\,(n_l+1)^{0.012}\,(n_d+1)^{0.082}}$<br>$B = 1.346\,\frac{L^{0.179}}{W^{0.394}}$<br>$E'$ is the inlet efficiency related to a width of half roadway with the width equal to 3 m.<br>$f$ varies with street geometry. | |
| Brown *et al.*<br>HEC-22 (2009)<br>US | Guideline for urban drainage | On grade: Johnson et al. 1984<br>In sag:<br>Weir flow:<br>$Q_{int} = C_{dw} P (d)^{\frac{3}{2}}$<br>Orifice equation:<br>$Q_{int} = C_{do} A_g \sqrt{2gd}$<br>P is the perimeter of grate disregarding the side against the curb, $A_g$ is the clear opening area of the grate.<br>$C_{dw}$= 1.66, $C_{do}$ = 0.67. | / |
| Guo *et al.* (2009)<br>Colorado, US | Investigated inlets in sump | Weir flow:<br>$Q_{int} = N_w C_{dw} \sqrt{2g} (2\mathrm{W} + \mathrm{L}) (d)^{\frac{3}{2}}$<br>Orifice flow:<br>$Q_{int} = N_o C_{do} \sqrt{2g} \mathrm{WL} (d)^{\frac{1}{2}}$<br>Mixing flow:<br>$Q_m = C_m \sqrt{Q_W Q_O}$<br>$Q_m$ is mixing flow, $C_m$ is the mixing flow coefficient to be calibrated | Setup size: 20x3.5m<br>Scale: 1:3<br>$S_L$: 1% $S_T$: 1%<br>Flow: <32 L/s |

| | | | |
|---|---|---|---|
| Gómez *et al.* (2009)<br>Barcelona, Spain | Investigated hydraulic efficiency of four types of continuous transverse grates for paved area. | $E = \alpha \left( Fr \left( \frac{d}{L} \right)^{0.812} \right) + \beta$<br>$\alpha$ and $\beta$ are coefficients depending on geometric characteristics of analyzed grates. | Setup size: 5.5m x 1.5m<br>Scale: full<br>$S_L$: 0 – 10% $S_T$: 0%<br>Flow: 6.7 – 66.7 L/s (unit width flow) |
| Gómez *et al.* (2007)<br>Barcelona, Spain | Investigated hydraulic efficiency of macro-inlet. | $E = A \left( \frac{Q_a}{d} \right)^{-B}$ | Setup size: 5.5m x3m<br>Scale: full<br>$S_L$: 0-10% $S_T$: 0-4%<br>Flow:20-200 L/s |
| Sipahi *et al.* (2006)<br>Turkey | Analysed efficiency of four types of continuous transverse grate inlets. | For 0.48 < Fr <1.0:<br>$E = (0.1579 + 0.858) Fr {Q_a}^{0.106}$ ;<br>For 1< Fr <1.74:<br>$E = (-0.1403 + 0.8403) Fr {Q_a}^{0.19}$ | Setup size: 12m x1m<br>$S_L$: 0-4% $S_T$: 0%<br>Flow: 0.16 – 7.46 L/s |
| Mustaffa *et al.* (2003; 2006)<br>Alberta, Canada | Described findings from a laboratory-scale model of flow through three types of grate inlets. | Weir and orifice equations (Lee 2012)<br>$C_{do}$= 0.35, 0.69, 0.81 | Setup size: 4.24m x 0.4m<br>$S_L$: 0-1% $S_T$: 0%<br>Flow: 1.76-37.12 L/s<br>n: 0.010-0.016(suggested) |
| Gómez *et al.* (2005)<br>Barcelona, Spain | Described a comparative study between three methodologies for grate inlet hydraulic efficiency. | / | / |
| Cromwell *et al.* (2001)<br>Florida, US | Reported hydraulic performance tests for two types of grated gutter inlets. | Graphics of:<br>$Q_a$ vs. $Q_{int}$<br>$y$ vs. $Q_{int}$ | Scale: 1:2<br>$S_L$: 0.8- 8% $S_T$: 6%<br>Flow: 10 -200 L/s |
| Spaliviero *et al.*<br>(2000) | Tested 21 types of grate inlets and determined the efficiency. | $E = \alpha - G \frac{Q_t}{h}$<br>$G = \frac{69}{A_g^{0.75} P^{0.5}} (n_t + 1)^{0.19} (n_l + 1)^{0.07} (n_d + 1)^{0.15}$ | Setup size: 4.9m x 1.5m<br>Scale: 1:1.28.<br>$S_L$: 1:200-1:15 |

| | | | |
|---|---|---|---|
| WallinFloword, UK | | $\alpha$ varies with grate inlets and is assumed to a average value 102.7.<br>$E = \frac{7.9}{1000} \frac{(S_T\, S_L^{0.5})^{\frac{9}{16}}}{n} \left(\frac{Q_t}{1000}\right)^{\frac{7}{16}}$ | $S_T$: 1:50-1:30<br>Flow: less than 150 L/s<br>n: 0.017 |
| Guo (2000)<br>Colorado, US | Described one design procedure for Setup size multiple-grate inlets considering clogging. | $C = \frac{C_0}{N} \sum_{i=1}^{i=N} e^{i-1}$<br>$Q_a = Q_0 \left(1 - \frac{L^2}{L_0''}\right)$ | / |
| McEnroe *et al.*<br>(1999)<br>Kansas, US | Determined the hydraulics of two types of grate inlets from hydraulic model tests and theoretical calculations. | $Q_{int} = \begin{cases} Q_a, & for\ Q_a \le Q_0 \\ Q_0 - (Q_t - Q_0)\left\{1 - \exp\left[-\left(\frac{Q_a - Q_0}{Q_t - Q_0}\right)\right]\right\}, & for\ Q_a > Q_0 \end{cases}$<br>Or<br>$Q_{int} = \begin{cases} Q_a, & for\ Q_a \le Q_0 \\ Q_a - (Q_a - Q_0)^m & for\ Q_a > Q_0 \end{cases}$<br>$Q_0$ is the largest approaching flow that can be completely captured; and $Q_t$ represents the upper limit on the captured discharge, which is approached asymptotically with increasing total discharge.<br>$m$ varies with each grate inlet. | Setup size:15m(length)<br>Scale: 1:4<br>$S_L$: 0.5 %<br>$S_T$: 1.6% - 3.1%<br>Flow: 10 – 250<br>n: 0.01 |
| NFCO (1998)<br>Wisconsin, USA | A manual by a CB inlets manufacturer. | $Q_{int} = K(\mathrm{d})^{\frac{5}{3}}$<br>$K$ varies for grate inlets. | / |
| Guo (1997)<br>Colorado, US | One book and computer model developed for street storm water analysis and street inlet sizing. | Extensive equations | N/A |
| Hotchkiss *et al.* (1991)<br>Bohac (1991)<br>Hotchkiss (1994) | Developing grate inlet efficiency curves for several types of grate inlets (single and series); | Efficiency versus gutter flow | Setup size: 13.4m x3.66m<br>$S_L$: 3% $S_T$:2%<br>Flow: 14.2-141.6<br>n=0.016 |

| | | | |
|---|---|---|---|
| McCallan *et al.* (1996)<br>Nebraska, US | analysed effect of resurfacing on inlet efficiency. | | |
| Johnson *et al.* (1984)<br>HEC-12 | A manual introducing drainage for highway pavements | $Q_{int} = R_f Q_f + R_s Q_s$<br>If $V_g \geq V_0$,<br>$R_f = 1 - 0.295(V_g - V_0)$<br>if $V_g \leq V_0$,<br>$R_f$ is equal to 1.0.<br>$R_s = \left(1 + \frac{K_s V_g^{1.8}}{S_x L^{2.3}}\right)^{-1}$<br>$E = R_f \left(\frac{Q_W}{Q_t}\right) + R_s \left(\frac{Q_s}{Q_t}\right)$ | / |
| Burgi *et al.* (1978)<br>Colorado, US | Reported results of comprehensive hydraulic, debris and bicycle safety tests on two types of grate inlets. | Graphics of:<br>$Q_{int}$ *vs.* $S_L$;<br>$Q_{int}$ *vs.* $S_T$;<br>$Q_{int}$*vs. E;*<br>*E vs. T* | Setup size: 18.3m x2.44m<br>$S_L$: 0.5-13%<br>$S_T$: 1:48 – 1:16<br>Flow: 160 L/s<br>n: 0.016-0.017 |
| Adam *et al.* (1974); Brandson (1971).<br>Manitoba, Canada | Described hydraulic analysis of Winnipeg sump inlets. | $Q_{int} = Cy^n$<br>Curves are provided that give C and n values as a function of the gutter slopes. | Scale: Full<br>Setup size: 7.3m x 2.4m<br>$S_L$: 0.5-6%<br>$S_T$: 2.1% & &4.2%<br>n: 0.012 (concrete) |
| Woo *et al.* (1974)<br>Washington, D. C. US | Investigated the influencing factors on efficiency of grate inlets. | Graphics of:<br>$Q_a$ *vs.* $E$ | Setup size: 8.84m x 0.89m<br>Scale: full & 1:1.27<br>$S_L$: 0.5 – 7.5%<br>$S_T$: 1:25<br>Flow: 0.008-0.091 |
| Appel (1972), Brune *et al.* (1972) | Provided information to aid in the design of spacing highway drainage inlets in grassed channels; to | Graphics of:<br>$Q_a$ *vs.* $E$. | Setup size: 10.1m x 4.9m<br>Scale: 1:2<br>$S_L$: 0.2-8% |

| | | | |
|---|---|---|---|
| Pennsylvania, US | determine experimentally the efficiency of three different types of grate inlets. | | $S_W$: 8-16%<br>$S_T$: 8-200%<br>Flow: 0.001 – 0.059 |
| Yucel *et al.* (1969)<br>Washington, D. C., US | A literature review on hydraulics of grate inlet. | / | / |
| Cassidy (1966)<br>Columbia, US | Described laboratory tests for hydraulic characteristic of grate inlets with varied bar configurations and orientation. | Graphics of:<br>$E$ vs. $\frac{v}{\sqrt{gy}}$ | Setup size: 0.75m x 0.36m<br>Scale: 1:2<br>$S_L$: 0.5-3.0%<br>$S_T$: 1:20.6; 1:50 |
| Black (1967) | Determined efficiency of grate inlets | Graphics of:<br>$E$ vs. $Q_a$<br>$E$ vs. $S_L$<br>$E$ vs. $S_T$ | Setup size: 9.6m x1.2m<br>Scale: Full<br>$S_L$: 0.4-6% $S_T$: 2-6%<br>Flow: 6.6-21.8 L/s |
| Guillou (1959)<br>Illinois, US | Determined interception capacity characteristics of several grate inlets. | Graphics of:<br>$E$ *vs.* $S_L$<br>$E$ *vs.* $v$<br>$Q_a$ *vs.* $Q_{int}$<br>$Q_a$ *vs.* $H$<br>H is the water depth over grate inlets. | Setup size: 8.53m x0.96m<br>Scale: full<br>$S_L$: 0.125-6%<br>Flow: 0.01-0.1<br>n: 0.017 |
| Johns Hopkins University (1956)<br>US | Developed one method to predicting the flow capacity of grate inlets. | / | / |
| Li *et al.* (1951)<br>US | Presented experimental tests of several grate inlets and developed formulas to describe inlet capacity. | Extensive equations and graphics. | Scale: 1:2<br>$S_L$: 0.5-6% |
| Larson *et al.* (1947)<br>Minnesota, US | Reported the results of an investigation of the flow of water and entrained debris | Graphics of:<br>$Q_C$ *vs.* $Q_{int}$ | Setup size: 4.88m x1.83m<br>$S_L$: 0.5-3.0% $S_T$: 1:20.6<br>Flow: 0.026-0.042 L/s |

| | | | |
|---|---|---|---|
| | through standard and experimental gutter inlets of the grate type. | $Q_C$ is carry-over flow. | **n**: 0.0103(Masonite) |

### 2.4.2 Under clogging conditions

Most studies assumed that grate inlets work in clean condition (without blockage). Debris like leaves and silt on roads could lead to partial and even full blockage of grate inlets, and hydraulic efficiency of the inlets could be significantly reduced, leading to inefficiency of the urban drainage system and even serious surface flooding during large rainfall events. Study on the clogging effect on grate inlet efficiency is needed to accurately determine grate inlet capacity under real conditions and help improve future design of CB inlets (Kemper et al., 2016). So far, only a few tests have been conducted (Gómez et al., 2013, 2018; Leitao et al., 2017; Hao et al., 2021) on clogging patterns, which are complex because both stormwater and debris vary from region to region.

The degree of blockage can vary considerably depending on the location of the road, the type of the grate, the season of the year, the antecedent weather conditions, and the frequency of road cleaning (Burgi et al., 1978; Spaliviero et al., 2000; Gómez et al., 2013, 2018; Russo et al., 2013; Leitao et al., 2017). Based on spatial analysis of their proximity to trees and evaluation of sewer inlet locations, Leitao et al. (2017) proposed one stochastic method for identifying the grate inlets most prone to clogging and conducted a Monte Carlo simulation on the capacity of inlets under clogging and subsequent simulation of flooding. Hao et al. (2021) tested grate inlets through physical experiments. The results revealed that clogging extent and position have a significant influence on grate inlet capacity, and clogging extent has a greater impact on grate inlet capacity than clogging position.

Early investigations (Larson et al., 1949; Burgi et al., 1978) conducted hydraulic tests in laboratory using Kraft paper and dry leaves to represent road debris. Larson et al. (1949) proposed the concept of “self-cleaning ability”, which represented the ability of the inlet to handle debris without clogging. The results demonstrated that an inlet with longitudinal opening had the best self-

cleaning ability compared to the inlet with the bars normal to the flow. Similarly, Burgi et al. (1978) claimed that a grate inlet's ability to handle debris without clogging largely depend on the spacing between its longitudinal bars. Guillou (1959) stated that the cleaning ability of smooth parallel bars is better than that of rough bars, and the self-cleaning ability increases with the increase of the smoothness.

To quantify blockage at CB inlets, the clogging factor, $C_0$(< 1.0), was used. The capacity of a grate inlet under clogging conditions, $Q_{int,cf}$, can be expressed as:

$$Q_{int,cf} = (1 - C_0)\, Q_{int} \tag{2.8}$$

where $Q_{int}$ is the intercepted flow with no clogging. A summary of $C_0$ is presented in Table 2.3. Similarly as $C_0$, Spaliviero et al. (2000) introduced a non-dimensional maintenance factor, *m*(shown in **Table 2.3**), to quantify the clogging effect, and recommended m = 1.0 for well-maintained roads, 0.9 for roads subject to less frequent maintenance, 0.8 for roads subject to substantial leaf falls or vehicle spillages, and 0.7 for sag points on road gradients.

In engineering practice, the clogging factor $C_0$ = 0.5 is commonly adopted for grate inlets in many local authorities (CCRFCD, 1990; CDOT, 2000; UDFCD, 2001). However, this value is not realistic but meat to be conservative (Gómez et al., 2013). Despotović et al. (2005) covered half of a grate inlet and found that the inlet efficiency significant decreased regardless of the clogging pattern. Gómez et al. (2013 & 2018) summarized the clogging patterns of grated inlets in Barcelona, Spain, and experimentally tested at full (1:1) scale to determine the reduction in hydraulic efficiency of grate inlets. Their results showed that $C_0$ = 0.23 - 0.50 for various clogging patterns in the most cases, while it could be close to 0.7 in the worst case. Veerappan et al. (2016) tested three types of CB grate inlets in Singapore through numerical simulation for the clogging portion

of 50%, 100%, and > 100% (clogging over the horizontal plane of the grate inlet). Compared with clean condition, their results showed that hydraulic efficiency varied slightly with different roadway longitudinal and transverse slopes, rain intensity, and types of inlets, for the 50% and 100% clogging cases. For > 100% clogging, the maximum $C_0$ can be around 0.7. It should be mentioned that the inlets tested by Veerappan et al. (2016) looked like combination inlets from the photographs. Abedin et al. (2019) used the GIS to model and map flood spatiotemporal variation in two urban catchments and found that $C_0$ = 0.83 and 0.14 to calibrate the model. Hao et al. (2021) tested grate inlets with various clogging extent and clogging position, and the results indicated clogging factors ranging from 0 to 0.45.

Studies revealed that it would be improper to adopt a value of clogging factor for CB inlet designs. In an urban area, the amount of debris is largely associated with the first flush volume, which can be the first 0.5 inch of a storm event (Guo and Urbonas, 1996). Guo et al. (2016) concluded that for an on-grade inlet, clogging effect is linearly proportional to the inlet length; but for a sump inlet, it is linearly proportional to the inlet opening area. While for curb opening inlets, Guo et al. (2006) pointed out that applying a clogging factor to the inlet capacity would result in inlets with an excessive length since it would overestimate the blockage length of inlets, and this discrepancy could be resolved by applying the clogging factor to the length of the inlet.

Guo (2000) proposed that the clogging effect on a multiple-grate inlet decays with respect to the length of inlet:

$$C_{0,i+1} = eC_{0,i} \tag{2.9}$$

where $C_0$ is the single-grate clogging factor, $e$ is the decay factor, and $i$ is the $i$-th grate. For grate inlets in series, the multiple grate clogging factor $C$ is:

$$C = \frac{C_0}{N} \sum_{i-1}^{i-N} e^{i-1} \tag{2.10}$$

where $C_0$ is the single-grate clogging factor, and $N$ is the number of grates. The calibrated values of $e$ = 0.5 and 0.25 using the field experimental data for grate inlets and curb opening inlets, respectively.

**Table 2.2** Summary of investigations considering clogging effect

| Study State/ Country | Study method | Equation / Chart | Experimental condition & scale | Clogging factor | Major conclusion |
|---|---|---|---|---|---|
| Hao et al. (2021) China | Experiment | / | Setup size: 9.6mx2.4m<br>Scale: 1:3<br>Flow: 0-20 L/s | 0.17 for clogging extent was 0.25;<br>0.45 for clogging extent was 0.5. | Clogging extent and clogging position have a significant influence on inlets discharge capacity; clogging extent has a greater impact than clogging position. |
| Abedin *et al.* (2019) Nevada, US | GIS-based | / | / | 0.83 For Blacklot;<br>0.10 For East Mall | N/A |
| Gómez *et al.* (2018) Barcelona, Spain | Experiment;<br>Covered with gypsum | / | Setup size: 5.5mx3m<br>Scale: full<br>$S_L$: 0-10%<br>$S_T$: 0-4%<br>Flow: 20-200 L/s | 0.25-0.7 | Clogging coefficients can be in the range of 0.23 to 0.50 for the most usual clogging patterns, while for the worst, clogging factor should be closer to 0.7. |
| Veerappan *et al.* (2016) Singapore | Experiment;<br>Closing some voids with sod | / | Setup size: 3m (width)<br>Scale: full<br>$S_L$: 1-3%<br>$S_T$: 4%<br>n: 0.015 | 0.7(Max.) | Rainfall intensities have little impact on the grate inlet hydraulic efficiencies. |
| Leitao *et al.* (2016) Coimbra, Portugal | Stochastic analyse | / | / | 0.72(Max.) | Considering variations in sewer inlet capacity could lead to more accurate representation of urban pluvial flooding. |
| Gómez *et al.* (2013) Riera Blanca Basin, Spain | Experiment;<br>Closing some voids in each inlet with gypsum. | $\boldsymbol{E = A\left(\frac{Q_a}{d}\right)^{-B}}$ | Setup size: 5.5mx3m<br>Scale: full | 0.265-0.674 | The reduction in terms of hydraulic efficiency depends on clogging patterns but is almost independent of flow |

| | | | | | |
|---|---|---|---|---|---|
| | | | $S_L$: 0-10%<br>$S_T$: 4%<br>Flow: 20-200 L/s | | conditions when high flow amount circulate on the street. |
| Guo (2006)<br>Colorado, US | / | / | / | / | For curb opening inlets, the interception of an inlet on a grade is proportional to the inlet length, and in a sump is proportional to the inlet opening area. |
| Artina et al. (2001)<br>Italy | / | / | / | 0.25 | / |
| Spaliviero *et al.* (2000)<br>WalinFloword, UK | Analytical | $Q_{int} = m\frac{\mathrm{E}}{100}Q_a$ | | 0.7 – 1.0 | Values of m are based on situations. |
| Guo (2000)<br>Colorado, US | Analytical | / | / | / | For grate inlet, applying clogging factor to the length of inlets is more promising. |
| CDOT (2000)<br>Colorado, US | / | / | / | 0.10 | / |
| CCRFCD (1999)<br>Nevada, US | / | / | / | 0.50 | / |
| Burgi *et al.* (1978)<br>Colorado, US | Experiment.<br>Brown craft paper | / | Setup size: 18.3mx2.44m<br>Scale: full<br>$S_L$: 0.5-13%<br>$S_T$: 4%<br>n: 0.016-0.017 | / | A grate's ability to handle debris without clogging was shown to be most dependent on the spacing of its longitudinal bars. |
| Yucel (1969)<br>Pennsylvania, US | Analytical | / | / | / | Inlets with the bars parallel to the direction of flow in the gutter have higher efficiency and self-cleaning ability than inlets, wherein the bars are not parallel to the direction of the flow. |
| Guillou (1959)<br>Illions, US | Analytical | / | / | / | The cleaning ability of smooth parallel bars is better than that of rough parallel. As the smoothness of the bars increases the self cleaning ability increases also. |

| | | | | | |
|---|---|---|---|---|---|
| Larson (1947)<br>Minnesota, US | Experiment,<br>Newsprint Paper,<br>Dried poplar leaves and grass | / | Setup size: 4.88x1.83<br>$S_L$: 0.5-3.0% $S_T$: 1:20.6<br>Flow: 0.026-0.042 L/s<br>**n**: 0.0103(Masonite) | / | The leaves passed through the inlet openings somewhat easier than did the pierces of paper, and when lodged on the grate bars, the leaves were washed off more readily. |

## 2.5 Curb opening inlets

Curb-opening inlets have been studied for more than 70 years, and relevant studies were reviewed by Izzard (1950), Holley et al. (1992), Hammonds et al. (1995), and Brown et al. (2009). Early studies proposed theoretical formulas for capacity and efficiency of curb-opening inlets and calibrated them with experiments to derive semi-empirical formulas (Izzard et al., 1950; Li et al., 1956; Forbes 1976). Early studies also investigated hydraulic performance and found the relationships between curb opening inlet capacity and the approaching flow conditions, gutter and geometry of transition from the road surface to curb-opening inlets, and inlet configurations (McEnroe et al., 1999; and Fiuzat et al., 2000; Kranc et al., 2001; Uyumaz, 2002). Recent studies aimed to optimize inlet designs and improve inlet capacity, considering the clogging effect and the presence of slabs and chambers (Hammonds et al., 1995; Guo et al., 2012).

The factors influencing the hydraulic performance of curb opening inlets are the longitudinal and transverse slopes of roadways, gutter geometry, transition geometry, approaching flow condition , clogging, and configurations of inlets (Izzard et al., 1950; Johns Hopkins University, 1956; Bauer et al., 1964; Uyumaz, 1977; Johnson et al., 1984; Holley et al., 1992; Kranc et al., 2001; Guo et al., 2012 ; Li et al., 2019). The interception capacity of a curb inlet can be enlarged by extending its length (Hammonds et al., 1995), depressing the gutter section at the inlet (Li, 1956), adding depression areas upstream and/or downstream of the inlet section (Hammonds et al., 1995, Li et al., 2019), and increasing the roadway transverse slope or roadway roughness (Muhammad, 2018).

The performance of a curb opening inlet can be divided into two categories: 100% efficiency (fully captured condition), i.e., the inlet capturing all the approaching flow; and < 100% efficiency (partially captured condition), i.e., there is carryover flow. Investigations on curb opening inlets

included two major types: with and without depression. Table 2.4 provided a summary of these studies.

### 2.5.1 Undepressed curb opening inlets

Izzard (1950) analyzed the flow into a curb inlet as flow over a broad-crested weir and assumed that the water depth could be treated as linearly decreasing along the inlet length. By modifying the Manning's equation for gutter flow, he proposed the velocity equation in the longitudinal direction ($V_L$) as a function of the flow depth upstream of the curb face, the Manning's roughness coefficient ($n$), and the roadway longitudinal slope. Based on that, the length of curb opening inlet required to fully capture the approaching flow, $L_r$, were derived as Eq. (2-11). Izzard (1950) also proposed the equation for the partially captured capacity and efficiency of curb opening inlets:

$$L_r = 1.51\, Q_t^{0.44}\, S_L^{0.28} \left(\frac{1}{n\, S_x}\right)^{0.56} \tag{2.11}$$

$$Q_{int} = K\, L_r\, y_n^{\frac{3}{2}} \left[1 - \left(1 - \frac{L}{L_r}\right)^{5/2}\right] \tag{2.12}$$

$$E = 1 - \left(1 - \frac{L}{L_r}\right)^{5/2} \tag{2.13}$$

where $K$ is a coefficient, $y_n$ is the normal depth of water and $L$ is the inlet length.

Hammonds et al. (1995) compared the analyses of Izzard (1950) and Li (1951) and revealed the effects of the different assumptions and inlet geometries on inlet capacity and efficiency. For a given approaching flow rate, Li's equation predicted that an inlet would capture at least two thirds more flow than that predicted by Izzard's equation. Compared to the experimental data of Hammonds et al. (1995), both Li's and Izzard's equations underestimated the capacity of the inlet for partially captured condition. Moreover, in terms of inlet efficiency, Li's equation predicted smaller efficiency than Izzard's equation for partially captured condition.

Li (1954) analysed the flow into curb opening inlets by comparing it with the free hydraulic drop. Li (1954) proposed analytical and empirical efficiency equations separately for the fully and partially captured flow cases. Li (1954)'s empirical and theoretical length required to fully capture the flow are:

$$\text{Empirical:} \quad L_r = V_L \sqrt{2y_n/g} \tag{2.14}$$

$$\text{Theoretical:} \quad L_r = V_L \sqrt{\frac{2y_n tan\theta}{g\, cos\theta}} \tag{2.15}$$

where the $\theta$ is the angle between vertical and gutter surface. The equation for the intercepted flow is:

$$Q_{int} = KL_r y_n \sqrt{g y_n} \tag{2.16}$$

The theoretical equation for the inlet efficiency is:

$$E = [\left(\frac{L}{L_r}\right)^2 - \left(\frac{L}{L_r}\right)^4] \tag{2.17}$$

Walsey (1960) analysed theoretically the flow as the superposition of 1) the instantaneous failure of a dam with a triangular reservoir and 2) a certain incoming velocity distribution upstream of the inlet. Walsey (1960) provided a formula for predicting the discharge of inlet required for fully captured condition.

Zwamborn (1966) conducted full scaled and 1:6-scaled experiments to analyse the capacity of curb opening inlets. Zwamborn defined the depth $y_0$ at the inlet after the sharp drop and related it to the normal water depth $y_n$ considering the effects of the nonlinear water surface profile. Zwamborn (1966) also assumed the flow into the inlet as a linear flow as Izzard (1950); however, the linear

profile was assumed to start at $y_0$ instead of $y_n$. Similar to Izzard (1950), Zwamborn proposed the following equation:

$$Q_{int} = 0.328 L_r \, y_n^{1.25} \tag{2.18}$$

Forbes (1976) used an analytical numerical method for calculating flow into undepressed curb inlets. Forbes compared his method to the weir formula of Li et al. (1956) and the experimental data of Zwamborn (1966) and Goldfinch. The results showed that Forbes's numerical method underestimated the inlet lengths for fully captured cases, and an empirical constant, 0.48, was needed to apply to g (the acceleration of gravity), compared with Li et al.'s and Zwamborn's data. Similarly, the empirical coefficient had to be 0.3 to match Goldfinch's data. Using the same empirical modifying constant (0.48), comparisons were then made with the Zwamborn (1966)'s formula. The comparison was generally good for the longitudinal slope of roadway up to 2.5%; but for the slopes > 2.5%, the numerical method showed a lower interception capacity and the difference became more marked as the slope increased.

For undepressed curb opening inlets, Johnson et al. (1984) stated that the length to fully capture the approaching flow is:

$$L_r = 0.076 \, Q_t^{0.42} \, S_L^{0.3} \left(\frac{1}{n \, S_x}\right)^{0.6} \tag{2.19}$$

Johnson et al. (1984) also proposed the efficiency formula as:

$$E = 1 - \left(1 - \frac{L}{L_r}\right)^{1.8} \tag{2.20}$$

For undepressed curb opening inlets under fully captured condition, Hammonds et al. (1995) report that both Izzard (1950)'s and Johnson et al. (1984)'s equations predicted lower captured capacity per unit length of inlets than the experimental data. For partially captured condition, Izzard's

equation slightly underestimated the capacity of the inlets, and Johnson et al.'s equation gave acceptable predictions.

Spaliviero et al. (2000) conducted full scaled experiments and provided an equation for partially captured condition:

$$E = 1 - 0.199 \frac{Q_t}{{y_n}^{1.5\mathrm{L}}} \tag{2.21}$$

$$L_r = 0.38\, Q_t^{0.51}\, S_L^{0.06} \left(\frac{1}{n\, S_x}\right)^{0.46} \tag{2.22}$$

Muhammad (2018) collected the experimental data from five studies, i.e., Li et al. (1951), Walsey (1960), Karaki et al. (1961), Hammonds et al. (1995), and Spaliviero et al. (2000). Non-linear regression analysis was conducted and the empirical formula for the fully captured condition was proposed as:

$$Q_t = 5.789\, d_n^{1.39}\, S_x^{0.23} n^{0.43} L_r \tag{2.23}$$

There were several different treatments regarding the water depth along the inlet length. Izzard (1950) assumed that the water depth along the inlet length could be treated as a linear decrease. However, Walsey (1960) and Zwamborn (1966) both observed the water depth decreased sharply from the upstream edge of the inlet and followed by a semi-linear profile until the end of the inlet length. stated that the treatment of the inlet flow as weir flow with a linear water profile that overestimates the depth would overestimate the flow into the inlet. Moreover, Muhammad (2018) pointed out that Izzard's assumption that transverse velocity in the approaching flow is negligible would underestimate the flow into the inlet.

There were also several assumptions on flow spread width. Li (1951) assumed that the flow spread width begins to decrease immediately at the cross-section of the upstream end of the inlet. Walsey

(1960) found that the flow spread remains constant for a given distance downstream of the beginning of the inlet before the spread width decreases. Muhammad (2018) reported that the assumption of a premature decrease of flow spread overestimates the flow into the inlet, and further suggested that inaccuracies of Walsey's predictions are due to the ignorance of the angle of flow into the inlet. Muhammad (2018) found that Brown et al. (2009)'s equations generally underestimates the inlet capacity for fully captured condition and overestimates the inlet efficiency for partially captured conditions.

Recently, Wang et al. (2021) examined curb opening inlets with a full-scale rainfall system and a road surface. It was found that methods from the literature for predicting the efficiency of curb opening inlets produced large errors in small rainfall (low approaching flow rate) situations. Compared with Wang et al. (2021)'s experimental data, average difference ranged from -26% to 16% for Brown et al. (2009) 's method, from -36% to 6% for Izzard et al. (1977)'s method.

### 2.5.2 Depressed curb opening inlets

Compared with undepressed curb opening inlets, the application of depression to curb opening inlets can significantly improve their interception capacities. Some studies modified the equations of undepressed curb opening inlets (Izzard, 1950; Li et al. 1956). Izzard (1950) modified the equations by introducing the depth of depression ($a$) into the equations and compared the equations with the data from North Carolina and the U.S. Army Corps of Engineers. Izzard (1950) found that his equations predicted larger fully captured capacity for the North Carolina inlets and underestimated the partially captured capacity of the Corps of Engineers inlets.

Hammonds et al. (1995) compared the analyses of Izzard (1950) and Li et al. (1951) for depressed curb opening inlets. For fully captured condition, Li et al.'s equation predicted larger required inlet length than Izzard's equation for lower approaching flow rates but smaller required inlet length for

higher flow rates. For partially captured condition, Li et al.'s equation predicted lower intercepted capacity than Izzard's equation.

Li (1956) modified the method of undepressed curb inlets for the capacity of depressed curb opening inlets. Firstly, the flow depth, $y$, is used instead of $y_n$, the normal depth. Secondly, $C$ is added into the formula for considering the increased inlet capacity due to the depression. They assumed the approaching flow was contained within the depressed gutter. The initial increase in length of depressed gutter would lead to an increase in inlet capacity, while beyond a certain length a decrease in inlet capacity was detected. Further, the triangular-shaped depressed gutter was found to have an inlet capacity of up to 80% higher than that of constant-width depressed gutter

Karaki et al. (1961) conducted a full-scaled experiment for depressed curb opening inlets with uniform, supercritical approaching flow and demonstrated the effects of geometric variables and roughness coefficient, but they did not develop conclusions. Bauer et al. (1964) used the data of Karaki et al. (1961) for depressed curb opening inlets. Firstly, they tested seven curb opening inlets with various geometries of upstream and downstream depression transition and found that a depression with depression width = 0.61 m and depression depth =0.05 m had the largest inlet capacity. Secondly, they developed inlet design curves and proposed that the efficiencies of curb opening inlets could be related to the dimensionless parameter.

Bauer et al. (1964) studied depressed curb opening inlets in sump with 1:4 model experiments. They treated the flow into the inlet as over a weir, and presented the results using curves allowing for direct comparison on the effect depression size on the inlet efficiency. Bauer et al. (1964) also proposed the empirical formula to calculate the intercepted capacity of curb opening inlets in sump and related it to the maximum gutter water depth. Bauer et al. (1964) also compared their results with the work of Izzard (1950) and Li (1956). It was found that Izzard's method substantially

underestimated the capacity of inlets with depression widths greater than 1 foot, while Li's curves showed higher interception rates due to differences in experimental conditions.

Zwamborn (1966) conducted tests on 1/6 scaled models, with longitudinal slope of roadway up to 2.5% for the former and 6.7% for the latter and treated the flow into the inlet as a weir. An empirical relationship was built between the depth of flow and capacity of inlets, in addition to charts. Zwamborn's charts gave smaller interception capacities for larger road longitudinal slopes and low approaching flows.

To examine whether Zwamborn's charts can be extrapolated for very steep road longitudinal slopes, Forbes (1976) presented a numerical method for calculating the flow into the depressed curb inlets. Forbes compared his method to Zwamborn (1966)'s full scaled tests and found that fairly close agreement. However, for longitudinal slope of roadway larger than 2.5% and for the upstream gutter length of 0.9 m, Forbes's method gave lower interception capacities than Zwamborn's predictions.

Izzard (1977) reanalysed the data of Bauer et al. (1964), simplified the method of designing depressed curb opening inlets and expanded the analysis by defining three characteristic lengths to describe the curb inlet performance. The reanalysis showed that the efficiency of the inlets can be represented as a dimensionless function of the parameter $L$ / $F_W$ / $T$ and the transverse slope of roadway, where $L$ is the length of curb opening inlet, $T$ is the flow spread width, $F_W$ is the flow Froude number at the flow spread edge.

Johnson et al. (1984) and Brown et al. (2009) stated the efficiency equation for undepressed curb opening inlets could be used for depressed curb opening inlets. But the equation for calculating $L_r$ was modified by replacing $S_x$ in the equation with an equivalent transverse slope, $S_e$, which is an equivalent cross slope having the same conveyance capacity as the given compound cross slope.

Hammonds et al. (1995) conducted 3:4 scaled experiments for depressed inlets. Based on empirical fitting of the experimental data, they proposed the intercepted capacity equation per unit length ($q_L$), which is related to the normal flow depth and effective inlet length required to fully capture the approaching flow.

Uyumaz (2002) conducted experiments and found the interception capacity of a depressed curb opening inlet could be related to several parameters as:

$$Q_{int} = f\left(\frac{1S_e}{F\,T}, \frac{L}{h_{gu.}}, \frac{Q_{int}}{Q_t}\right) \tag{2.24}$$

where $h_{gu}$ is the water depth in the gutter.

Comport (2009) and Comport et al (2012) conducted 1:3 scaled experiments on depressed curb opening inlets. They found that the method of Brown et al. (2009) underestimated the inlet efficiencies by an average of 8.7% compared with the observed values. They re-determined the coefficients of Brown et al.'s method using the collected test data.

Schalla (2016) and Schalla et al. (2017) conducted full-scale experiments and the results were compared with Brown et al. (2009)'s method at full interception. It showed a good agreement for the short inlet (1.52m in length) except for extremely small longitudinal slopes, but large difference for longer inlet (4.57m). For the long inlet tested, Brown et al.'s method always over-predicted the fully captured capacity of inlets. Schalla (2016) attributed the over-prediction to the assumption of a linearly decreasing water surface over the entire length of inlet. Similarly, Muhammad (2018) conducted experiments, and assessed the interception capacity and the assumptions used in Brown et al. (2009)'s analysis. For the fully captured condition, the experiments showed that the equation of Brown et al. (2009) overestimated the capacity for the longer inlets and underestimated for

shorter inlets. Muhammad stated that the assumed profile by Brown et al. was the main reason for the overestimation.

### 2.5.3 Special design of curb opening inlets

In addition to the depressed and undepressed curb opening inlet, some studies focused on the influence of road sags (Brandson, 1971; Adam et al., 1974; Guo et al., 2009), recessions (Holley et al., 1992), slab supports (Brown et al., 2009; Schalla, 2016; Hodges et al., 2018; Muhammad 2018), and channel extensions (Hodges et al., 2018) on the interception capacity of curb opening inlets.

Brandson (1971) and Adam et al. (1974) presented experimental investigations on hydraulic performance of undepressed and depressed curb opening inlets located in road sags for the City of Winnipeg, Canada. It was found that the interception capacity of undepressed inlets at a particular depth of ponding was inversely proportional to the longitudinal slope of the gutter, and the capacity of inlets was independent of the transverse slope of roadway. For depressed curb opening inlets, both the longitudinal slope of the gutter and the transverse slope of roadway had little effect on the capacity of inlets. Johnson et al. (1984) and Brown et al. (2009) pointed out that the capacity of a curb opening inlet in a sag depends on water depth at the curb, the length and the height of the curb opening.

Bauer et al. (1964) conducted 1:4 scaled experiments and treated the flow into the inlet as over a weir. For the condition tested for the curb opening inlets in sag, capacity of inlet was calculated as:

$$Q_{int} = K\ (L_i + 1.8W)(d_{max} + W/12)^{1.85} \tag{2.25}$$

where $d_{max}$ is maximum gutter water depth, $K$ is a coefficient and varies with the depression configurations.

Johnson et al. (1984) and Brown et al. (2009) revealed that the inlet operates as a weir to depths equal to the curb opening height and as an orifice at depths greater than 1.4 times the opening height. The equation for the capacity of a curb opening inlet operating as a weir is (Johnson et al., 1984; Brown et al., 2009):

$$Q_{int} = C_{dw}(\mathrm{L} + 1.8\mathrm{W})(d)^{\frac{3}{2}} \tag{2.26}$$

where $C_{dw}$ is 1.25 for depressed curb opening inlets (1.6 for undepressed curb opening inlets), $d$ is the depth at curb, W is the lateral width of depression (equal to 0 for undepressed curb opening inlets). The capacity equation for both depressed and undepressed curb opening inlets operating as orifices is:

$$Q_{int} = C_{do}A\left(2g\left(d_i - \frac{h}{2}\right)\right)^{\frac{3}{2}} \tag{2.27}$$

where $C_{do}$ is 0.67, $d_i$ is the effective head on the center of the orifice throat, $A$ is the clear area of opening, h is the depth at lip of curb opening, $h$ is the height of curb opening orifice.

Guo et al. (2012) stated that flow into a curb opening inlet in sump operated like weir, orifice, or mixing flow. Similar to grate inlet in a sag, the modified weir and orifice formulas for a curb opening inlet are:

$$Q_{int} = C_{dw}L_c(d)^{\frac{3}{2}} \tag{2.28}$$

$$Q_{int} = C_{do}\sqrt{2g}(d - 0.5L_c) \tag{2.29}$$

where $L_c$ is the length of curb opening, and $H_c$ is the height of curb opening inlet. The 1:3 scaled experimental data showed significant difference from the predictions using the method of Brown et al. (2009), but agreed with Guo et al.'s equations.

Holley et al. (1992) conducted 3:4 scaled experiments on recessed curb opening inlets. Tests were performed to evaluate linear and reverse curve transitions upstream and downstream of inlet opening as well as the slope of the recessed portion of the curb line and the actual inlet opening. The results showed that recessed curb opening inlets behaved similarly to the undepressed curb opening inlets of greater length in terms of flow captured.

Flush structural slab supports are widely used in long curb opening inlets. However, conclusions of the influence of structural slab supports on curb opening inlets are not consistent. Brown et al. (2009) stated that slab supports placed with the curb line can significantly reduce the interception capacity of curb opening inlets. According to tests of Brown et al. (2009), such supports could reduce the capacities of openings downstream of the supports by as much as 50%. Schalla (2016) and Hodges et al. (2018) conducted full scaled experiments investigating the effect of the structural slab supports on the performance of undepressed curb opening inlets, and found no observable difference in the intercepted flow due to the slab supports. Muhammad (2018) conducted full scaled experiments, and the results were also consistent with those of Schalla (2016) and Hodges et al. (2018).

Hodges et al. (2018) conducted a series of tests to investigate the effect of the constrict upstream extension on the overall interception of the inlet, and found that the effect is negligible as the inlet intercepted the same flow rate as a conventional inlet of the same length. Their tests for curb opening inlets in a sag showed that the method of Brown et al. (2013) significantly overestimates

the interception capacity of the extension. An equation was proposed for the capacity of the extension as a function of the depth at the inlet, as:

$$Q_{int} = 0.094(d_i + 0.292)^{0.5} \quad (2.30)$$

**Table 2.3** Summary of investigations of hydraulic performance of curb opening inlets

| Reference/ Research campaign | Major interests | Design Equation | Investigation Conditions |
|---|---|---|---|
| Wang *et al.* (2021)<br>China | To evaluate curb opening inlet efficiency under unsteady rainfall. | $E_t = E_{et} + a_0 e^{-b_0 Q_t}$<br>$a_0$ *(%) and* $b_0$ *(h/m³) are adjusted parameters;*<br>$E_t$ is efficiency at time *t;* $E_{et}$ is efficiency calculated using existing method at time *t;* $Q_t$ is approaching flow rate at time t ($m^3$/h). | Setup size: 18m x 4m<br>Scale: full<br>$S_L$: 3%-10% $S_T$: 1.5%-3%<br>Rainfall: return year of 1, 3 and 5 years with 1 hr rainfall duration. |
| Zaman *et al.* (2021)<br>Malaysia | Sensitivity analysis on the parameters influencing capacity of curb opening inlets. | $E = A\ ln(Q_a) + B$<br>$P_f = a\ E + b\ (Q_a)^c$<br>A, B, a, b, and c vary for types of curb opening inlets.<br>$P_f$ is probability of failure. | Setup size: 6.04m x 3.83m<br>Scale: full<br>$S_L$: 0.5% $S_T$: 2.5% $S_g$ 4%<br>n: 0.016<br>Flow: < 30 L/s |
| Muhammed (2018)<br>US | Verified past design methods for depressed curb inlets and developed a new approach. | Undepressed:<br>$Q_{int} = 5.789\ d_n^{1.39}\ S_T^{0.23} n^{0.43} L_r$<br>Depressed:<br>For 100% interception:<br>$Q_{int} = C_f\ Q_{HEC}$<br>$C_f = 2.8\left(\frac{a}{d}\right)^{0.24}\left(\frac{W}{T}\right)^{0.8}(S_L + S_{Tr})^{-0.13}(S_L)^{0.22}$<br>For less than 100% efficiency:<br>$Q_{int} = Q_t[1 - m(1 - \frac{L}{L_r})]$<br>$m = \left(\frac{L_r}{y_{n,100}}\right)^{0.22}$<br>$S_{Tr}$ is the transition slope. | Setup size: 19.5m x 3.2m<br>Scale: full<br>$S_L$: 0.1-4% $S_T$: 2-6%<br>Flow: < 14.2 L/s<br>n: 0.012 |

| | | | |
|---|---|---|---|
| | | $Q_{HEC}$ is the capacity calculated using the method of Brown et al., 2013.<br>$y_{n,100}$ is the normal water depth associated with fully captured capacity | |
| Hodges *et al.* (2018)<br>Texas, US | The effect of structural slab supports on the performance of curb inlets; the effect of potential flow restrictions on the interception capacity of curb inlets with channel extensions. | For 100% interception without depression:<br>$Q_{int} = 8.4\ L\ n^{\frac{1}{3}}(S_T)^{\frac{7}{8}}(S_L)^{-\frac{1}{8}}$ | Setup size: 19.0m x 3.2m<br>Scale: 3:4<br>$S_L$: 0.1-4% $S_T$: 2-6%<br>Flow: < 198.2 L/s<br>n: 0.0166 |
| Schalla *et al.* (2016; 2017; 2018)<br>Texas, US | Investigate effects of flush slab supports on the hydraulic performance of depressed curb opening inlets and an analysis of design equations | Graphics of comparison between HEC-22 and experiments. | Setup size: 19.0m x 3.2m<br>Scale: full<br>$S_L$: 0.1-4% $S_T$: 2-6%<br>Flow: < 198.2 L/s<br>n: 0.0166 |
| Guo and MacKenzie, CDOT, (2012)<br>Colorado, US | Investigated the hydraulic efficiency of the Type R curb inlet in the sump and on-grade conditions. | Depressed:<br>$L_r = 0.048\ Q_t^{0.51}\ S_L^{0.06}\left(\frac{1}{n\ S_x}\right)^{0.46}$<br>$E = 1 - \left(1 - \frac{L}{L_r}\right)^{0.8}$<br>In sump:<br>Weir flow:<br>$Q_w = n_w C_{dw}\sqrt{2g}L_c d^{\frac{3}{2}}$<br>Orifice flow through throat:<br>$Q_o = n_o C_{do}\sqrt{2g}L_c H_w d^{\frac{1}{2}}$<br>Orifice flow through curb opening:<br>$Q_o = n_o C_{do}\sqrt{2g}L_c H_c (d - 0.5H_c)^{\frac{1}{2}}$ | Setup size: 19.2mx5.5m<br>Scale: 1:3<br>$S_L$: 0.5-4%<br>$S_T$: 1-2%<br>n: 0.015 |

| | | | |
|---|---|---|---|
| | | Mixing flow:<br>$$Q_m = C_m\sqrt{Q_w Q_o}$$<br>Suggested capacity of curb opening inlets:<br>$$Q_i = \min(Q_w, Q_o, Q_m)$$<br>$n_w$ is weir length opening ratio after subtracting steel bar's width; $n_o$ is orifice areal opening ratio; $C_m$ is the mixing flow coefficient; $H_w$ is the width of throat. | |
| Comport (2009), Comport and Thorton, (2012)<br>Colorado, US | Presented hydraulic efficiency analysis of depressed curb inlets. | $$L_r = 0.493\, Q_a^{0.62}\, S_L^{-0.021} \left(\frac{1}{n\, S_e}\right)^{0.49}$$ | Setup size: 19.2m x 5.5m<br>Scale: 1:3<br>$S_L$: 0.5-4% $S_T$: 1-2%<br>Flow depth: 0.1 - 0.15m<br>n: 0.015 |
| Uyumaz (1994; 2002),<br>Istanbul, Turkey | Developed a new hydraulic design procedure for curb inlets based on experimental data. | $$E = A\left(\frac{L}{FT}\right)^3 + B\left(\frac{L}{FT}\right)^2 + C\frac{L}{FT}$$<br>A, B, and C are coefficients; F is Froude number at the beginning of the curb opening inlet.<br>Graphic of E versus. $\frac{L}{FT}$ | Scale: 1: 4<br>$S_L$: 0-6%<br>$S_T$: 2-6%<br>$S_g$: 4-8% |

| | | | |
|---|---|---|---|
| Brown *et al.* (2009). HEC-22. | FHWA's guidelines and recommended design procedures for the drainage of highway pavement. | Undepressed:<br>$$L_T = 0.817\, Q_g^{0.42}\, S_L^{0.3} \left(\frac{1}{n\, S_x}\right)^{0.6}$$<br>$$E_{ci} = 1 - \left(1 - \frac{L_{ci}}{L_T}\right)^{1.8}$$<br>$$L_T = K_u\, Q_g^{0.42}\, S_L^{0.3} \left(\frac{1}{n\, S_e}\right)^{0.6}$$<br>$$S_e = S_x + S_w' E_0$$<br>Depressed:<br>$$E = \frac{1}{\left\{1 + \frac{S_w \frac{1}{S_x}}{\left(1 + \frac{S_w \frac{1}{S_x}}{\frac{T}{w} - 1}\right)^{2.67} - 1}\right\}}$$ | / |
| Spaliviero *et al.* (2000),<br>Florida, US | Determined efficiency for curb inlets through experiments. | $$E = 1 - 0.199 \frac{Q_t}{{y_n}^{1.5}\mathrm{L}}$$<br>100% efficiency is achieved under the condition:<br>$$1.53 \gg \frac{Q_t}{{y_n}^{1.5}\mathrm{L}}$$ | Setup size: 4.9x1.5<br>Scale: 1:1.28.<br>$S_L$: 1:200-1:15<br>$S_T$: 1:50-1:30<br>Flow: less than 150 L/s<br>n: 0.017 |
| Kranc *et al.* (1998, 2001)<br>Florida, US | Reported a performance analysis of several curb inlets. | $$Q_{int} = A + BQ_a + C{Q_a}^2$$<br>A, B, and C are coefficients. | Setup size:<br>Scale: 1:2<br>$S_L$: 0.8-8%<br>$S_T$: 2-6%<br>Flow: <283 L/ |

| | | | |
|---|---|---|---|
| McEnroe *et al.* (1999)<br>Kansas, US | Investigated the performance characteristics of KDOT'S stand curb inlets from hydraulic model tests and theoretical calculations. | Weir flow:<br>$Q = 1.075\left(L\left(\frac{d}{1000}\right)^{\frac{3}{2}} + \frac{125}{26}\left(\left(\frac{d}{1000}\right)^{\frac{5}{2}} - \left(\frac{d}{1000}\right)^{\frac{3}{2}}\right)\right)$<br>Orifice flow:<br>$Q = 0.823(0.101)(L - 0.3)\sqrt{19.62(d + 0.091)}$<br>Noted that coefficients are specific for inlets and experiment conditions. | Setup size:15m (length)<br>Scale: 1:4<br>$S_L$: 0.5-5 %<br>$S_T$: 1.6%, 3.1%<br>Flow: 10 – 250 L/s<br>n: 0.01 |
| Hammonds and Holley, 1995.<br>Texas, US | Presented the results of a research project to determine the hydraulic characteristics and developed design equations for depressed curb inlets | 100% efficiency:<br>$q_L = \frac{Q}{L_{e,r}} = 0.196y_n - 0.0023$<br>Less than 100% efficiency:<br>$E = \frac{\left(\frac{a}{y_n} + 1\right)^{\frac{5}{2}} - \left(\frac{a}{y_n} + 1 - \frac{L_e}{L_{e,r}}\right)^{\frac{5}{2}}}{\left(\frac{a}{y_n} + 1\right)^{\frac{5}{2}} - \left(\frac{a}{y_n}\right)^{\frac{5}{2}}}$ | Setup size: 19.5mx4.3m<br>Scale: 3:4<br>$S_L$: 0.4-6%<br>$S_T$: 2.08-4.17%<br>Flow: < 250L/s<br>n: 0.017 |
| Uyumaz, 1988&1992<br>Istanbul, Turkey | Developed a new hydraulic design procedure for curb inlets based on experimental data. | For efficiency less than 60%:<br>$E = A\left(\frac{L}{FT}\right)$<br>For efficiency larger than 60%:<br>$E = B\left(\frac{L}{FT}\right)^3 + C\left(\frac{L}{FT}\right)^2 + D\frac{L}{FT}$<br>A, B, C, and D are coefficients varying with roadway slopes. | Scale: 1:4<br>$S_L$: 0-6.0%<br>$S_T$: 2-6%<br>$S_g$: 4-8% |
| Holley *et al.* 1992<br>Texas, US | Hydraulic characteristics of recessed curb inlets for different flow conditions and curb inlet geometries and develop design information related. | For 100% efficiency:<br>$q_L = 0.118y^{1.5}$<br>For less than 100% efficiency:<br>$E = f(Fr, L_e)$ | Setup size: 19.5mx3.2m<br>Scale: 3:4<br>$S_L$: 0.4-6%<br>$S_T$: 2.08-4.17%<br>Flow: < 250L/s |

| | | | |
|---|---|---|---|
| | | | n: 0.017 |
| Soares. 1991<br>South Carolina, US | Studied the effects of altering a curb inlet's entrance and exit transitions with the hope of improving inlet efficiency. | / | / |
| Hotchkiss et al. 1991<br>Bohac 1991<br>Hotchkiss 1994<br>Macallan et al. 1996<br>Nebraska, US | Studies the effects of altering a curb inlet's entrance and exit transitions with the hope of improving inlet efficiency. | / | Setup size: 13.4mx3.66m<br>Scale: full<br>$S_L$: 3%<br>$S_T$: 2%<br>Flow: 14.2-141.6 L/s |
| Johnson *et al.* (1984)<br>(HEC-12)<br>US | Guidelines and recommended design procedures for the highway inlets | Undepressed<br>For 100% efficiency:<br>$L_T = 0.82\ Q_g^{0.42}\ S_L^{0.3} \left(\frac{1}{n\ S_x}\right)^{0.6}$ (Empirical)<br>For < 100% efficiency:<br>$\mathrm{E} = 1 - \left(1 - \frac{L_{ci}}{L_T}\right)^{1.8}$<br>Depressed<br>For 100% efficiency:<br>$L_T = 0.82\ Q_g^{0.42}\ S_L^{0.3} \left(\frac{1}{n\ S_e}\right)^{0.6}$ (Empirical)<br>$S_e = S_x\ (1 - E_0) + \frac{a}{\mathrm{W}} E_0$<br>For < 100% efficiency:<br>$\frac{\mathrm{N}}{\mathrm{A}}$ | / |

| | | | |
|---|---|---|---|
| Izzard (1977)<br>US | Reanalysed the data of Bauer et al. (1964) and developed another method. | $E = f\left(\frac{L}{T\ Fr_w}, S_T\right)$ | Data of Bauer et al. (1964). |
| Forbes (1976)<br>US | Presented an interesting numerical procedure to calculate the flow into both depressed and undepressed curb inlets. | Extensive charts and tables. | Compared with experiments of Zwamborn (1966) and Goldfinch's model tests. |
| Goldfinch (N/A)<br>Durban | Carried out a total of 155 tests for steep gradients on a one – sixth scale model. | / | Scale: 1:6<br>1.9-12.1 percent<br>2-3.33 percent<br>Flow: 24-111 L/s<br>n: 0.017 |
| Adam *et al.* (1974)<br>Brandson (1971)<br>Manitoba, Canada | Investigated the hydraulic analysis of two types of sump curb inlets with depression and without depression. | Weir and orifice equations:<br>$Q_{int} = Cy^n$<br>Graphics of C versus. n are provided. | Setup size: 7.315mx2.438m<br>Scale: full<br>$S_L$: 0.5-6%<br>$S_T$: 2.1% & &4.2%<br>FLOW: N/A<br>n: 0.012 (concrete) |

| | | | |
|---|---|---|---|
| Zwamborn (1966)<br>US | Reported the results of comprehensive tests on both full and reduced scaled model. | Undepressed:<br>$y_0 = 0.43\, y_n^{0.83}$<br>$Q_{int} = 0.328 L_r\, y_n^{1.25}$<br>Less than 100% captured<br>$\mathrm{E} = 1 - \left(1 - \frac{L_{ci}}{L_T}\right)^{\frac{3}{2}}$<br>$\frac{Q}{L} = 1.67 H^{1.85}$ (in sag)<br>Depressed:<br>$\frac{Q}{L} = 0.0077 H^{1.85}$ (in sag) | Scale: 1:6 & full<br>$S_L$: 0.5-6%<br>$S_T$: 2% & 3.3% |
| Yong (1965)<br>New South Wales, Australia | To determine the efficiency of the curb inlet, and effect of with recess and with deflectors. | A series of curves. | 1:4 Setup size: 4.57mx0.91m<br>$S_L$: 1:32 &1:12<br>$S_T$: 0.5-15%<br>n: 0.011- 0.012 |
| Bauer *et al.* (1964)<br>Washington, D.C. US | Presented new design curves for depressed curb inlet based on experimental results. | Depressed:<br>$E = 1 - \left(1 - \frac{W}{T}\right)^{\frac{8}{3}}$<br>$\frac{L_i}{F_W T} = K \frac{W}{T} \sqrt{\frac{d_W}{a}}$<br>Depressed curb opening inlets in sump: | Scale: full & 1:4<br>$S_L$: 0.01&0.04; 0&0.002<br>$S_T$: 0.015&0.06; 0.016&0.058<br>n: 0.016 & 0.01 |

| | | | |
|---|---|---|---|
| | | $Q_{int} = 1.4(L + 1.8W)\left(d_{max} + \frac{W}{12}\right)^{1.85}$<br>$d_{max}$ is the maximum gutter water depth, $d_W$ is the water depth at distance $W$ from the curb face, $K$ is empirical coefficient of transverse acceleration, $F_W$ is Froude number at distance W from the curb face. | |
| Karaki *et al.* (1961)<br>Colorado, US | Presented the laboratory data for depressed curb inlets with uniform approach flow at supercritical velocities. | Graphics of:<br>$E$ *versus.* $\frac{L}{FT}$ | Setup size: 25.6mx3.66ft<br>Scale: full<br>$S_L$: 1%, 4%<br>$S_T$: 1.5%, 6%<br>n: 0.01&0.016 |
| Wasley (1960; 1961)<br>US | Applied a complex theoretical approach to describe the velocity filed in the vicinity of the inlet and conducted a numerical study of the hydrodynamic of curb inlets. | $L_r = \frac{TC}{\mathrm{g}}\left(1 + \frac{1}{\sqrt{2}}\right)$<br>$C = 0.552\sqrt{\frac{8gS_L}{f}}$<br>$f$ is Darcy's friction coefficient. | Setup size: 9.75mx1.83m<br>Scale: full<br>$S_L$; 0.5-5%<br>$S_T$: 1/96&1/12<br>Flow: 0.084-84.94 L/s |
| John Hopkins University (1956)<br>US | | $\frac{Q}{L} = kL(gy)^{0.5}$<br>For $\tan\theta$= 12, 24 and 45,<br>K = 0.23, 0.20 and respectively | Setup size: 6.1 x 0.9 m<br>q/Q: 0-0.7<br>$\frac{v}{(gy)^{0.5}}$ : 1 – 3 |
| Li *et al.* (1951);<br>Li (1954)<br>US | Investigated curb inlets capacity using free fall approach | Undepressed:<br>$L_r = V_L\sqrt{\frac{2y_n}{g}}$ | / |

| | | | |
|---|---|---|---|
| | | $$L_r = V_L \sqrt{\frac{2y_n tan\theta}{g\ cos\theta}}$$ $$Q_{int} = KL_r y_n \sqrt{gy_n}$$ $K$ = 0.35 (theoretical), 0.72(empirical) for $S_x$ = 8.33%, and 0.626 (empirical) for $S_x$ = 2.083% and 4.167%. $$E = \left[\left(\frac{L}{L_r}\right)^2 - \left(\frac{L}{L_r}\right)^4\right]$$ Depressed: $$Q_{int} = (K + C)L_r \mathrm{y} \sqrt{g\mathrm{y}}$$ $$C = \frac{0.45}{1.12^M}$$ $$M = \frac{L\ {V_L}^2}{\mathrm{agytan\theta}}$$ | |
| Izzard (1949; 1950) Washington, D.C. US | Investigated hydraulic performance of curb inlets treating flow into the inlet opening as flow over a broad-crested weir. | Undepressed: $$Q_{int} = k\ L_r\ y_n^{\frac{3}{2}}\left[1 - \left(1 - \frac{L}{L_r}\right)^{\frac{5}{2}}\right]$$ $$L_r = 1.51\ Q_t^{0.44}\ S_L^{0.28}\left(\frac{1}{n\ S_x}\right)^{0.56}$$ $E = 1 - \left(1 - \frac{L}{L_r}\right)^{\frac{5}{2}}$ $k$ is a coefficient and $k$ = 0.679 (theoretical), 0.39 (empirical). Depressed $$Q_{int} = mL_r\ y_n^{\frac{3}{2}}(\left(\frac{a}{y_n} + 1\right)^{\frac{5}{2}} - (\frac{a}{y_n} + 1 - \frac{L}{L_r})^{\frac{5}{2}})$$ | Scale: 1:3&1:2 |

| | | | |
|---|---|---|---|
| | | $E = \frac{\left(\frac{a}{y_n}+1\right)^{\frac{5}{2}} - \left(\frac{a}{y_n}+1-\frac{L}{L_r}\right)^{\frac{5}{2}}}{\left(\frac{a}{y_n}+1\right)^{\frac{5}{2}} - \left(\frac{a}{y_n}\right)^{\frac{5}{2}}}$<br>$m$ is coefficient and $m$ = 0.679 (theoretical), 0.39 (empirical). | |
| U.S. Corps of Engineers (1949) | Reported tests on curb inlets installed on a cross section. | N/A | Scale: 1:2 |
| Guillou (1948)<br>US | Presented a general summary of plans to construct and operate hydraulic models for gutter and inlet flow. | N/A | N/A |
| Conner *et al.* (1945)<br>North Carolina, US | Design and capacity of curb inlets | / | / |

## 2.6 Combination inlets

Compared with grate inlets and curb opening inlets, there are fewer studies on combination inlets despite extensive use of combination inlets on streets. Investigations have demonstrated that the interception capacity of combination inlets would be affected by grate type and position, sump condition, water ponding depth above the inlet and clogging condition (Li et al., 1954; Black 1967; Adam et al., 1974; Brown et al., 2009; Guo et al., 2009).

Li et al. (1954) experimentally studied the effects of grate type and position (relative to curb opening) on the efficiency of depressed combination inlets. It was found that using a more efficient grate was a better way to increase efficiency than putting the grate upstream or downstream of the curb opening. The combination inlet without transverse bars is the most efficient compared with that with transverse bars, and placing the grates with transverse bars either upstream or downstream of the curb opening would increase intercepted flow. When the grate was downstream of the curb opening, some of the water-carried debris will not reach the grate; and if debris forms a dam, the capacity of the curb-opening inlet will be increased due to the backing up of water.

Bock et al. (1956) developed a simplified method to determine the capacities of single and multiple combination inlets. They used two assumptions: the velocity is uniform throughout the cross-section of the gutter flow, and there is no carry-over flow across the grate in a single inlet or across the downstream grate in a multiple inlet. A series of flow diagrams based on the simplified method were developed both for depressed and undepressed combination inlets. Black (1967) tested 5 types of combination inlets and determined the efficiency curve as a function of approaching flow rate and longitudinal and transverse slopes of roadways.

The capacity of a combination inlet in sump is dependent upon the depth of ponding above the inlet as well as clogging conditions (USWDCM, 2001). Adam et al. (1974) tested one type of

combination inlets under the road sump condition and showed that neither the gutter slope nor the cross slope of the roadway affected the amount of water passing through the inlet openings. They found that the curb opening behaved like a simple weir, up to the point where the water was just below the top of the curb opening, beyond which, the inlet appeared to impose orifice control on the flow. Brown et al. (2009) stated that the interception capacity of the combination inlet in sump is essentially equal to that of the grate inlet alone in weir flow condition, and in orifice flow condition, the capacity of the combination inlet is equal to the capacity of the grate plus the capacity of curb opening. However, Guo et al. (2009) found that the method of Brown et al. (2009) overestimates the capacity of combination inlets in sump, and concluded the inlets are dominated by the grate when water is shallow, and by the curb opening when water becomes deep. Guo et al. (2009; 2012) proposed a new method to calculate the interception capacity ($Q_p$) of combination inlets in sump:

$$Q_p = Q_g + Q_c - K\sqrt{Q_g Q_c} \tag{2.31}$$

where $Q_g$ is the interception for grate, $Q_c$ is the interception for curb opening, and $K$ is the reduction factor obtained from experiments. A higher value of $K$ implies that the higher influence between the grate and the curb opening.

In addition to theoretical analysis, Comport (2009) and Comport et al. (2012) developed an empirical equation for combination inlets to predict the interception efficiency:

$$E = N\ (V/\sqrt{g\frac{A}{T}})^a\ \ (\frac{LT}{A})^b(\frac{hT}{A})^c(S_C)^d(S_L)^e \tag{2.32}$$

where $a$, $b$, $c$, $d$, and $e$ are regression exponents and $N$ is coefficient of regression, all of which need to be determined based on experimental data, $A$ is cross-sectional flow area, $L_{com}$ is length of inlet, and $T$ is the top width of street flow spread from the curb face.

### 2.7 Numerical studies on CB inlets

Three-dimensional (3D) numerical simulation is a great tool for investigating hydraulics of CB inlets, which is time and cost efficient in comparison to laboratory tests. Moreover, numerical simulation is able to provide results that are difficult to measure such as flow streamline and velocity field to further understand and improve the hydraulic performance of CB inlets. The commonly utilized software packages for modelling CB inlets are FLOW-3D, FLUENT and OpenFOAM. Current studies on CB inlets was summarized in **Table 2.5.**

Fang et al. (2010) used FLOW-3D to develop models for unsteady free-surface, shallow flow through curb-opening inlets. The predicted intercepted flow and inlet efficiency agreed well with laboratory measurements of Hammonds et al. (1995). The simulations were extended to smaller slopes of roadways for which laboratory tests were not conducted. The results were used to develop a linear regression equation between the inlet efficiency and water spread. Sezenoz (2014) conducted numerical modeling on the continuous transverse grate inlets using FLOW-3D, and calculated the inlet efficiency as a function of approaching flow rate and Froude numbers. The results of efficiencies of the continuous transverse grate inlets were compared with the experiments of Sipahi (2006) and Gómez and Russo (2009). It was found that the numerical results were similar to the experimental results of Sipahi (2006), but showed smaller efficiencies compared to experimental results of Gómez and Rosso (2009). Sezenoz (2014) stated that this difference is due to the bypass flow in the experiments of Gómez and Russo (2009). Kemper et al. (2016) used FLOW-3D to investigate grate inlet capacity with partially clogged grate openings. The numerical

model was validated against the physical model test results of Kemper et al. (2016) with errors of less than 10% and 15% for the water depth and velocity upstream of the inlet, respectively.

Gómez et al. (2016) reproduced the experimental results of Gómez et al. (2011) using FLOW-3D and showed that the water depth upper the grate inlet and total flow captured had mean absolute relative errors of 10% and 4%, respectively. Moreover, they reported the frontal interception was the main mechanism for flow capture, representing 60-80% of the total volume of flow captured. Kemper et al. (2018) simulated a grate inlet with supercritical approaching flow using FLOW-3D. An analytical approach and physical model tests were used to calibrate the numerical model. An empirical approach was also developed to estimate the discharge through different part of the grate inlet.

Begum et al. (2011) performed a 3D numerical study of the hydraulic capacity through a combination inlet using FLUENT, aiming to predict the efficiency of the combination inlet as a function of flow rate. And the numerical modelling results were in good agreement with the experimental data. Galambos (2012) used OpenFOAM to model the linkage between the road surface and below ground drainage systems and various grate inlets were tested. The numerical simulation was validated with the experiments conducted by Sabtu (2012) regarding the water depth on the road surface and grate inlet efficiency. Galambos' work also helped understand the effect of various inlet geometric and road alignment on inlet capacity. Lopes et al. (2016) built one numerical model using the solver interFOAM within the OpenFOAM packages to reproduce the efficiency of a continuous transverse grate inlet, and the inlet efficiency attained from the numerical model is calibrated against experimental data.

**Table 2.5** Summary on CFD numerical studies on CB inlets hydraulics

| Reference | Inlet type | Data for model verification | Model setup |
|---|---|---|---|
| Ampoman et al. 2021 | Curb opening inlet | Ampoman et al. 2021 | Software: FLUENT<br>Mesh size: 0.01-0.04m<br>Turbulence model: Standard k-ε |
| Shevade et al. 2020 | Curb opening inlet | Field survey data in Shevade et al. 2020 | Software: Flow-3D<br>Turbulence model: RNG |
| Kemper *et al.* 2018 | Grate inlet | Kemper et al. 2018 | Software: FLOW-3D<br>Mesh size: 1.5-6mm<br>Roughness: 1.5mm<br>Turbulence model: RNG k-ε |
| Lopes *et al.* 2016 | Transverse grate inlet | Gómez et al. 2009 | Software: OpenFOAM<br>Mesh size: 1-3mm |
| Gómez *et al.* 2016 | Grate inlet | Gómez et al. 2011 | Software: FLOW-3D<br>Mesh size: 10-20mm<br>Roughness: 0.9&0.5mm for channel and grate<br>Turbulence model: RNG |
| Kemper *et al.* 2016 | Grate inlet | Kemper et al. 2016;<br>Kemper et al. 2019 | Software: FLOW-3D<br>Mesh size 3-4mm near the bars; 3-12mm in the approach channel;<br>Turbulence model: RNG k-ε<br>Roughness: 1.5 &0.3mm for the channel and grate, respectively. |
| Martins *et al.* 2014 | Grate inlet | Martins et al. 2014 | Software: OpenFOAM |
| Sezenoz 2014 | Transverse grate inlet | Sipahi 2006;<br>Gómez et al. 2009 | Software: FLOW-3D<br>Mesh size:10-20mm |
| Galambos 2012 | Grate inlet | Sabtu 2012 | Software: OpenFOAM<br>Mesh size: 2-70mm<br>Turbulence model: K-ω |

| | | | |
|---|---|---|---|
| Fang *et al.* 2010 | Curb opening inlet | Hammonds & Holley, 1995 | Software: FLOW-3D<br>Mesh size:15-76mm<br>Turbulence model: RNG<br>Roughness: 7.6mm |
| Begum *et al.* 2010 | Grate inlet; curb opening inlet | Begum et al. 2010 | Software: FLUENT<br>Mesh size: 13mm<br>Turbulence model: K-ε |

## 2.8 Performance of CB inlets in extreme weathers

Hailstorm is one of severe extreme weathers, often accompanied with storm events. The hailstone could severely clog road gutter and CB inlets, resulting in severe floods and even losses of life and property. Severe urban floods caused by hailstorms have been reported in many places in the world in the past few years, including Alberta in Canada, Colorado in US, and Madrid in Spain. Currently, there is no investigation on the mechanism of flooding due to CB clogging caused by hail. There is a need to specifically study the clogging effects of hail, accompanied with debris such as leaves, to ensure the proper operation of urban drainage systems and reduce losses caused by this weather extreme.

During the last 60-70 years, urban drainage research mainly has been focusing on summer (temperate and warm) conditions. There are few research attempts for cold climates. In cold climates, low temperature and snowfall would affect the operation of drainage systems through changing the hydrologic cycle and urban runoff. Seepage into soil would be reduced due to frozen ground surface, frost penetration into the ground, and the existence of snow on ground. Urban runoff would be dependent on rain on snow, natural and man-made snow redistribution (Thorofsson, 2001). It is obvious that hydraulic performance of CB inlets would be affected or impaired due to the blockage of ice and snow (Bengtsson et al., 1980), and surface ponding or flooding would occur on roadways, affecting pedestrians and vehicles. Once temperature drops below zero, surface flow would freeze, and CB inlets would be clogged more severely. Often in cold regions especially in early spring with rain-on-snow, the melt snow and ice would result in large runoff and bring challenge for CB inlet interception. So far, there has been no study on the hydraulic performance of CB inlets under cold climates.

## 2.9 Summary and recommendations

This study provides a comprehensive review on CB inlet hydraulics. The types of CB inlets were first generalized; then the experimental investigations on the three primary CB inlets (grate inlets, curb opening inlets and combination inlets) were reviewed; afterwards, numerical studies using CFD packages were summarized; and finally the performance of CB inlets in extreme weathers was discussed. Based on this review, research gaps are summarized in Table 2.6.

Despite of different experimental studies on CB inlet hydraulics, a full assessment on existing studies is still lacking. For CB grate inlets, most of current equations for capacity and efficiency are empirical, and a few adopted the modified theoretical formulas of weir and orifice flow. The experimental scales, flow conditions, flume slopes and sizes were quite different for different research campaigns. Particularly, early investigations adopted small-sized flumes or reduced-scale tests. As a result, comparisons among the existing results or methods should be cautious. Currently, the limited studies on clogging effect of grate inlets were all based on representative clogging patterns, and future research should investigate the mechanism of the clogging and the clogging effect due to different clogging materials, and clogging with various conditions of surface flow.

Regarding curb opening inlets, most studies were theoretical analysis with simplifications and assumptions, and the results were then calibrated with experimental data. The rest of existing studies proposed empirical equations or used the formulas of weir and orifice flow, adjusted based on experiments. More mechanism studies on curb opening inlets are in need considering various factors, including inlet throat geometry, curb opening geometry, and clogging due to large debris. Current studies of combination inlets evaluated the interception capacities of the two parts: grate and curb opening. To better understand combination inlets, more studies are required, including under the effect of clogging effect.

Various experimental and numerical studies have been conducted to understand the hydraulics of CB inlets. However, laboratory studies condition can be limited, and specific conditions such as large runoff and cold climate can not be investigated. Moreover, laboratory studies usually only consider single CB inlet, ignoring the influences of the up- or downstream CB inlets, and the impacts of vehicles and buildings. More field experiments are needed to improve the understanding of CB inlets under real conditions.

Real or simulated rainfall are needed both for physical experiments and numerical simulations. The flow captured by CB inlets was a continuous process and approaching flow rate might change with time. Most of previous studies adopted constant, specific approaching flow rates for evaluating CB inlet hydraulic performance. To evaluate hydraulic performance of CB inlets during rainfall events is greatly need. For example, it was necessary to assess CB inlets hydraulics under both small and large rainfall events.

Extreme weather can be more common in future in the context of climate change, but few studies consider it. For instance, hailstorm is generally accompanied with large rainfall, and the clogging on grate inlets due to mixture of hail balls, debris, leaves should be assessed. Hydraulic performance of CB inlets during cold climates should be also paid more attention to. In cold regions, blockage of inlets by ice could be serious during cycle of melting and refreezing especially in early spring, causing ponding or flooding on roadway surface, which needs to be investigated. Future studies are needed under flooding conditions.

**Table 2.6** Future research directions recommended for CB inelts

| Recommended research | Objectives |
|---|---|
| Clogging effect studies | • To investigate the clogging progress during storm events;<br>• To predict clogging effect of grate inlets due to different materials or with various surface flow and underground drainage conditions. |
| Extreme weathers | • To study discharge of CB inlets during flashing flooding;<br>• To study the hydraulics of inlets during small rainfall.<br>• To study CB inlets hydraulics with ice and snow in cold regions.<br>• To figure out the performance of inlets during hailstorm events |
| In site (field) experiments | • To collect more field data to figure out the real performance of inlets during rainfall or in other extreme weather; |
| Grate inlets | • To improve designs of grate inlets considering skipping mitigation under large street longitudinal slope; |
| Curb opening inlets | • To determine the influence of clogging, inlet throat geometry, and curb opening geometry on hydraulics of curb opening inlets. |
| Combination inlets | • To conduct more tests on the interaction between grate part and curb opening part;<br>• To assess the hydraulics of combination inlets with the grate part clogged. |

## Chapter 3 Numerical study on the clogging effects to CB grate inlet

### 3.1 Introduction

There have been numerous studies on the capacity and/or efficiency of the three types of CB inlets, with the majority used laboratory experiments (e.g., Cassidy, 1966; Brandson, 1970; Uyumaz, 1992; Mustaffa et al., 2006; Gómez et al., 2011; Kemper et al., 2019) and only a few using computational fluid dynamics (CFD) models, e.g., FLOW-3D, FLUENT, and OpenFOAM (Fang et al., 2010; Galambos, 2012; Kemper et al., 2018). Moreover, these studies examined CB inlets in clean (non-clogging) condition. In **Chapter 2**, numerical studies on CB grate inlets was comprehensively reviewed, and therefore it will not be repeated here.

It is common to see clogging on CB grating inlets caused by leaves, debris, and other objects, which lowers the inlet capacity and efficiency. The following equation is commonly used to represent the clogging effect of a grate inlet on its capacity:

$$Q_{int,cf} = (1 - c_0)\, Q_{int} \tag{3.1}$$

where $Q_{int,cf}$ is the intercepted flow considering clogging of the grate, $Q_{int}$ is the intercepted flow with no clogging, and $c_0$ is the clogging factor. In engineering practice, a value of 0.5 for the clogging factor is commonly adopted by many local authorities (Clark Count Regional Flood District, 1990; Colorado Department of Transportation, 2000; Urban Drainage and Flood Control District, 2001). However, the clogging factor of 0.5 is not that realistic but meant to be conservative (Gómez et al. 2013).

In fact, the clogging factor can vary substantially. Despotovic et al. (2005) covered half of the grate inlet in their experiments and found significant decrease in the inlet efficiency regardless of the clogging patterns. The maximum clogging factor value determined by the result is 0.62. Gómez

et al. (2013, 2018) classified the clogging patterns for the most widely used grate inlets in Barcelona, Spain, experimentally tested them at a full scale, and discovered that the clogging factor could range from 0.23 to 0.70. Abedin et al. (2019) numerically investigated flood spatiotemporal variation in two urban micro-watersheds using GIS, and the calibrated clogging factors were 0.83 and 0.14, respectively. Veerappan et al. (2016) investigated three types of grate inlets in Singapore through simulating the clogging portion of 50%, 100%, and > 100% (clogging over the horizontal plane of the grate inlet). For 50% and 100% clogging levels, results showed that hydraulic efficiency varied slightly with different roadway longitudinal slope, roadway transverse slope, rain intensity, and types of inlets when compared to clean conditions. The maximum clogging factor for clogging over the horizontal plane of the grate inlet can be around 0.7. Spaliviero et al. (2000) introduced a non-dimensional maintenance factor, *m*, in addition to the clogging factor, to account for the effect of a partial blockage, and recommended clogging factor values ranging from 0 to 0.3.

A potential law had been reported by Russo (2010) and Gómez et al. (2011) when they investigated grate inlets hydraulics in clean condition through experiments:

$$E = A(\frac{Q_a}{d})^{-B} \tag{3.2}$$

where *d* is water depth upper grate inlet, and *A* and *B* are two parameters that can be obtained from the experimental data. Gómez et al. (2013) found that *E* of clean and clogged grate inlets can be all derived using this potential law when they tested *E* of inlets with clogging.

There is currently no CFD research on the clogging effects of CB inlets. CFD models can circumvent the limitations of laboratory space and experimental settings (e.g., flow and slopes), hence reducing expenses and saving time. CFD models can also provide other characteristics, including as streamlines, velocity field, and vortices, to better comprehend the hydraulics of CB

inlet. Using ANSYS FLUENT, this study created a numerical model to explore the clogging consequences of various clogging patterns on a CB grate inlet. After model calibration, additional clogging patterns in terms of inlet capacity, efficiency, and clogging factor will be investigated. Then, the effects of real clogging digitized from photographs were compared to conceptually generalized clogging. In addition, the situation of deep water on the road was investigated for serious flooding on the road. Finally, a 0.02 m vertical depression of the CB grate was simulated to study the influence of vertical depression on the hydraulics of the grate inlet.

### 3.2 The CFD model

#### 3.2.1 Governing equations

The software of FLUENT 2021 was used in this study to build the CFD model on a CB grate inlet under different conditions. The Reynolds-Averaged Navier-Stokes (RANS) approximation was used because it was documented to perform well for hydrodynamics of engineering problems (Garcia et al. 2004). The RANS equations for the mass and momentum conservation of incompressible viscous flows are described as follows:

$$\frac{\partial u_i}{\partial x_i} = 0 \tag{3.3}$$

$$\frac{\partial U_i}{\partial t} + u_j \frac{\partial U_i}{\partial x_j} = -\frac{1}{\rho}\frac{\partial p}{\partial x_i} + \frac{\partial}{\partial x_j}\left(v\frac{\partial U_i}{\partial x_j} - \overline{u_i' u_j'}\right) \tag{3.4}$$

where $x_i$ is the Cartesian space coordinate with $i$ =1, 2, 3; $u_i$ is the mean velocity component in the $i$ direction; $t$ is the time; $\rho$ is the water density; $p$ is the pressure; $v$ is the kinematic viscosity of water; and $\overline{u_i' u_j'}$ denotes the Reynolds stress tensor.

In this study, two turbulence models, the standard $k$-$\varepsilon$ model and the Renormalisation Group (RNG) $k$-$\varepsilon$ model, were compared for modeling hydraulics of CB grate inlet. The standard $k$-$\varepsilon$ model, the

most commonly used turbulence model, is stable and delivers reasonably realistic results, although it may produce a high turbulent viscosity and does not capture the proper behavior of turbulent boundary layers up to separation (Bates et al., 2005; European Research Community On Flow, Turbulence And Combustion, 2000). The RNG *k*- $\varepsilon$ model can simulate complex flow phenomena effectively without requiring major modification of constants or functions (Yakhot et al. 1992; Nektarios et al. 2012). The transport equations of the turbulent kinetic energy *k* and the turbulent dissipation rate $\varepsilon$ for the RNG *k*- $\varepsilon$ model are shown as:

$$\frac{\partial}{\partial t}(\rho k) + \frac{\partial}{\partial x_i}(\rho k u_i) = \frac{\partial}{\partial x_j}\left(a_k \mu_{eff} \frac{\partial k}{\partial x_j}\right) + G_k + G_b - \rho\epsilon - Y_M + S_k \qquad (3.5)$$

$$\frac{\partial}{\partial t}(\rho\varepsilon) + \frac{\partial}{\partial x_i}(\rho\varepsilon u_i) = \frac{\partial}{\partial x_j}\left(a_\varepsilon \mu_{eff} \frac{\partial \varepsilon}{\partial x_j}\right) + C_{1\varepsilon}\frac{\varepsilon}{k}(G_k + C_{3\epsilon}G_b) - C_{2\epsilon}\rho\frac{\epsilon^2}{k} - R_\varepsilon + S_\varepsilon \qquad (3.6)$$

In these equations, $G_k$ represents the generation of turbulence kinetic energy due to mean velocity gradients, $G_b$ is the generation of turbulence kinetic energy due to buoyancy, $Y_M$ represents the contribution of the fluctuating dilatation in compressible turbulence to the overall dissipation rate, the quantities $a_k$ and $a_\varepsilon$ are the inverse effective Prandtl number for *k* and $\varepsilon$, respectively, $R_\varepsilon$ And $S_\varepsilon$ are the user-defined source terms, $\mu_{eff}$ is the effective viscosity, and $C_{1\varepsilon}$, $C_{2\varepsilon}$ and $C_{3\varepsilon}$ are the model constants.

The volume of fluid (VOF) technique proposed by Hirt and Nichols (1981) was used in this study to capture the interface between the water and air phases, i.e., the free water surface. The governing equation is:

$$\frac{\partial \alpha}{\partial t} + \frac{\partial \alpha u_i}{\partial x_i} = 0 \tag{3.7}$$

where $\alpha$ is the volume fraction of water in a cell. $\alpha = 1$ means the cell is full of water, $\alpha = 0$ means it is full of air, and $0 < \alpha < 1$ denotes a water interface in the cell (Ubbink, 1997; Koutsourakis et al., 2019).

### 3.2.2 Computation domain and grid

To simulate the hydraulics through a CB grate inlet, Gómez et al. (2013)'s physical experiment was used for model calibration, and therefore the model was constructed in the same manner as the actual configuration used in their study. Gómez et al. (2013) did a general survey of a catchment and three main clogging patterns were identified (clogging pattern 1-3 in Fig. 3.1). Then they calculated efficiency loss for each clogging pattern through experimental tests. Tests were made in a 1:1 scale model of a roadway measuring 5.5 m long and 3 m wide. Gómez et al. (2013) simulated grate inlets with a transversal slope up to 4% and longitudinal slope up to 10%. Pumps supply the flow up to a tank placed approximately 15 m above the platform. The flow circulates through the model, first through a tank located up stream of the platform. This tank dissipates the flow energy and provides a horizontal profile to the surface water level. The discharge intercepted by the inlet is conveyed to a V-notch triangular weir and the flow measurement is carried out through a limnimeter with an accuracy of 0.1 mm. Flow depth measurements on the platform are obtained directly with a thin graduated invar scale.

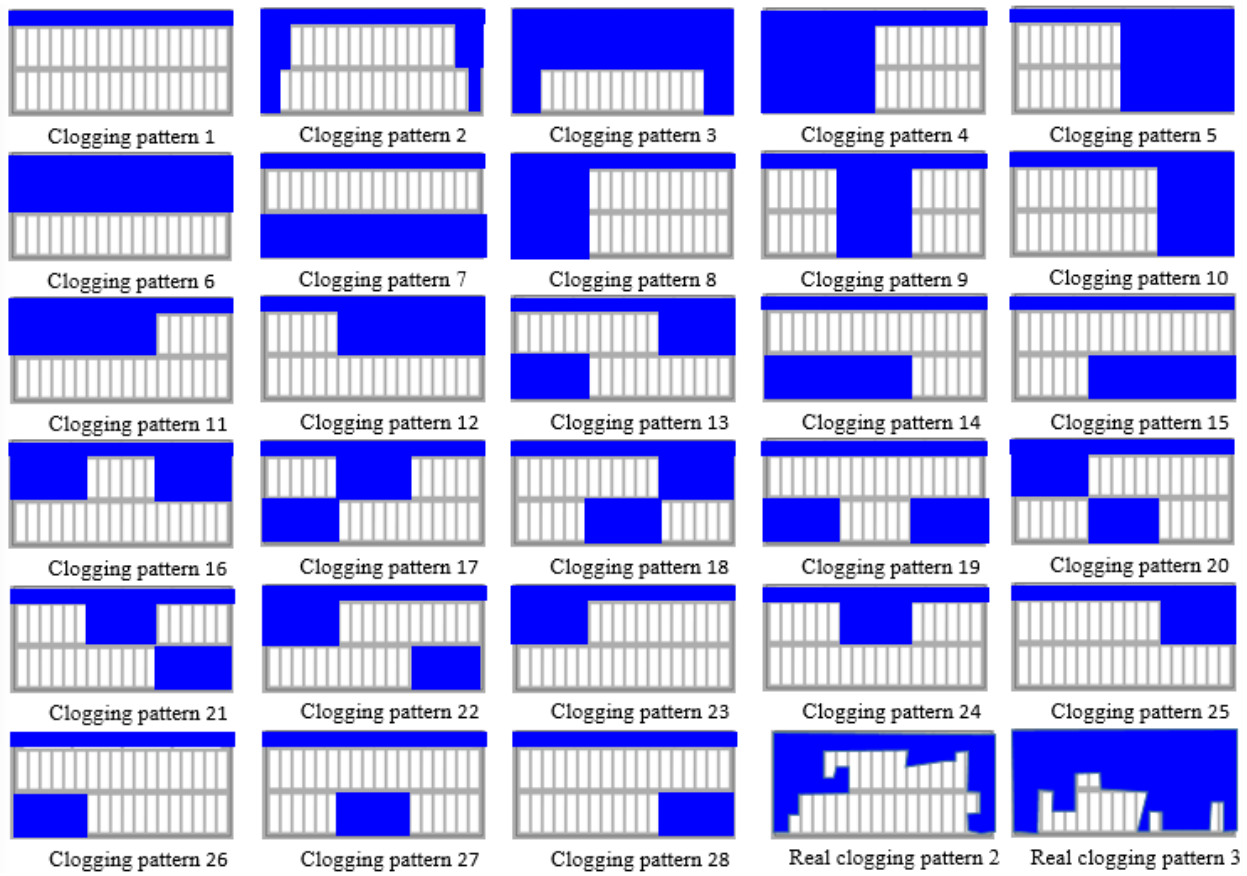


Figure 3.1 Sketch of clogging patterns. The curb side of the grate is on the top side, and the approaching flow is from left to right.

Fig. 3.2 depicts the computation domain. At the top of the flume was a supply water tank that was 0.5 m long, 3 m wide, and 0.8 m high. The flume was 5.5 m long and 3 m wide. The flume's two side walls were made to be 0.4 m high to prevent runoff from exiting the side walls. The grate inlet was positioned 3 m downstream of the supply water tank and along one side wall, which is 78 cm long and 34 cm wide as illustrated in Fig. 3.2. The surfaces of the grate inlet were at the same elevation of the flume. There was a bottomless tank constructed beneath the grate inlet to capture the flow that entered the inlet.

The precision and speed of the computations are significantly influenced by the grid's quality. Grid sizes did not exceed 70 mm when they are farther from the grate entrance. Three grid sizes of 6

mm (fine), 9 mm (medium), and 12 mm (coarse) at the grate inlet were tested for the CB clean condition to assess the impact of grid independence on the numerical results, resulting 0.89 million, 1.35 million, and 2.3 million cells, respectively.

The governing equations for mass, momentum, and turbulence model were numerically solved in FLUENT (ANSYS Inc, 2021). The computation schemes applied the second-order upwind discretization for momentum, pressure, turbulent kinetic energy, and turbulent dissipation rate, which is commonly used (Gagan et al., 2014; Zhu et al., 2014; ANSYS Inc, 2021). The time step has a 0.05s specification for balancing time consuming and calculation accuracy.

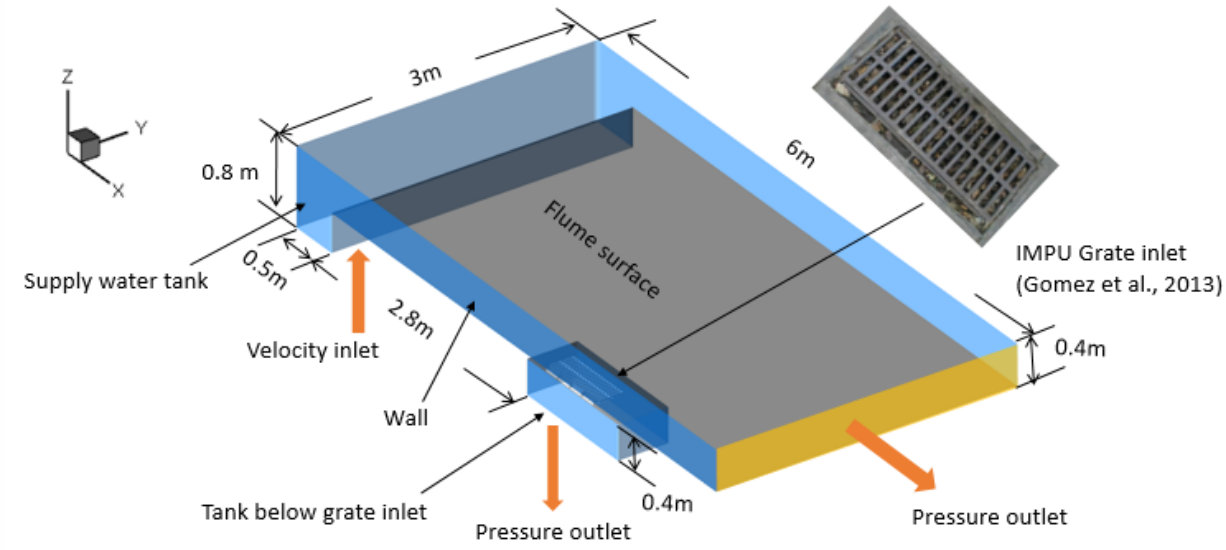


Figure 3.2 Sketch of the numerical model and boundary conditions.

### 3.2.3 Initial and boundary conditions

Different boundary conditions were set for the inlet and outlet of the numerical model. Runoff was supplied through the supply water tank's bottom using the velocity inlet boundary (Fig. 3.2). The bottom of the tank beneath the grate inlet and the outlet of the flume both had pressure outlet boundaries. Gravity was divided into the x, y, and z axes to simulate the variation of the

longitudinal and transverse slopes of the road in order to simplify the model setup. Manning's roughness coefficient for flume surface adopted for simulation was 0.015 (asphalt). At the beginning of simulation, there was no water in the supply water tank and the tank beneath the grate inlet.

### 3.2.4 Model calibration scenarios and methodologies

Based on the physical experiment of Gómez et al. (2013), four scenarios were first modeled for model calibration, including the clean condition and the clogging patterns 1-3 as depicted in Fig. 3.1. Gómez et al. (2013) developed the testing protocol in their physical experiments as: discharges from 0-200 L/s, longitudinal slopes from 0-10% and transverse slopes from 0-4%. Considering accuracy and running time of modelling, two approaching flow rates: 25 and 200 L/s were employed in calibration, together with four slope combinations: 2%_2%, 0%_4%, 0%_0%, and 10%_0%. It should be noted that the slopes combinations utilized in this paper are denoted by the notation $S_x$_$S_T$.

In addition, additional scenarios were modeled to investigate the hydraulics of the grate inlet, including more clogging patterns (patterns 4-28), large water depth on roads during large storm events, vertical depression of the grate inlet (i.e., grate surface is lower than road surface), and outflow from the grate inlet to road surface due to surcharging of underground sewers (**Table 3.1**).

To evaluate the validity of the generalized clogging patterns defined by Gómez et al. 2013, two real clogging patterns 2 and 3 were created (Fig. 3.1) by digitizing from the real clogging photos (Fig. A4 in the appendix) and modeled in this study. Except for the four longitudinal voids (near the flume's left side), the rest of the clogging voids ratios were 16.6% for the generalized clogging pattern 2, 61.1% for the generalized clogging pattern 3, 23.6% for the real clogging pattern 2, and 76.4% for the real clogging pattern 3. Three road slope combinations of 2%_2%, 0%_4%, and

10%_0% were chosen, as well as five approaching flow rates of 25, 50, 100, 150, and 200 L/s, for the simulation.

The physical experiment of Gómez et al. (2013) summarized three of the most representative clogging patterns based on field observations. Actually, clogging patterns can be quite varied and arbitrary. As a result, additional clogging patterns, clogging patterns 4 to 28, were generated as illustrated in Fig. 3.1, and simulated, to better understand clogging consequences.

For all the new clogging patterns, the four longitudinal voids (near the left side the flume) of the grate inlet were also first clogged. In addition, different areas were covered to simulate clogging: if 50% of the rest voids were covered, the numerical series was named as series 50% clogged, including clogging patterns 4-7; if one-third of the rest voids were covered, the series was called 33% clogged, including clogging patterns 8-22; if the one-sixth of the rest voids were covered, it was called 17% clogged, including clogging patterns 23-28. Four approaching flow rates: 25, 50, 100 and 200 L/s were employed, together with three slope combinations: 2%_2%, 4%_2%, and 10% 2%.

For assessing grate inlet hydraulics with large water depths (during flooding), the scenario of large water depth was modeled. To produce a deep-water depth, the flume was numerically extended from 5.5 m to 9.27 m, leaving 5.0 m between the grate inlet and flume outlet. In addition, a 0.15 m high gate was numerically added at the flume end. These two modifications assume that the grate inlet can accommodate orifice flows. One slope combination, 0%_4%, and two approaching flow rates, 25 L/s and 200 L/s. The scenarios of large water depth were tested in this study for clean condition and generalised clogging pattern 1, 2, and 3. The orifice flow equation shown below can be used in this situation to analyze the grate inlet operation:

$$Q = C_{do} A_o \sqrt{2gh} \tag{3.8}$$

where $Q$ is the discharge, $A$ is the orifice cross section area, $h$ is the water depth measured upstream of the grate inlet, $g$ is the gravitational acceleration, and $C_{do}$ is the orifice discharge coefficient.

Grate inlet vertical depression may be caused by high traffic volumes, road shoulder erosion and settlement, aging processes, and the ensuing road layers. The effects of vertical depression on grate inlet efficiency have only been proven experimentally once (Wakif et al., 2019). In comparison to the non-depressed grate inlet, Wakif et al. (2019) found that a vertical depression of 0.02 m caused a 6–10% drop in efficiency. Additionally, no numerical analysis has been done to investigate how vertical depression affects grate inlet. Therefore, the scenario of grate inlet with a 0.02 m vertical depression was modeled (see Fig. 3.3). In this investigation, the surface of the grate surface elevation was lowered by 0.02 m below the flume bed. In order to analyze the combined impacts of vertical depression and clogging, the clean condition and clogging patterns 1, 2, and 3 were modeled under the conditions of four street slope combinations (2%_2 %, 10% _2%, 0% _0%, and 0%_4%) and two approaching flow rates (25 L/s and 200 L/s).

CB inlets allow drainage system runoff to be discharged to the ground surface. In this work, the outflow to both the wet and dry streets was numerically studied. For the wet street scenario, boundary condition for the bottom of the tank beneath the grate inlet was changed from previous pressure outlet to velocity inlet for outflow to a wet street; for the dry street scenario, the supply water tank's boundary condition was modified to pressure outlet, and the tank's boundary condition was changed to pressure outlet. These two adjustments are depicted in Appendix Fig. A6. First, the street transverse slope was kept constant at 2% for the simulation, while the longitudinal slope was varied between 0%, 2%, 4%, and 10%. Then the longitudinal slope was kept constant at 2%, while the transverse slope was varied between 0%, 1%, and 2%. For both the dry and wet streets,

the flow rate from the grate inlet to the flume surface was set at 10, 50, 100, and 200 L/s. The supply water tank runoff flow rate was set to 50 and 100 L/s for the wet plain, respectively. Fig. A7 in the appendix indicated the positions of nine water level measurement stations in order to precisely get the mean piezometric head above the grate inlet. The discharge coefficient of the grate inlet was calculated using Eq. 3.8. It should be noted that this scenario was tested only in clean condition, because there was much chance that the clogging would be cleaned by the outflow from the CB.

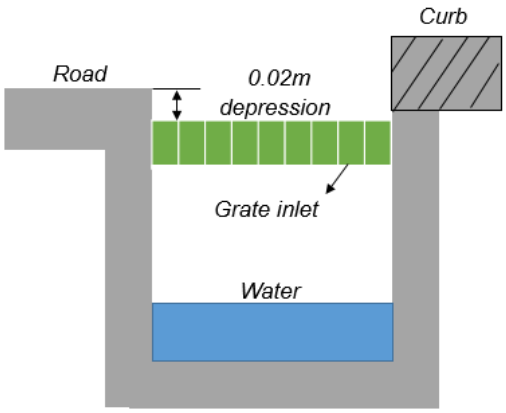


Figure 3.3 Sketch of the grate inlet with a 0.02 m vertical depression

As demonstrated in **Table 3.1**, additional testing circumstances were applied to investigate the hydraulics of the grate inlet in greater depth.

**Table 3.1** Summary of calibration and additional scenarios

| Scenarios | Contents |
|---|---|
| Calibration scenarios | • Clean condition<br>• Clogging pattern 1, 2, and 3. |
| Additional scenarios | • Real clogging pattern1 & 2.<br>• More clogging patterns (Clogging pattern 4 - 28)<br>• Large water depth<br>• Vertical depression<br>• Outflow from grate inlet |

### 3.3 Results and discussion

#### 3.3.1 Model calibration

Compared to the standard $k$-$\varepsilon$ model, the RNG $k$-$\varepsilon$ model was chosen as the turbulence model in this study, because it has better performance when compared with the experimental results as shown in Fig. A1 in the appendix. The result of grid independence is shown in Fig. A2 in the appendix, using the three different mesh sizes for modeling the grate inlet capacity and water depth. The medium grid size of 9 mm (i.e., 1.35 million cells) close to the grate entrance was selected for the subsequent computation considering the balance of numerical precision and computation speed. A view of the mesh around the grate inlet is shown in Fig. A3 in the appendix.

With the RNG $k$-$\varepsilon$ model and medium grid size, the simulation results were compared with the experimental data of Gómez et al. (2013) in Fig. 3.4 to assess the model performance. The comparison shows the numerical and experimental data are in good agreement in terms of data locations. There existed obvious power functions between $E$ and $Q_a/d$ for simulation results, which were in the same form as the Eq. 2 proposed by Gómez et al. (2013), and high coefficients of determination ($R^2$) were obtained, with the values ranging from 0.93 to 0.99. In terms of efficiency, $R^2$ between the simulated and the predicted using the set of equations of Gómez et al. (2013) were 0.93 for clean condition, 0.71 for clogging pattern 1, 0.70 for clogging pattern 2, and 0.76 for clogging pattern 3, and Root Mean Square Weighted Error (RMSE) were 0.05 for clean condition, 0.11 for clogging pattern 1, 0.11 for clogging pattern 2, and 0.07 for clogging pattern 3. The average absolute efficiency difference between the simulated and the predicted using the set of equations of Gómez et al. (2013) were 0.04 for clean condition, 0.08 for clogging pattern 1, 0.08 for clogging pattern 2, and 0.05 for clogging pattern 3. Based on the model calibration, the 3-D CFD model developed in this study is suitable for investigating the hydrodynamics of grate inlet.

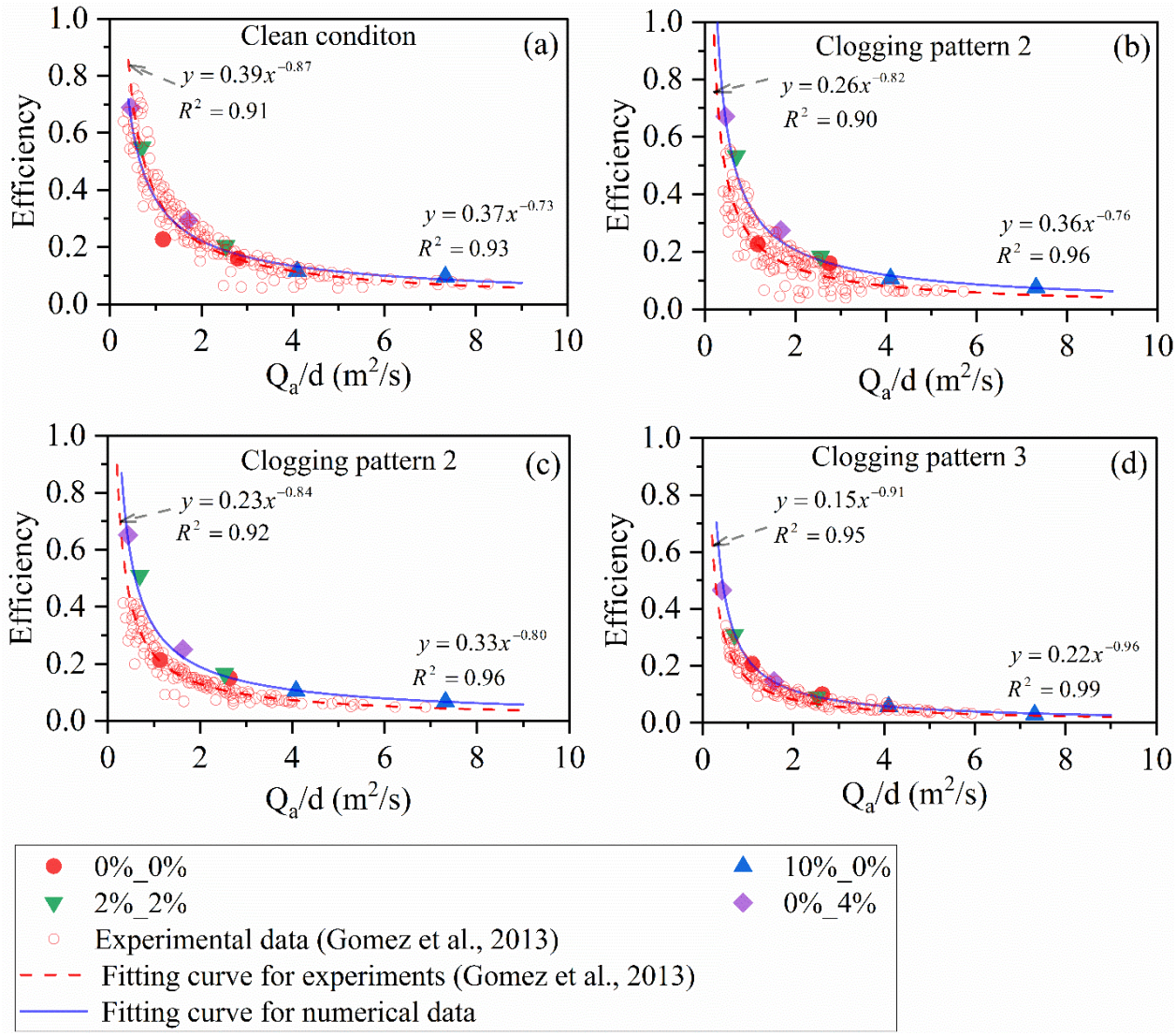


Figure 3.4 Comparison of the simulated results (filled dots) against experimental results (empty dots) of Gómez et al. (2013) for: (a) clean condition; (b-d) clogging pattern 1-3.

### 3.3.2 Impact of hydraulic parameters and clogging

The grate inlet intercepted flow rate is affected by both the approaching flow and road slopes (see Fig. 3.5). According to Fig. 3.5, the grate inlet intercepted flow rate would increase as the approaching flow rate increases. As the approaching flow rate increased from 25 L/s to 200 L/s, the grate inlet intercepted flow rate increased from the range of 5.67-17.18 L/s to the range of

32.17–59.12 L/s, from Fig. 3.5(a); increased from the range, 11.41-13.71 L/s to the range, 34.26-44.46 L/s, from Fig. 3.5(c). This is because as the approaching flow rate increased, more approaching flow will flow towards the inlet and be captured by the inlet. The inlet intercepted flow rate also increased with the road transverse slope as expected (see Fig. 3.5(a)), because the large transverse slope means larger portion of the approaching flow will be distributed towards the inlet. On the other hand, the longitudinal slope had a minimal impact on the inlet capacity (see Fig. 3.5(c)), for the range of 0% to 4%. Evidently, a 10% large longitudinal slope reduced the inlet capacity, which is attributed to the high flow velocity that make the flow "skip" the inlet in a quick manner, resulting less flow captured by the inlet.

Similarly, as shown in Fig. 3.5, the grate inlet efficiency is also affected by the approaching flow and road slopes. As the approaching flow increased, the inlet efficiency would decline because larger portion of the approaching flow will be uncaptured by the grate inlet even the grate inlet capacity increased. With the road slopes = 0%_0%, the grate inlet efficiency decreased from 0.23 to 0.16 (by 21.7% in percentage); with the road slopes =0%_4%, efficiency decreased from 0.69 to 0.29 (by 58.0% in percentage); with 10%_2%, changing from 0.46 to 0.17 (by 63.0% in percentage); with 0%_2%, changing from 0.55 to 0.20 (by 63.6% in percentage). Under the same approaching flow rate and longitudinal slope, the inlet efficiency would increase as the road transverse slope increased, e.g., from 0.23 to 0.69 (by 200% in percentage) as the approaching flow = 25 L/s, 0.16 to 0.29 (by 81.3% in percentage) as the approaching flow = 200 L/s. This can be explained by that the approaching flow would accumulate towards the grate inlet, and the existence of the side wall near the grate inlet would help accumulate more approaching flow. Under the same approaching flow rate and the road transverse slope, larger road longitudinal slope would reduce the inlet efficiency, but the impact was minor. For example, the inlet efficiency increased

from 0.46 to 0.55 (by 19.6% in percentage) for the approaching flow = 25 L/s, 0.17 to 0.22 (by 29.4% in percentage) for the approaching flow = 200 L/s. This is because the larger road longitudinal slope would increase the ability of the approaching flow 'fleeing' from the grate inlet. Therefore, it was clear that the road transverse slope and approaching flow had the larger impact on the grate inlet efficiency, when compared with the road longitudinal slope.

It was found that clogging could significantly reduce the grate inlet's intercepted flow rate and efficiency (seen in Fig. 3.6a&b and Table 3.2). Compared with the clean condition, the clogging pattern 1 decreased the inlet intercepted flow rate by 0.26-3.01 L/s (3.1%-9.3% in percentage), and decreased the inlet efficiency by 0.01 (3.2%-9.2% in percentage); the clogging pattern 2 decreased the intercepted flow rate by 0.53-5.57 L/s (5.2%-16.0% in percentage), and decreased the efficiency by 0.03 (6.9%-17.5% in percentage); the clogging pattern 3 decreased the intercepted flow rate by 3.39-19.49 L/s (34.1% -53.5% in percentage), and decreased the efficiency by 0.10-0.14 (34.3% -53.4% in percentage). This is because the smaller the grate opening is, less the approaching flow captured by the grate inlet. As the clogged grate opening increased, more portion of approaching flow would pass above the clogged grate opening, the less the possibility of approaching flow captured by the grate inlet.

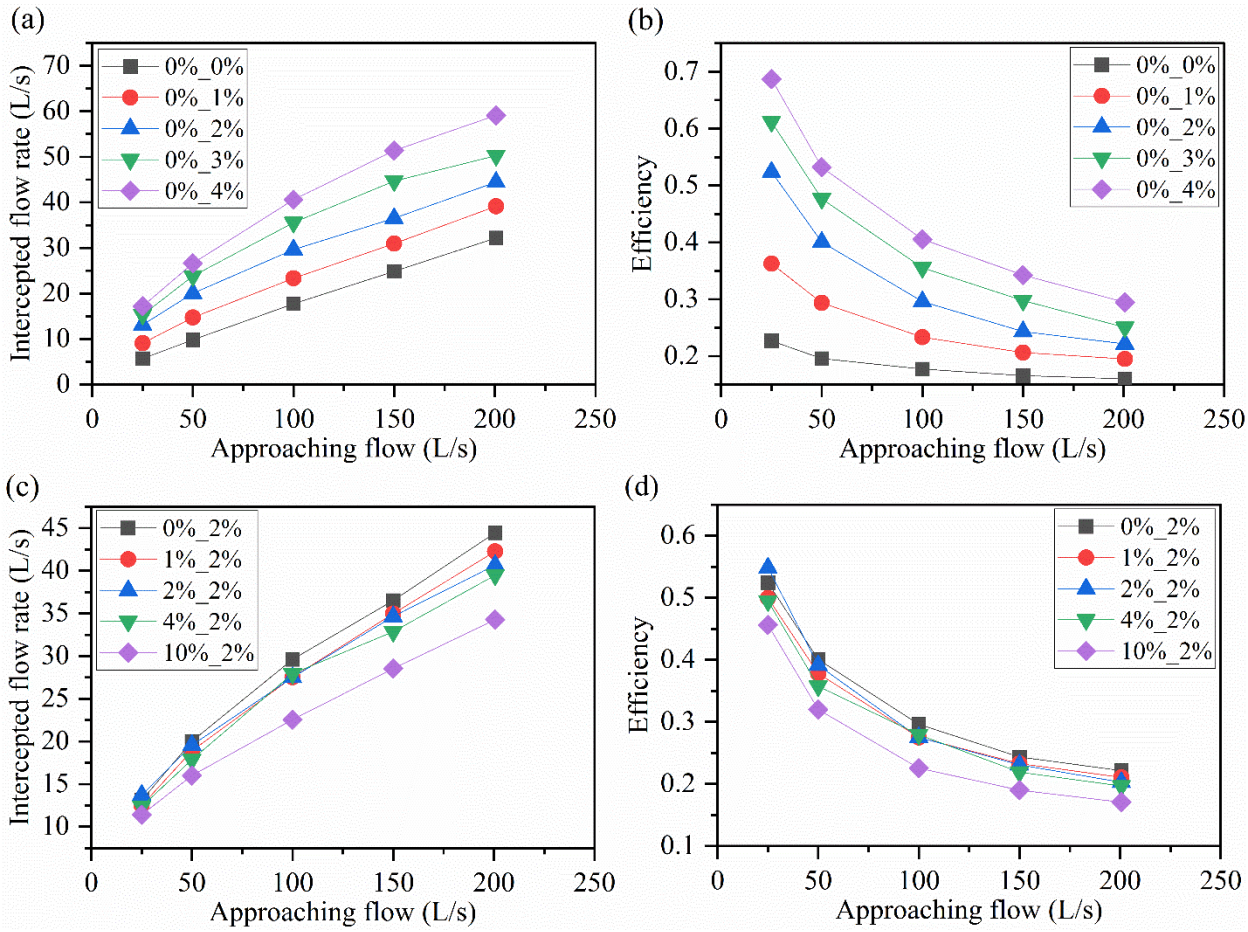


Figure 3.5 Variations of the CB grate inlet intercepted flow rate (left figures) and efficiency (right figures) with the approaching flow and street slopes, under clean condition. In Fig. 3.5 (a, b) the street transverse slope is changed from 0% to 4%, while the street longitudinal slope is maintained at 0%; in Fig. 3.5(c, d), the longitudinal slope is changed from 0% to 10%, while the transverse slope is maintained at 2%.

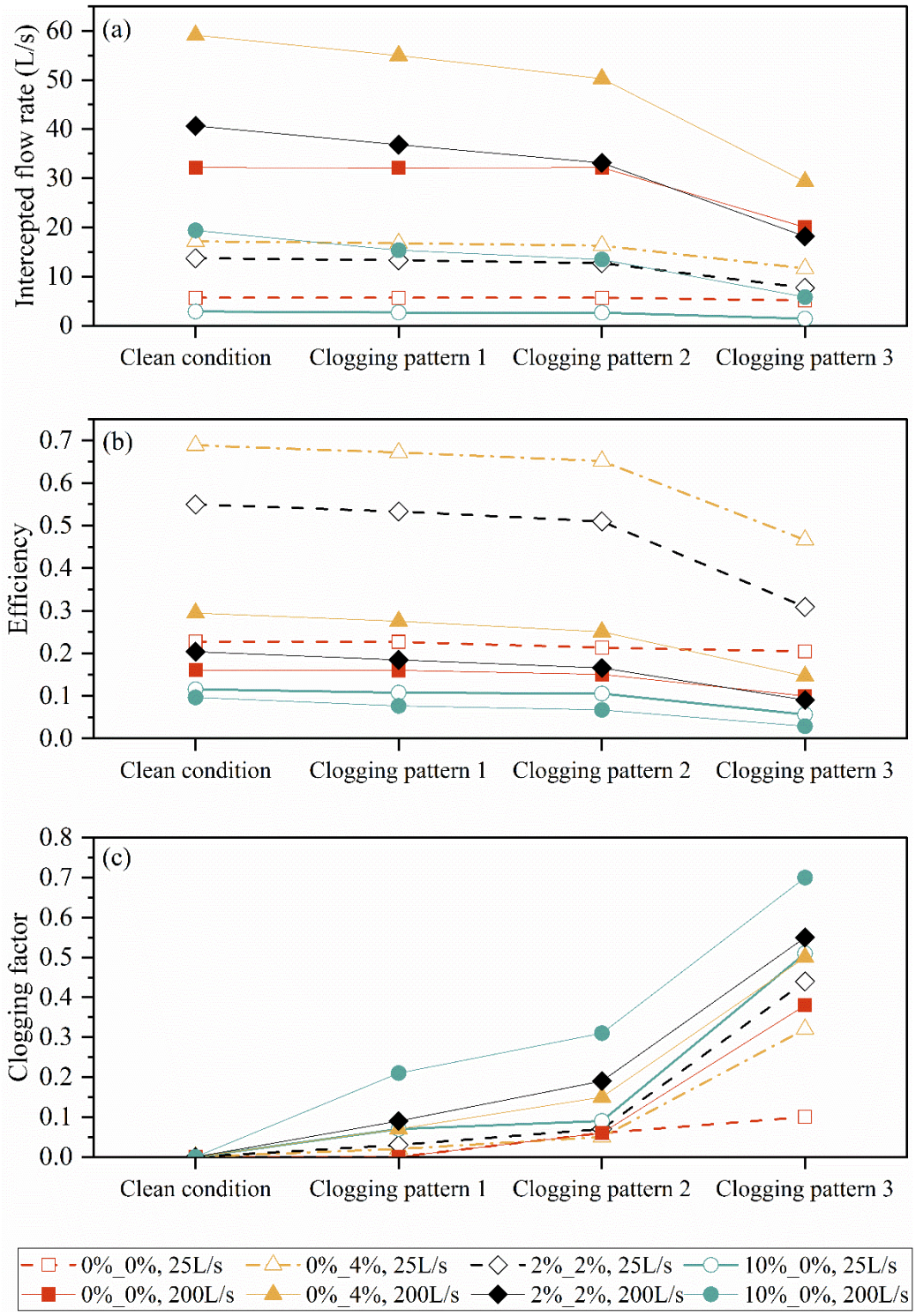


Figure 3.6 Variations of the CB inlet (a) intercepted flow rate, (b) efficiency and (c) clogging factor with the approaching flow, street transverse and longitudinal slopes, with three different clogging patterns.

**Table 3.2** The averaged difference of the grate inlet intercepted flow rate and efficiency between clean condition and each clogging pattern

| | The averaged difference of the grate inlet intercepted flow (L/s) | | The averaged difference of the grate inlet efficiency | |
|---|---|---|---|---|
| | 25 L/s | 200 L/s | 25 L/s | 200 L/s |
| Clogging pattern 1 | -0.26 (-3.1%) | -3.01 (-9.3%) | -0.01 (-3.2%) | -0.01 (-9.2%) |
| Clogging pattern 2 | -0.53 (-5.2%) | -5.57 (-16.0%) | -0.03 (-6.9%) | -0.03 (-17.5%) |
| Clogging pattern 3 | -3.39 (-34.1%) | -19.49 (-53.3%) | -0.14 (-34.3%) | -0.10 (-53.4%) |

### 3.3.3 Water fraction and velocity contours under clean conditions

To better examine the water inception mechanism by the grate inlet, the water fraction and velocity field near the inlet were examined in Fig. 3.7, where the inlet location is shown by a red dashed line. The horizontal plane selected to show the horizontal velocity contour (U_xy) is at 0.005 m above the flume bed.

The results show that both the approaching flow rate has an impact on the water fraction and velocity field. As the approaching flow rate increased, the water contour within the grate inlet indicated more approaching flow will enter the region of the grate inlet (see Fig. 3.7(1), (2), and (3)), especially the part of the grate inlet near the upstream and the part of the grate inlet away from the side wall. In addition to these, there the velocity field within the inlet expanded as the approaching flow rate increased. These are because the grate inlet intercepted more approaching

flow, and the parts mentioned above were the earliest portions of the inlet to capture approaching flow. As the approaching flow rate increased, the approaching flow will be able to arrive at the center part of the grate inlet.

The results also indicated that road slopes have an impact on the water fraction and velocity field. With a larger road transverse slope, water fraction within the inlet increased and the velocity towards the side wall near the inlet increased (see Fig. 3.7(a) and (b)). This is because more approaching flow will enter the region of the inlet with a larger road transverse slope. As the longitudinal slope increased (see Fig. 3.7(a) and (c)), water velocity towards the side wall near the inlet reduced, and the water velocity towards the flume outlet increased. These are due to that as the longitudinal slope increased, which means that the approaching flow rate increased, the velocity towards the flume outlet will increased. Besides these, it is interesting that a larger area without the water phase suddenly appeared just downstream of the grate inlet, close to the side wall, with the largest road longitudinal slope of 10%, as shown in Fig. 3.7(c). On the other side, there approaching flow was intercepted by the downstream side of the inlet (see in Fig 3.7(a)). This difference between Fig. 3.7(a) and Fig. 3.7(c) is because a larger longitudinal slope will result in a higher flow velocity, and the approaching flow tended to 'skip' over of the grate inlet. These findings from water fraction and velocity contour are consistent with the those of the impacts of hydraulic parameters.

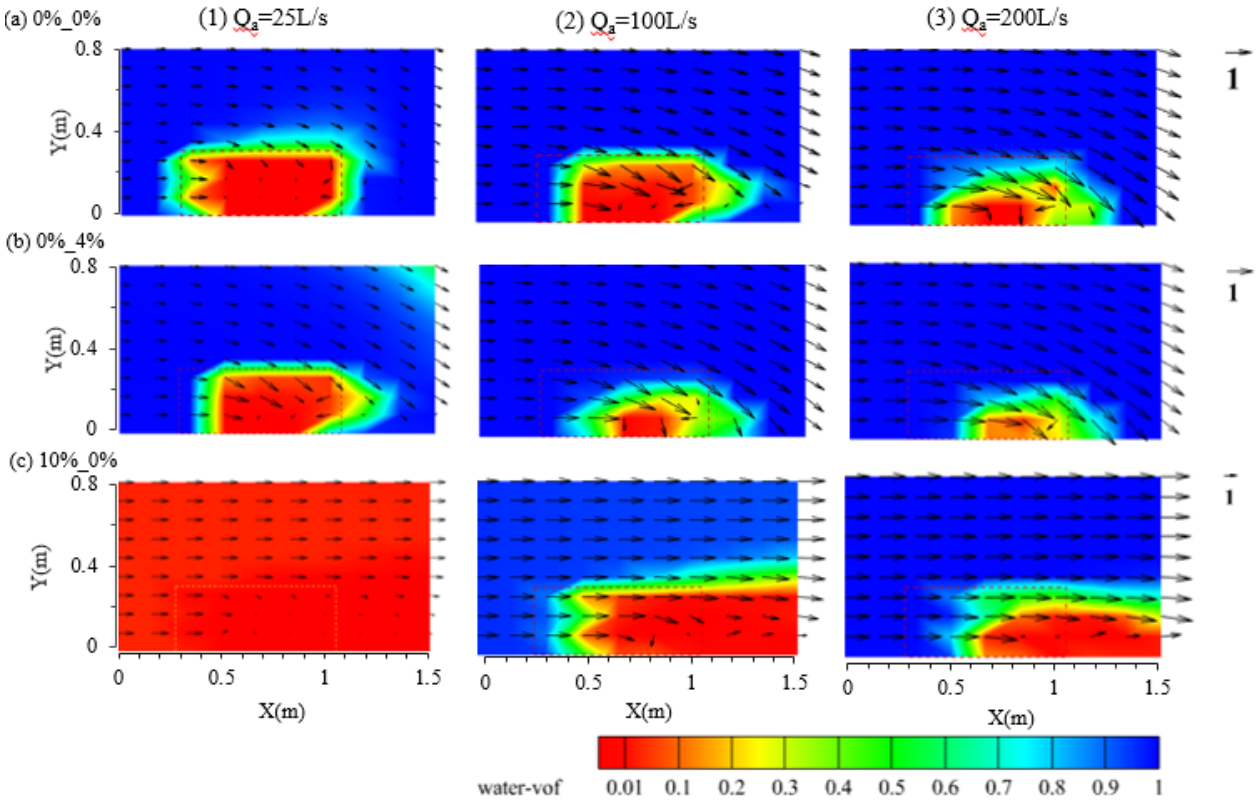


Figure 3.7 Contours water fraction and velocity field around the grate inlet under clean condition (velocity vector unit is m/s).

### 3.3.4 Clogging factors

The simulation results in Fig. 3.6(c) show that the clogging factor increased with the increase of clogging area. The clogging factors for clogging pattern 1, 2 and 3 (see Fig. 3.2) ranged from 0 to 0.21, 0.05-0.31, and 0.10-0.70, respectively. Moreover, the real clogging pattern 2 and 3 had larger clogging factors than the generalized clogging pattern 2 and 3 for all the three slopes combinations, separately. These trends of clogging factor are reasonable, since as clogged grate inlet opening increased, the inflow captured capacity of grate inlet would be reduced.

Furthermore, Fig. 3.6c shows that the clogging factor generally increased when the approaching rate increased from 25 L/s to 200 L/s with the same street slopes (longitudinal and transverse).

This means that the inlet efficiency owing to clogging will decrease (see Fig. 3.6b) during large rainfall events that have larger flow rate. It was because the inlet can not handle large amount of approaching flow during large rainfall events. So it is needed to clean the clogged inlet in time especially during the season with large rainfall. In the experiment of Gómez et al. (2013), the clogging factor of the inlet ranged from 0.27 to 0.68 at the highest test range of $Q_a/d$ = 10. In this simulation, the maximum $Q_a/d$ = 7.3 with the slope 10%_0% and the approaching flow $Q_a$ = 200 L/s, and the related clogging factor ranged between 0.21 and 0.70.

Furthermore, when compared to the other three slope combinations (i.e., 0%_0%, 0%_4% and 2%_2%), the slope combination 10%_0% had the largest clogging factor for both small (25 L/s) and large runoff (200 L/s), which indicated the largest efficiency loss. This is because the approaching flow skipped over the grate inlet due to high flow velocity. So large longitudinal slope of street will lead to more severe clogging of the inlet. Compared to the slope combination of 0%_0%, the slope combination 0%_4% had larger clogging factors, indicating that clogging effect would be increased with large street transverse slope. This is because more approaching flow will accumulate around the grate inlet, the inlet will have larger difficulty in intercepting the flow. So large longitudinal or transverse slopes of road will make the clogging effect more serious.

### 3.3.5 Real clogging scenarios

According to Fig. 3.8 and **Table 3.3**, the generalized clogging patterns approach overestimated the inlet intercepted flow rate by 0-0.49 L/s (0-27% in percentage), overestimated efficiency by 0~0.07 (0-27% in percentage) and underestimated the clogging factor by 0-0.21 (0-66% in percentage). Even for the typical road slopes, 2%_2%, the difference was 1.3-3.6 L/s (12%-25%) for the inlet intercepted flow rate, 0.02-0.07 (12%-25% in percentage) for the inlet efficiency, 0.09-0.12(14%-66% in percentage). This is reasonable since the grate opening using the generalized approaching

was larger than that of real clogging pattern approach, more approaching flow was able to be intercepted by the grate inlet. Based on these findings, it is vital to digit the real clogging patterns from photographs for accurately assessing the inlet hydraulics in clogging conditions.

**Table 3.3** Difference between real and generalized clogging patterns

| | | Difference | | |
|---|---|---|---|---|
| | | 2%_2% | 0%_4% | 10%_0% |
| Intercepted flow (L/s) | Pattern 2 | 1.7~3.6 (12%~15%) | 0.2~2.6 (1%~8%) | 0.3~2.8 (15%~27%) |
| | Pattern 3 | 1.3~3.6 (20%~25%) | 1.2~4.9 (11%~20%)) | 0~0.8 (0%~19%) |
| Efficiency | Pattern 2 | 0.02~0.07 (12%~15%) | 0.01~0.03 (1%~8%) | 0.01~0.02 (15%~27%) |
| | Pattern 3 | 0.02~0.05 (20%~25%) | 0.02~0.06 (11%~20%) | 0~0.01 (0%~19%) |
| Clogging factor | Pattern 2 | -0.09~-0.12 (-33%~-66%) | -0.01~-0.07 (-17%~45%) | -0.15~-0.21 (-32%~55%) |
| | Pattern 3 | -0.09~-0.10 (-14%~-18%) | -0.07~-0.1 (-14%~-23%) | 0~-0.04 (0%~-12%) |

Note: Difference = generalized clogging – real clogging. The values in the brackets are difference in percentage.

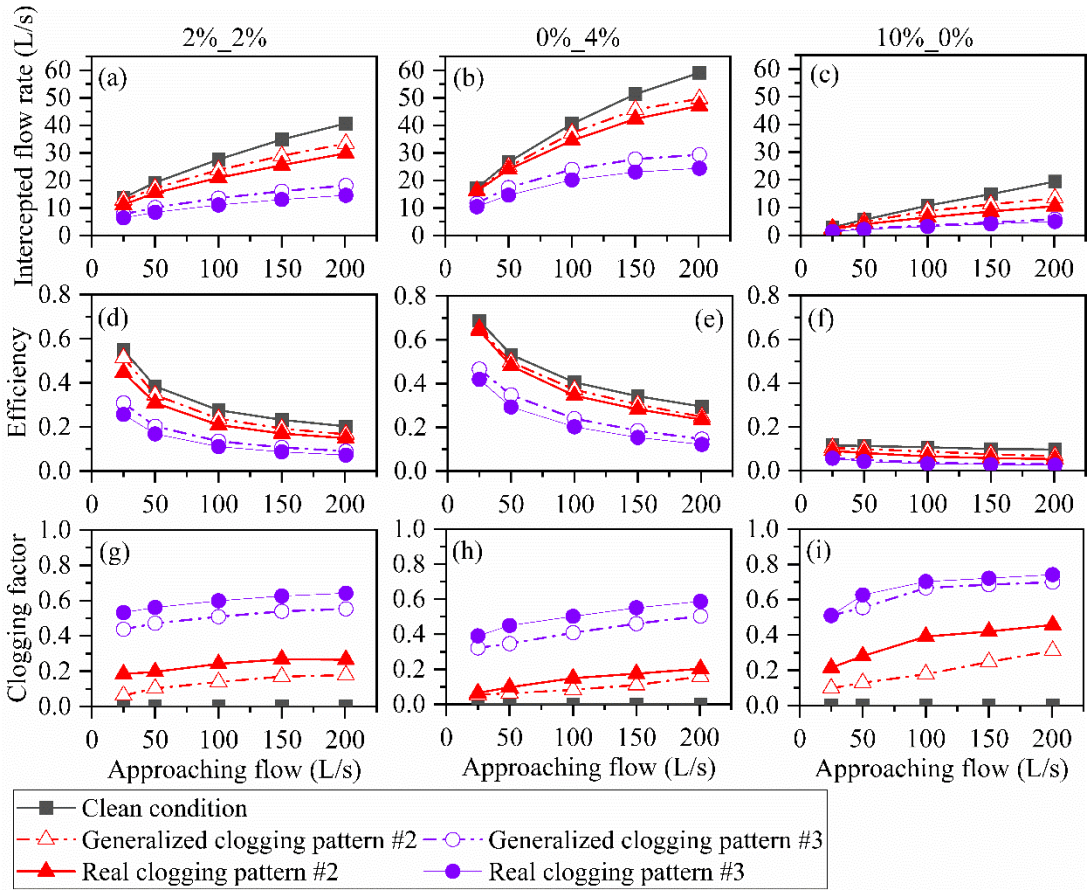


Figure 3.8 Comparison of the CB inlet intercepted flow rate, efficiency and clogging factor between generalized (empty dots) and real clogging (filled dots) cases, with street slopes of (a, d, g) 2% and 2%; (b, e, h) 0% and 4%; and (c, f, i) 10% and 0%.

The contours of water fraction and horizontal plane velocity field (at 0.5 cm above the flume bed) were examined (Fig. 3.9) to further examine the difference between the generalized clogging approach and the real clogging approach. As shown in Fig. 3.8, when compared to the real clogging patterns, the generalized clogging patterns had larger water fraction within the grate inlet. It indicated that the generalized clogging patterns intercepted more approaching flow. It was consistent with earlier conclusions about capacity and efficiency.

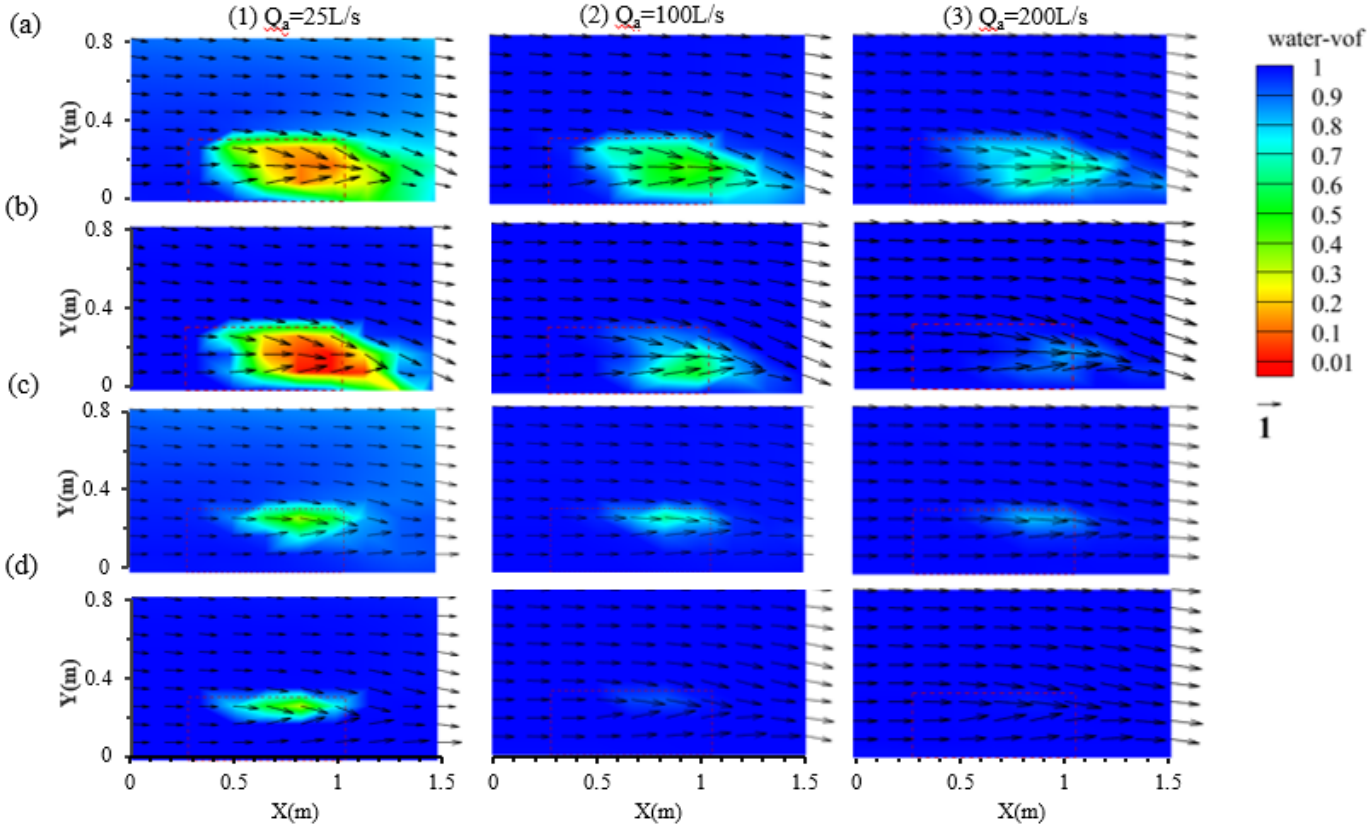


Figure 3.9 Contours of water fraction and velocity field around the grate inlet for (a, c) real clogging pattern 2 and 3, and (b, d) generalized clogging pattern 2 and 3, with road slopes 2%_2%. (The velocity vector unit is m/s.)

### 3.3.6 More clogging patterns

The simulation results for the grate inlet intercepted flow rate, efficiency, and clogging factor are shown in Fig. 3.10 for the additional clogging patterns 4-28. In the series of 50% clogged, grate inlet capacities ranged from 4.35 to 30.83 L/s, efficiencies ranged from 0.06 to 0.47, and clogging factors ranged from 0.22 to 0.66. It was found that clogging patterns 4 and 5 intercepted more runoff than clogging patterns 6 and 7, emphasizing the more importance of grate inlet effective (unclogged) width than the effective length or area, where the width is defined in the transverse direction (perpendicular to the flow direction) and the length is in the longitudinal direction. The

similar results (intercepted flow rate, efficiency and clogging factor) of clogging patterns 4 and 5 are not surprising, because the only difference between these two is the location of the open voids (upper half or lower half) in the grate inlet. Clogging patterns 6 and 7 produced comparable results for the similar reason – the open voids are either on the left or right side of the grate inlet.

In the series of 33% clogged, grate inlet intercepted flow rate range from 6.83 to 39.81 L/s, efficiencies ranged from 0.08 to 0.57, and clogging factors range from 0.05 to 0.5. Clogging patterns 8-22 had larger inlet capacity and efficiency and lower clogging factor, compared to the series of 50% clogged, as expected. Overall, the clogging patterns 8-22 produced similar results in terms of capacity, efficiency and clogging factor for the grate, despite of some variation within these patterns. This suggests that the clogging pattern itself has a marginal impact to the grate inlet hydraulics, as long as the total clogged area is the same. Interesting, clogging pattern 9 produced larger inlet capacity and lower clogging factor, compared to other clogging patterns. The possible reason is that the clogging in clogging pattern 9 changed the original inlet into two small inlets, the upstream one and the downstream one. These two small inlets were not connected directly, and the clogging between these two inlets increased the intercepted flow amount by intercepting flow from the downstream side of the upstream inlet and intercepted flow from the upstream side of the downstream inlet. This joint contribution to interception can help increase the whole inlet capacity. In the series of 17% clogged, grate inlet intercepted flow rate ranged from 8.49 to 44.3 L/s, efficiencies ranged from 0.11 to 0.60, clogging factors ranged from 0.02 to 0.37. The results are remarkably similar to the results of the series of 33%.

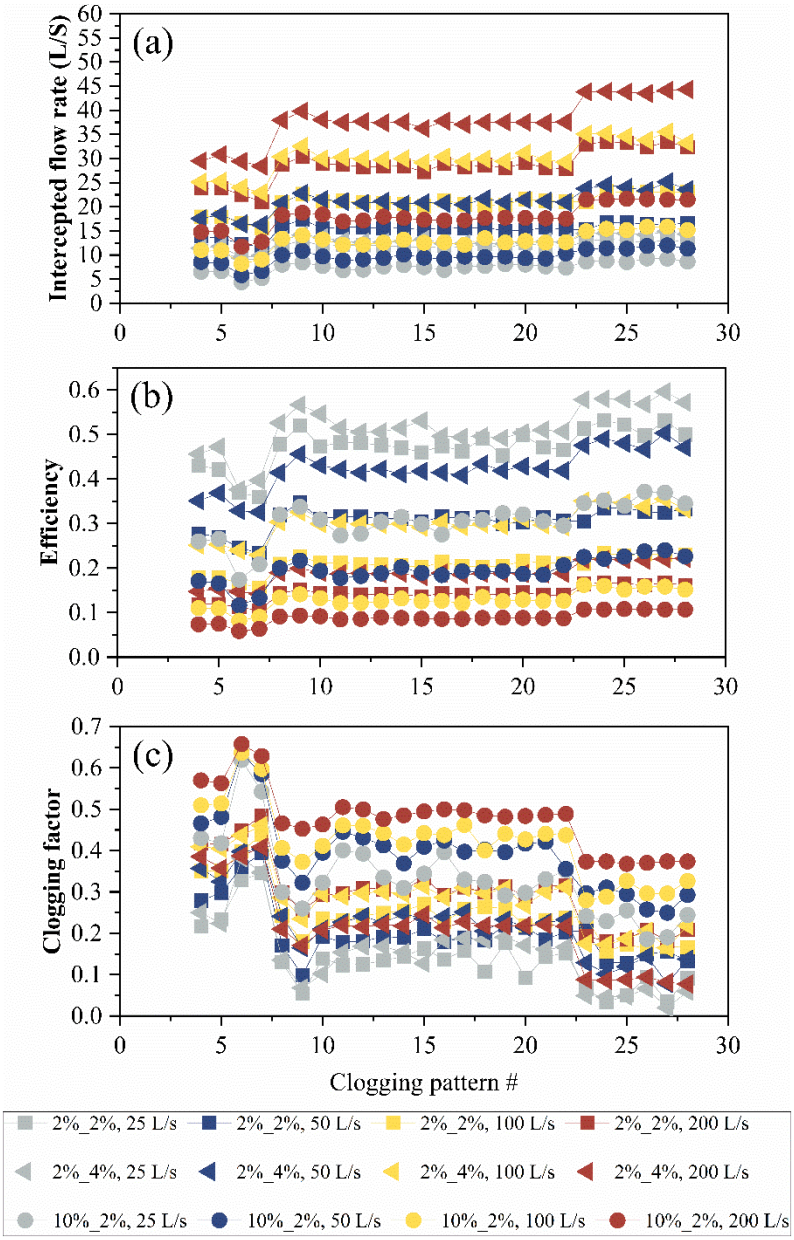


Figure 3.10 Simulation results for the CB inlet (a) intercepted flow rate, (b) efficiency and (c) clogging factor for the additional clogging patterns 4-28.

The results above suggest that the clogging factor was most affected by the approaching flow, street slopes, and clogging area, but marginally affected by the clogging site or pattern. Based on these results, predicted equations for the CB inlet efficiency and clogging factor were developed in this study. The equations for the inlet efficiency and clogging factor are as follows:

$$E = (48 - 0.24Q_{int})/175\text{-}0.29C_{Percent} - 0.53S_L + 3.18S_T + 0.2 \quad (3.9)$$

$$C_0 = (0.11Q_{int} - 22)/175 + 0.88C_{Percent} + 2.03S_L + 0.79S_T - 0.14 \quad (3.10)$$

where $C_{Percent}$ is the percentage of clogged void area over the total void area of the grate inlet. The prediction equations use the results of all the 28 clogging patterns as well as the clean condition.

As illustrated in Fig. 3.11, it was found that the inlet efficiency and clogging factor obtained using the predicted equation for the grate inlet mostly agreed with the values from the CFD model. $R^2$ between the simulated inlet efficiency and the predicted efficiency using the equation was 0.60, and $R^2$ between the simulated clogging factor and the predicted clogging factor was 0.93. Therefore, the two equations are recommended for future use to forecast grate inlet efficiency and clogging factor.

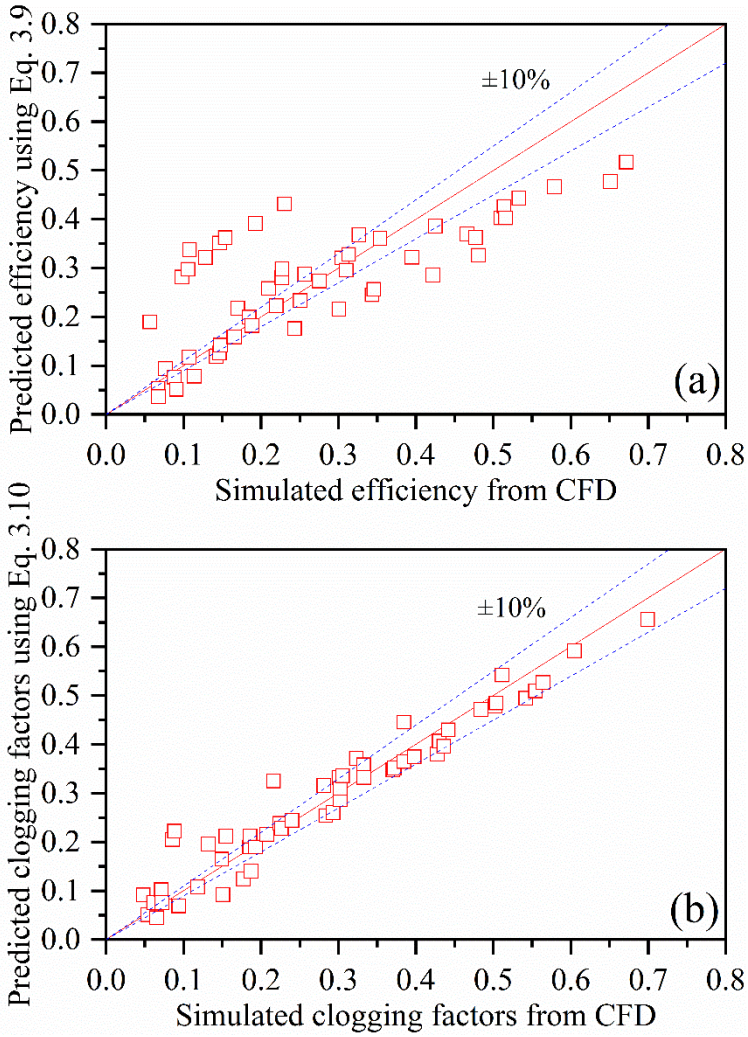


Figure 3.11 Comparison of the predicted (a) efficiency and (b) clogging factor with the CFD modeling results, for the grate inlet.

### 3.3.7 Large water depth

As the approaching flow rate increased, the grate inlet intercepted flow rate increased, as seen in Fig. 3.12(a). The impact of approaching flow rate on the inlet capacity is similar to the smaller approaching flow rate as discussed above. Clogging lowered grate inlet capacity as clogging area increased. This is also similar to the simulated results for smaller approaching flow rate. Furthermore, it was evident from Fig. 3.11(b) that the efficiency of the grate inlet decreased with

the increase of the approaching flow rate or clogging area. This impact was also similar for small water depth. The results on the clogging factor (Fig. 3.12(c)) showed that clogging pattern 3 had the largest clogging factor value (0.61 to 0.63), and clogging pattern 1 had the lowest values (0.20-0.21). All of these results suggested that grate inlet capacity and efficiency would be decreased by the deep water with clogging effects.

In general, a value of 0.6 is commonly used to describe orifice flow through a grate inlet. In Fig. 3.12(d), the simulated values for the inlet orifice discharge coefficient were compared for different clogging patterns. The orifice discharge coefficient ranged from 0.61 to 0.64 for clean condition, ranging from 0.58 to 0.59 for clogging pattern 1, ranging 0.60 to 0.62 for clogging pattern 2, and ranging from 0.61 to 0.63 for clogging pattern 3. It was found that the clogging pattern had a minimal impact on the inlet orifice discharge coefficient, and the suggested value for orifice discharge coefficient 0.6 is suitable for calculating intercepted capacity for the grate inlet during large rainfall events.

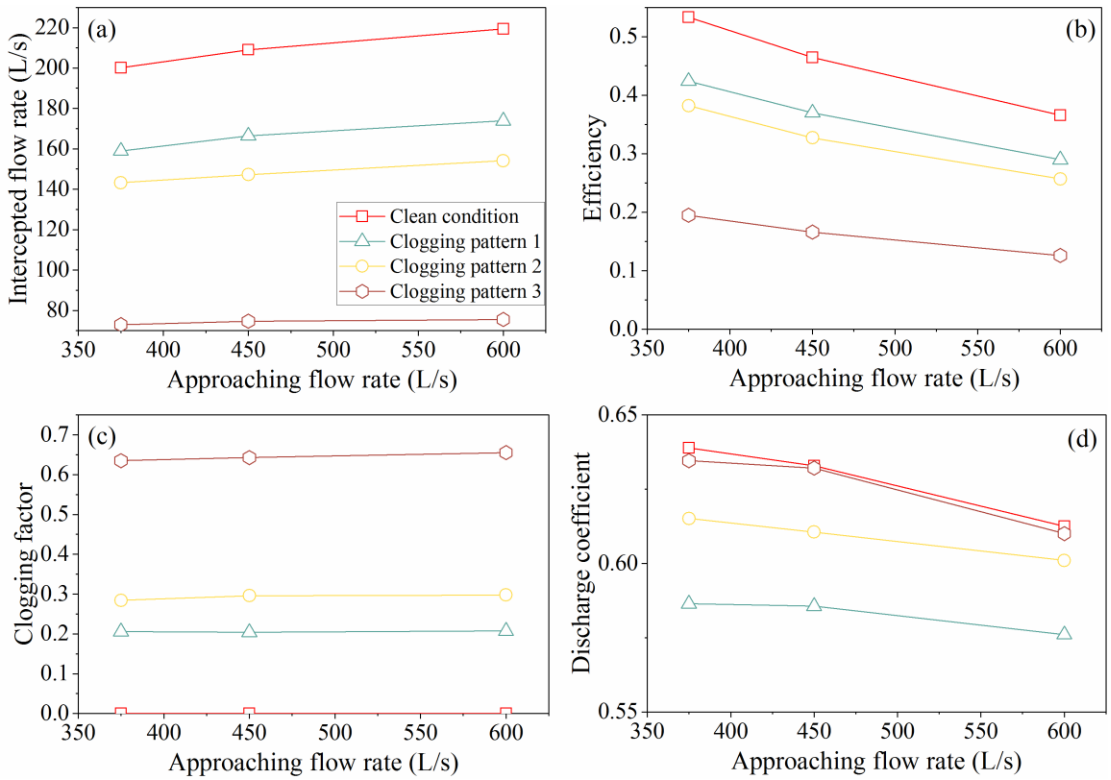


Figure 3.12 Simulation results for large approaching flow on streets: (a) intercepted flow, (b) efficiency, (c) clogging factor, and (d) discharge coefficient, for the CB grate inlet.

### 3.3.8 Vertical depression

The grate inlet capacity, efficiency, and clogging factor are individually shown in Fig. 3.13. With the small approaching flow of 25 L/s, the vertical depression had a negligible affect on inlet hydraulics (intercepted flow rate, efficiency, and clogging factor). However, with a large approaching flow of 200 L/s, the 0.02 m vertical depression increased the inlet intercepted flow rate by 2.5 - 6.8 L/s, and increase efficiency by 0 – 0.04, while it decreased the clogging factor by 0 - 0.08. It is clear that the 0.02 m vertical depression is only important for large approaching flow rather than the low approaching flow. As for a large approaching flow rate (200 L/s) without the grate inlet depression, the high velocity of approaching flow will lead the flow to skip over the grate inlet. With the vertical depression, such skipping is not likely to happen, and the approaching

flow near the side of the inlet will drop into the grate opening. So, the difference between the inlet without a vertical depression and with can be explained. But for a small approaching flow rate (25 L/s), there the possibility of skipping was near zero whether there was a vertical depression or not.

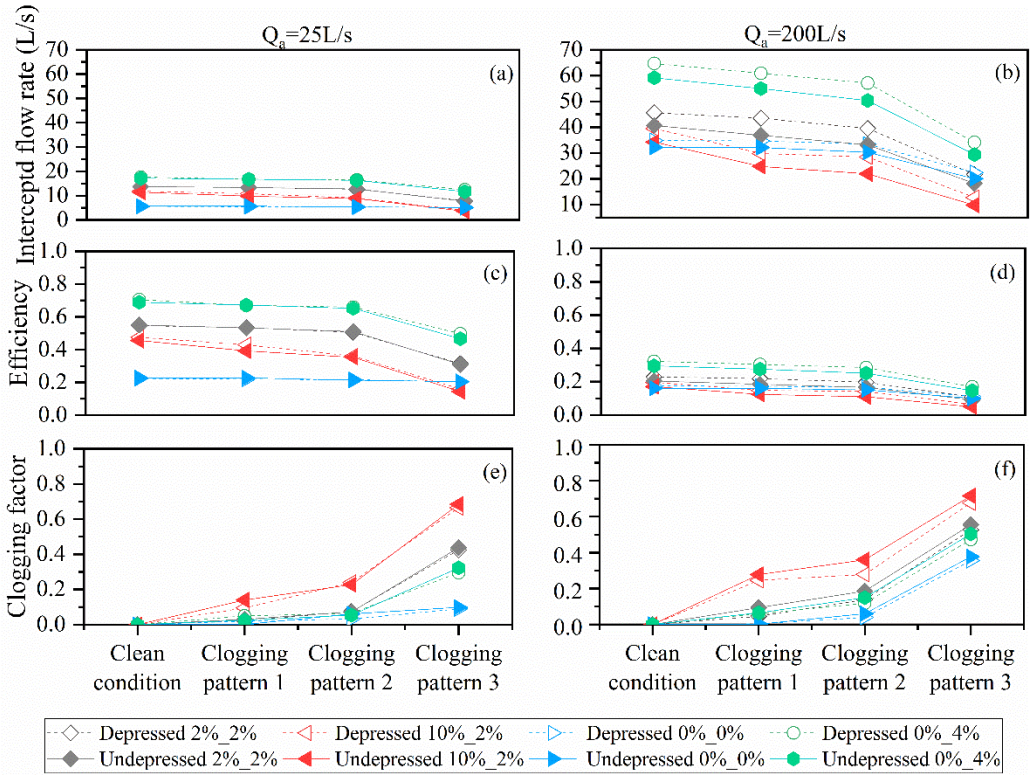


Figure 3.13 Simulation results of (a, b) intercepted flow rate, (c, d) efficiency and (e, f) clogging factor of the CB grate inlet with a 2 cm vertical depression, under both clean and clogging conditions

Wakif et al. (2019) reported opposite results on the impact of a vertical depression on the capacity and efficiency of grate inlets from this study. Wakif et al. (2019) found that a vertical depression of 0.02 m depression would result in a reduction of about 6% to 10% of the inlet efficiency, They stated that this is because the inlet openings (holes) nearest to the approaching flow are not utilized/fully utilized, so the approaching flow will skip over the grate inlet.

The opposite results between this study and Wakif et al. (2019) can be explained by possible reasons: 1) the flume sizes are quite different: in Wakif et al. (2019)'s study, the inlet and the inlet

was 0.67 m far away from the supply water tank and located at the middle of the flume near the side wall (see in Fig. A5), while in this study, the inlet was 3 m far away from the supply water tank and located at the downstream of the flume. In Wakif et al.'s study, the flow intercepted by the inlet may be influenced by the supply water tank due to the short distance between the inlet and water supply tank. (2) the configurations of the inlets are different. In wakif et al. (2019)'s experiments, there were 7 interior gratings perpendicular to the side wall (also the main direction of the approaching flow) in the grate inlet (see Fig. A5), while in this study there was only one interior grating. In the undepressed condition, the 7 interior gratings can retard the approaching flow effectively, while in this study, this retard effect is quite smaller. As a result, the difference due to the retard effect of the vertical bars was minimal whether there was a vertical depression or not. (3) the approaching flow rates employed in these two studies are quite different. In Wakif et al. (2019)'s experiment, the approaching flow rate ranged from 4 to 12 L/s, while in this study it ranged from 25 to 200 L/s. In this study, the approaching flow accumulated or near the inlet can be pretty larger than that in Wakif et al. (2019)'s study. As there the depression existed, the approaching flow will be intercepted more easier in this study.

### 3.3.9 Outflow from the grate inlet

According to the dry street results, neither longitudinal nor transverse slope had an evident effect on the discharge coefficient $C_{do}$ (Fig. 3.14(a) and (b)), and $C_{do}$ increases as the outflow rate via the grate inlet increases (Fig. 3.14(c)). Overall, with the outflow ranging 10 - 200 L/s, the modeling showed that the $C_{do}$ ranged from 0.09 to 0.57. It can be concluded that the suggested value, 0.6, for the discharge coefficient may overestimate the outflow from the sewer (e.g., CB) to the street via the CB inlet; the road slopes (longitudinal and transverse) had very poor influence on the discharge coefficient. As the outflow rate range from 10 to 50 L/s, the modeling results suggest a

value range of 0.09 - 0.26 for $C_{do}$, whereas the experiments of Gómez et al. (2019) reported a larger range of 0.14 - 0.40. The possible reason for this difference may be the different configurations of the inlets tested separately by Gómez et al. (2019) and this study, e.g., the inlet sizes, the gratings numbers and directions.

According to Fig. 3.14(d), the road slopes (longitudinal and transverse) had very marginal impact on discharge coefficient, but the existence of the approaching flow, i.e., the wet street condition, would influence the discharge coefficient. For the outflow = 50 L/s, the discharge coefficient decreased from 0.26 to 0.20 as the approaching flow increased from 0 to 200 L/s; for the outflow = 50 L/s, the discharge coefficient decreased from 0.40 to 0.35 as the approaching flow increased from 0 to 200 L/s The discharge coefficient $C_{do}$ was smaller as the supply water tank's approaching flow increases, because the approaching flow from the supply water tank would retard the exit of the outflow via the grate inlet. The actual discharge via the inlet would be reduced for the wet street than the discharge with dry street. This conclusion indicated that the suggested discharge coefficient, 0.6, would significantly overestimate the outflow via the grate inlet.

Based on the results, the prediction equation for $C_{do}$ was developed under the dry street condition. The discharge coefficient was linked to the longitudinal and transverse slopes of the road, as well as the outflow rates:

$$C_{do} = 0.10 * S_L - 0.31 * S_T + (0.46Q_{out} - 92)/190 + 0.6 \quad (3.11)$$

where $Q_{out}$ is the flow rate of outflow from the grate inlet to the street. The prediction from Eq. 3.11 was compared to the simulation results from the CFD model, as illustrated in Fig. 3.15. The $R^2$ between the simulated discharge coefficient and predicted discharge coefficient using the equation above is 0.95. It can be concluded that the prediction outcomes were consistent with the

simulations, and the prediction equation can be used for calculating the discharge coefficient accurately.

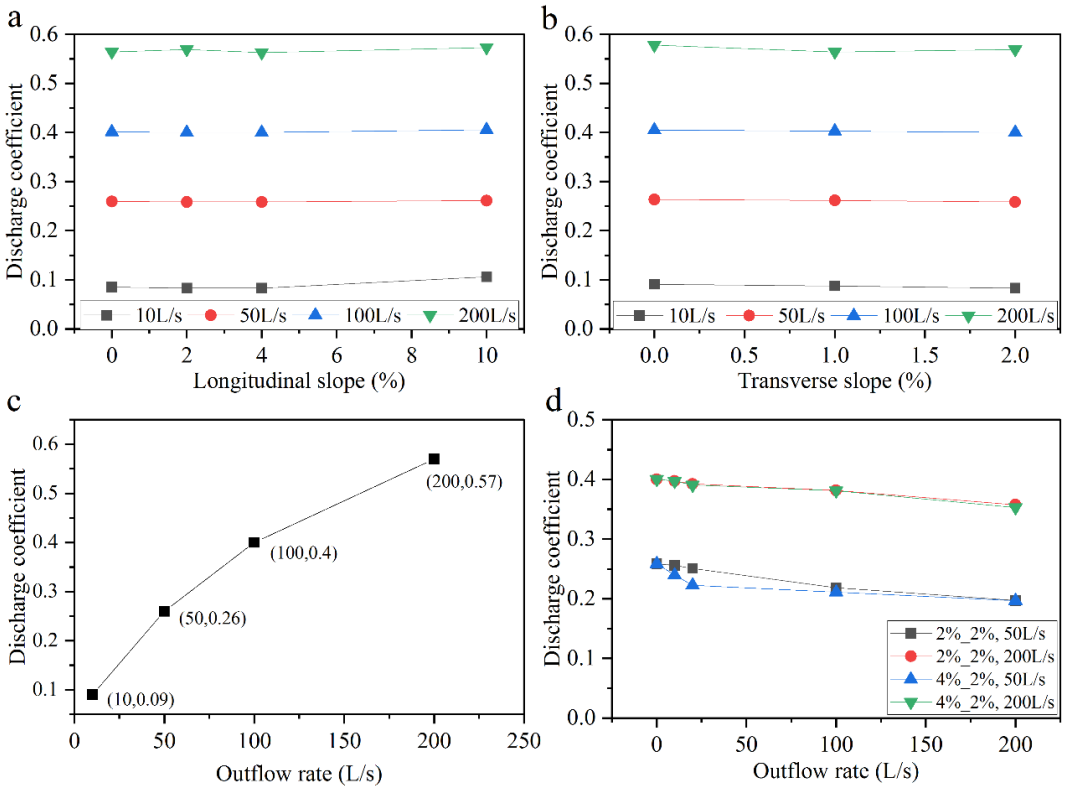


Figure 3.14 Simulation results of discharge coefficients of the CB grate inlet under (a - c) dry street and (d) wet street conditions

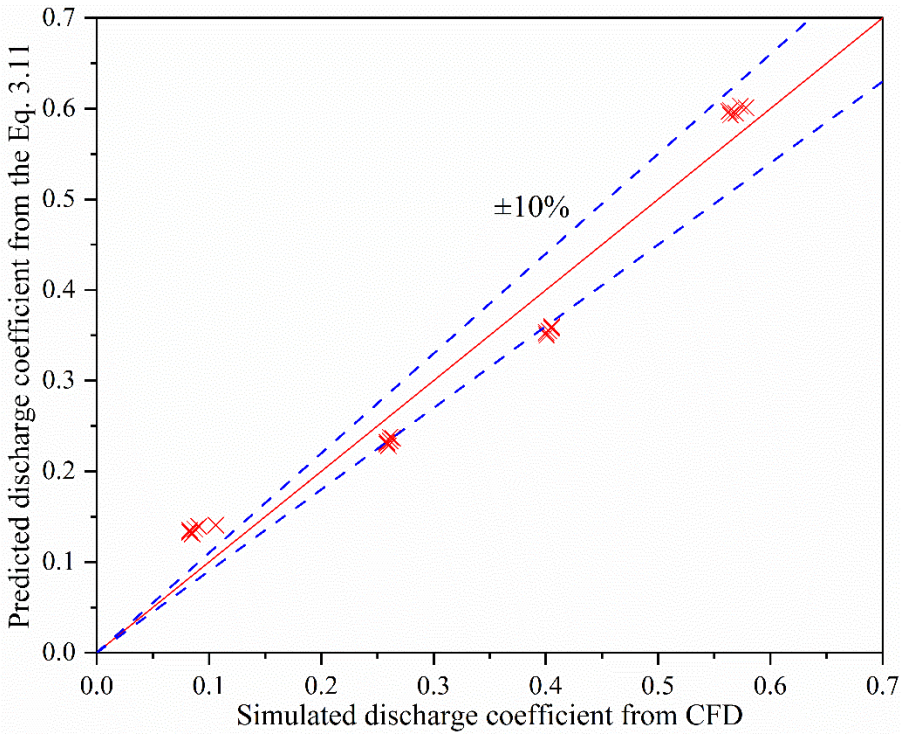


Figure 3.15 Comparison of the predicted discharge coefficients against the ones from the CFD model under the dry street condition.

### 3.3.10 Research limitations

This research still has some limitations. First, the prediction formulas (Eqns. 3.9, 3.10 and 3.11) proposed in this study are still limited to certain conditions, particularly under certain flow rate range. Their application on other CB grate inlets under other conditions needs verifications. Moreover, there was only one type of grate inlet tested in this research, and therefore the conclusions may not be general for other grate inlets.

## 3.4 Conclusions

In this study, the RANS and RNG $k$-$\varepsilon$ equations, as well as the VOF approach, were employed to build a mathematical model for assessing a grate inlet under both clean and clogging conditions. The simulated results agree well with the experimental results of Gómez et al. (2013). The

calibrated model was utilized to quantify the hydraulics of the grate inlet under various conditions, such as real clogging patterns, different clogging areas and patterns, large water depth on streets during large storm events, vertical depression of the grate inlet, and outflow from the grate inlet. Main conclusions are as follows:

- The clogging factor can range from 0 to 0.7 in the scenarios tested in this work, which is affected by the clogging area, approaching flow, and street longitudinal and transverse slopes. The locations of clogging on the grate inlet would not significantly alter the hydraulics of the grate inlet.
- Generalized clogging patterns tend to increase the grate inlet intercepted flow rate (by 0.2-4.9 L/s) and lower the clogging factor (by 0.02-0.12), compared to the real clogging patterns.
- Under large water depth condition on streets, the clogging factor is independent of the approaching flow rate. A value of 0.6 is acceptable for the discharge coefficient when the orifice flow through CB inlet is used.
- A 0.02 m vertical depression of the grate inlet was found to increase the inlet intercepted flow rate by 2.5-6.8 L/s, and increase efficiency by 0-0.04, and decrease the clogging factor by 0-0.08, compared to the non-depressed grate inlet.
- Under the condition of outflow from the grate inlet, neither street longitudinal slope nor transverse slope has an influence on the discharge coefficient $C_{do}$ both for the wet and dry streets, and the presence of a approaching flow on street would reduce $C_{do}$ in wet street scenario. The suggested value for the discharge coefficient, 0.6, would overestimate the outflow via the grate inlet.
- The new equations proposed for predicting the grate inlet efficiency and clogging factor can be used for calculating these two parameters. The equation developed for the discharge coefficient of outflow is useful for accurately estimating the outflow from the CB, which can improve the calculation in current commercial software.

Future research is suggested in the following areas: (a) the true clogging impact of leaves, debris, and other items; (b) more clogging patterns; (c) CB inlets with other designs and other vertical depression depths; (d) additional street slope combinations for large water depth scenarios; (e) the retard effect of the approaching flow on the outflow of grate inlet on wet street.

**Chapter 4 General conclusions and future work**

This thesis was written in paper-based format and is composed of two pieces of work: a critical literature review on stormwater CB inlet hydraulics; and a numerical simulation study on CB grate inlets under different conditions. The contributions of this thesis include:

- The literature review is so far the most comprehensive review on the topic, covering 104 relevant studies in the past 70 years.
- The 3-D numerical model developed in this study help us explore CB grate inlet hydraulics under the following four conditions that have been numerically examined: under clogging condition; large water depth condition on road; vertical depression compared to road surface; and outflow via inlets to roads due to surcharging of underground sewers.
- New formulas were proposed for CB grate inlet efficiency and clogging factor under clogging conditions, which have not been reported.

Detailed conclusions on this research have been provided in Chapter 2 and 3 of the thesis. Herein, general conclusions are summarized below:

- There are four major types of CB inlets: grate inlet, curb opening inlet, combination inlet, and slotted inlet. Among these four types, grate inlet and curb opening inlet

are the most investigated types. After 1990s, studies on CB inlets increased substantially, especially on CB grate inlet.

- Most previous studies assessed CB inlet hydraulics considering CB inlet geometries, approaching flow and road conditions, and developed empirical equations for inlet capacity and/or efficiency based on physical experiments. Notice that there are applicable ranges for these equations due to different experimental conditions.
- There are 3D CFD packages, e.g., FLOW-3D, FLUENT, and OpenFOAM, applied in the research of CB grate inlets. Compared to physical experiments, numerical simulations can help understand flow near and through CB inlets.
- A 3D CFD model was successfully built in this study using FLUENT to assess CB grate inlet hydraulics under the four specific conditions that have been less studied and have not been numerically explored.
- Based on the calibrated model, the clogging factor to the grate inlets was calculated to be 0 - 0.7, depending on the clogging area, approaching flow and road slopes. Generalized clogging patterns tend to overestimate grate inlet capacity, i.e., with a smaller clogging factor, compared to the real clogging patterns. Large water depth on streets generate near constant clogging factor, independent of approaching flow rate; and a value of 0.6 for discharge coefficient can be used with the orifice flow equation to predict the inlet capacity. A vertical depression will increase the inlet capacity and efficiency and decrease the clogging factor, compared to the non-depressed case. When underground sewers are surcharging via CBs to road surface, it was found that road slopes (longitudinal or transverse slope) have no impact on the discharge coefficient $C_{do}$, and the approaching flow on road will decrease $C_{do}$.

- Prediction equations on CB grate inlet efficiencies, clogging factors, and orifice discharge coefficient have been proposed based on the simulation results, with good agreement among the equations and the simulation results.

To improve understanding of CB inlet hydraulics, **it is suggested to conduct the following future research:**

- To conduct full scale experiments so as to avoid the scaling effect of physical models;
- To assess CB inlets on real streets, particularly considering underground CB components and connecting pipes, i.e., considering the interaction between street flow and underground sewage flow;
- To evaluate CB inlet under more real environment conditions, e.g., unsteady rainfall, extreme rainfall, hailstorm event, and in cold regions with the effects of snow, ice and melting.
- To conduct more investigations for CB inlets under clogging condition. Specifically, it is vital to understand the dynamics of clogging on grate inlet during storm events, including the formation, and change of clogging with time and different materials. The goal is to build a more detailed guideline for choosing clogging factors for CB inlets in the engineering design.
- To conduct more studies on the behaviors of surface runoff, sand, silts and debris approaching and through CB inlets. Existing studies only consider runoff, and the joint effects of water, solids and debris will improve the accuracy of CB inlet capacity and efficiency calculation.

- To conduct neighborhood-scale numerical and physical experiments to assess CB inlet performance in urban drainage systems. Current studies only consider single CB inlet, and the interactions among CB inlets on the same and/or different streets need to be better understood for urban flood mitigation, especially under clogging conditions and in cold regions where ice effect is important.
- To further examine the hydraulics of combination inlets. Currently, combination inlet hydraulics are poorly understood, but they are widely adopted in urban drainage systems.
- To develop equations for CB inlet capacity and efficiency that can be more widely and universally used in engineering design, i.e., they are less limitations on these equations and larger applicable ranges.

**References**


Adam, K. M. and Brandson, N. B. (1974). Hydraulic analysis of Winnipeg sump inlets. *Journal of the Water Pollution Control Federation,* 46(12), 2755–2763.

Almedeij, J., Alsulaili, A. and Alhomoud, J. (2006). Assessment of grate sag inlets in a residential area based on return period and clogging factor. *Journal of Environmental Management*, 79(1), 38–42.

ANSYS Inc. (2021). ANSYS FLUENT tutorial guide.

Appel, E. and Appel, E. (1972). Hydraulic performance of Pennsylvania highway drainage inlets installed in grassed channels. M. S. thesis.

Artina, S., Calenda, G., Calomino, F., Cao. C., La Loggia, G., Modica, C., … Veltri, P. (2001). Sistemi di fognature, Manuale di progettazione. Milano, Italy: Hoepli.

Argue, J. R. and Pezzaniti, D. (1996). How reliable are inlet (hydraulic) models at representing stormwater flow? *Science of the Total Environment,* 189–190, pp. 355–359.

Burgi, P. H. and Gober, D. E. (1978). Hydraulic and safety characteristics of selected grate inlets.

Burgi, P. H. & Gober D. E. (1977). Bicycle-Safe Grate Inlets Study: Volume 1 – Hydraulic and Safety Characteristics of Selected Grate Inlets on Continuous Grades. *Report No. FHWA-RD-77-24,* US Department of Interior, Bureau of Reclamation, Colorado, USA.

Bates, P. D., Lane, S. N., Ferguson, R. I. (2005). Computational Fluid Dynamics - Applications in Environmental Hydraulics. John Wiley & Sons Ltd..

Bauer, W. J. and Woo, D. (1964). Hydraulic Design of Depressed Curb-Opening Inlets", Highway Research Record, (58), 158–164.

Begum, S., Rasul, M., Brown, R., Subaschandar, N. & Thomas, P. (2011). An experimental and computational investigation of performance of the Green Gully for reusing stormwater. *Journal of Water Reuse and Desalination*. 1 (2), 99–112.

Brandson, N. B., (1971). Hydraulic behavior of the City of Winnipeg Standard storm water sump inlets. M. S. thesis, Dept. of Civil Eng. Univ. of Manitoba, Winnipeg, Canada.

Brune, A. W., Yee, P. P. and Graf, W. H. (1972). Hydraulic performance of Pennsylvania highway drainage inlets installed in paved channels , August 1972 ( 75-40 ) PB 222 488.

Bock, P., Li, W. H. and Geyer, J. C. (1956). Hydraulic Behavior of Storm-Water Inlets: V. A Simplified Method of Determining Capacities of Single and Multiple Inlets", Sewage and Industrial Wastes, 28(6), 774–784.

Bouchard, M. G and Townsend , R. D. (1984). Laboratory tests on the influence of grating pattern on street inlet hydraulics. Proceedings, Annual Conference Candian Society for Civil Engineering, Montreal, v2, 685 – 698.

Bowman, N. K. (1988). Hydraulic analysis of alternative South Carolina curb inlet structures. PhD thesis, Clemson University.

Brown, S. A., Schall, J. D., Morris, J. L., Doherty, C. L., Stein, S. M. & Warner, J. C. (2009). *Urban Drainage Design Manual – Hydraulic Engineering Circular 22 (HEC-22), 3rd edn.* FHWA-NHI-10-009, US Department of Transportation, Federal Highway Administration, Washington, DC and National Highway Institute, Virginia, USA.

Brown, S. A., Schall, J. D., Morris, J. L., Doherty, C. L., Stein, S. M. & Warner, J. C. (2013). *Urban Drainage Design Manual – Hydraulic Engineering Circular 22 (HEC-22), 3rd edn.* FHWA-NHI-10-2009, US Department of Transportation, Federal Highway Administration,

Washington, DC and National Highway Institute, Virginia, USA.

Bohac, D. E., (1991). Assessing the utility of previously derived equations measuring the efficiency of inlets: Comparison of data results from a laboratory analysis of gutter inlets with equations derived by previous research. M. S thesis. University of Nebraska-Lincoln, 106p.

Butler, D., Davies J. W. (2004) Urban drainage, 2nd Edition.

Cassidy, J. J. (1966). Generalized Hydraulic Characteristics of Grate inlets. Paper Sponsored by Committee on Surface Drainage of Highways and Presented at the 45th Annual Meeting. Washington DC, No. 123, 36-48.

Clacrk Country Regional Flood Control District (CCRFCD), (1999). Hydrologic criteria and drainage design manual.

Conner, N. W. (1945). Design and Capacity of Gutter inlets. *In Highway Research Board Proceedings.* 25, 101-104.

Comport, B. (2009). Hydraulic effficiency of grate and curb inlets for urban storm drainage. MS thesis, Dept. of Civil and Environmental Engineering, Colorado State Univ. Fort Collins, CO.

Comport, B. C. and Thornton, C. I. (2012). Hydraulic efficiency of grate and curb inlets for urban storm drainage. *Journal of Hydraulic Engineering,* 138(10), 878–884.

Cromwell, C. J., Rabens, C., and Kranc, S. C. (2001). Hydraulic Performance of a Grated Gutter Inlet. Bridging the Gap : Meeting the World"s Water and Environmental Resources Challenges Congress 2001.

Dai, H. B., Jin, S., Qian, C., Yang, N., Ma Y. L. & Liang, C. (2021). Interception efficiency of grate inlets for sustainable urban drainage systems design under different road slopes and approaching discharges, *Urban Water Journal,* 18:8, 650-661,

Despotovic, J. et al. (2005). Inefficiency of storm water inlets as a source of urban floods. *Water Science and Technology,* 51(2), 139–145.

Djordjević, S. et al. (2013). Experimental and numerical investigation of interactions between above and below ground drainage systems. Water Science and Technology, 67(3), pp. 535–542. doi: 10.2166/wst.2012.570.

Emily C. O'Donnell and Colin R. T. (2020). Driver of future urban flood risk. *Philosophical Transactions of the Royal Society A: Mathematical, Physical and Engineering Sciences.* 378-2168.

ERCOFTAC. (2000). Best Practice Guidlines for Industrial Computational Fluid Dynamics of Single-Phase Flows, Lausanne.

Fang, X., Jiang, S. and Alam, S. R. (2010). Numerical simulations of efficiency of curb-opening inlets. *Journal of Hydraulic Engineering,* 136(1), 62–66.

Farouk, M. Z. (2017). The Efficiency of A Depressed Gully Inlet of A Malaysian Drain." Degree Thesis, Universiti Sains Malaysia.

Feng, B., Zhang, Y. & Bourke, R. (2021). Urbanization impacts on flood risks based on urban growth data and coupled flood models. Nat Hazards 106, 613–627.

Fiuzat, A., Soares, C., and Sill, B. (2000). Design of curb opening inlet instructure.

Forbes, H. J. C. (1976). Capacity of Lateral Stormwater Inlets. *Civ Eng S Afr,* 18(9), 195–205.

Gagan, J., Smierciew, K., Butrymowicz, D., Karwacki, J. (2014). Comparative study of turbulence models in application to gas ejectors. *Int. J. Therm. Sci.* 78, 9–15.

Galambos, I. (2012). Improved Understanding of Performance of Local Controls Linking the

Above and Below Ground Components of Urban Flood Flows. PhD Thesis, University of Exeter, UK. Available from: https://ore.exeter.ac.uk/repository/handle/10036/4063.

Garcia, N., Lara, J.L., Losada I.J., (2004) 2-D numerical analysis of near-field flow at low-crested permeable breakwaters, *Coastal Engineering,* 51(10), 991-1020.

Gómez, M and Russo, B. (2005). Comparative study among different methodologies to determine storm sewer inlet efficiency from test data. Paper presented at the 10th International Conference on Urban Drainage, Copenhagen/Denmark, August. pp. 21–26.

Gómez, M., Russo, B. (2007). Hydraulic efficiency of macro-inlets. 1157–1164.

Gómez, M. & Russo, B. (2009). Hydraulic efficiency of continuous transverse grates for paved areas. Journal of Irrigation and Drainage Engineering 135 (2), 225–230.

Gómez, M. & Russo, B. (2011). Methodology to estimate hydraulic efficiency of drain inlets. *Proceedings of the Institution of Civil Engineers – Water Management,* 164 (2), 81–90.

Gómez, M., Hidalgo, G. & Russo, B. (2013). Experimental campaign to determine grated inlet clogging factors in an urban catchment of Barcelona. *Urban Water Journal,* 10 (1), 51–60.

Gómez, M., Recasens, J., Russo, B. & Martínez-Gomariz, E. (2016). Assessment of inlet efficiency through a 3D simulation: numerical and experimental comparison. *Water Science and Technology,* 74 (8), 1926–1935.

Gómez, M., Parés, J., Russo, B. and Martínez-Gomariz, E. (2018). Methodology to quantify clogging coefficients for grated inlets. Application to SANT MARTI catchment (Barcelona). *Jourtnal of Flood Risk Management,* 12(4), 1–10.

Gómez, M., Russo, B. and Tellez-Alvarez, J. (2019). Experimental investigation to estimate the discharge coefficient of a grate inlet under surcharge conditions. *Urban Water Journal.*

Taylor & Francis, 16(2), 85–91.

Guillou, J. C. (1959). The Use and Efficiency of Some Gutter Inlet Grates" Univ. of Illinois, Engrg. Exp. Sta., Bull. No. 450.

Guo, J. C. Y. (1997). Street Hydraulics and Inlet Sizing. ISBN Number 1-887201-00-9, Water Resources Publication Company, Littleton, Colorado, USA.

Guo, J. C. Y. (2000). Design of grate inlets with a clogging factor", *Advances in Environmental Research,* 4(3), 181–186.

Guo, J. C. Y. (2000). Street Stormwater Storage Capacity. *Water Environment Research,* 72(5), pp. 626–630.

Guo, J. C. Y. (2006). Design of Street Curb Opening Inlets Using a Decay-Based Clogging Factor. *Journal of Hydraulic Engineering,* 132(11), 1237-1241.

Guo, J. C. Y. and Mackenzie, K. (2012). Hydraulic Efficiency of Grate and Curb-Opening Inlets under clogging effect. Colorado.

Guo. J. C. (2012). Hydraulic Capacity of CDOT Type C and D area Inlets ( Installed in flat , depressed , and inclined configurations).

Guo, J. C. Y., Mackenzie, K. A. and Mommandi, A. (2016). Flow Interception Capacity of Inclined Grate, 142(4), 2–6.

Hammonds, M. & Holley, E.(1995). Hydraulic Characteristics of Flush Depressed Curb Inlets and Bridge Deck Drains. FHWA/TX-96/1409-1. Rep. No. 1409-1. Center for Transportation Research, University of Texas at Austin, Austin, Texas, USA.

Hao X. L., Jie Mu, J., and Shi H. J. (2021). Experimental Study on the Inlet Discharge Capacity

under Different Clogging Conditions. *Water*, 13-826.

Hirt, C. W. & Nichols, B. D. (1981). Volume of fluid (VOF) method for the dynamics of free boundaries. Journal of Computational Physics 39, 201–225.

Holley, E. R., Woodward, C., Brigneti, A., and Ott, C. (1992). Hydraulic characteristics of recessed curb inlets and bridge drains. Texas Department of Transportation (TxDOT), Austin, Texas.

Hodges, B. R., Barrett, M. E. and Schalla, F. E. (2018). Interception Capacity of Conventional Depressed Curb Inlets and Inlets with Channel Extension.

Hotchkiss, R., D. Bohac. (1991). Efficiency of highway stormwater inlets. Report RES1 (0099) P440. Nebraska Department of Roads.

Hotchkiss, Rollin H. (1994). Improvements in curb-opening and grate inlet efficiency. Transportation Research Record, (1471), 24–30.

Izzard, C. F. (1949). Tentative Results on Capacity of Inlets. In Proceedings of the 29th Annual Conference of the Highway Research Board, Washington, DC, USA, 36–54.

Izzard, C. F. (1950). Tentative results on capacity of curb opening inlets. In Highway Research Board, 11–13.

Izzard, C. F. (1977). Simplified Method for Design of Curb-Opening Inlets. Transportation Research Record, (631), 39–46.

Katopodes, N. D. (2019). Volume of Fluid Method. *Free-Surface Flow*, 766–802.

Karaki, S. S., Hanie, R. M. (1961). Depressed curb opening inlets: Supercritical flow, Experimental data. Colorado State Univ. Res. Foundation, Civil Eng. Sect.

Kemper, S. & Schlenkhoff, A. (2016). Capacity of street inlets with partially severed grate

openings. In the 6th International Junior Researcher and Engineer Workshop on Hydraulic Structures (IJREWHS 2016), Lübeck, Germany.

Kemper, S. & Schlenkhoff, A. (2018). Numerical simulation of intake structures like street inlets with supercritical flow conditions. In the 7th International Symposium on Hydraulic Structures, Aachen, Germany.

Kemper, S. & Schlenkhoff, A. (2019). Experimental study on the hydraulic capacity of grate inlets with supercritical surface flow conditions. *Water Science and Technology,* 79 (9), 1717–1726.

Kranc, S., Romano, F., Ethier, S., Wilmot, J., Deavers, R., Kromolicki, J., Rabens, G., and Cowell, C. (1998). *Hydraulic performance of drainage structures*, phase i and ii. Technical report.

Kranc, S. C., Cromwell, C. J., Rabens, C. J. and Killian J. D. (2001). Hydraulic performance of several curb and gutter inlets.The department of Civil and Environmental Engineering, College of Engineering, Univ. of South Florida.

Koutsourakis, N., Bartzis, J.G. & Markatos, N.C. (2012) Evaluation of Reynolds stress, k-ε and RNG k-ε turbulence models in street canyon flows using various experimental datasets. *Environ Fluid Mech.* 12, 379–403

Larson, C. L. (1947). Investigation of Flow Through Standard and Experimental Grate Inlets for Street Gutters. Retrieved from the University of Minnesota Digital Conservancy, Available at: http://purl.umn.edu/108101.

Larson, C. L., (1948). Experiments on Flow Through Inlet Grating For Street Gutters. St. Anthony Falls Hydraulic Laboratory.

Lee, S. et al. (2012). Study on Inlet Discharge Coefficient Through the Different Shapes of Storm Drains for Urban Inundation Analysis. *Journal of Japan Society of Civil Engineers*, Ser. B1

(Hydraulic Engineering), 68(4), I_31-I_36.

Li, X. et al. (2019). Evaluating Curb Inlet Efficiency for Urban Drainage. *Water,* 11(851), 1–18.

Li, W. H., Geyer, J. C. and Benton, G. S. (1951). Hydraulic Behavior of Storm-Water Inlets: I. Flow into Gutter Inlets in a Straight Gutter without Depression. Sewage and Industrial Wastes, 23(1), 34–46. Available at: https://www.jstor.org/stable/25031491.

Li, W. H., Sorteberg, K. K., and Geyer, J. C. (1951). Hydraulic behavior of storm- water inlets: Ii. flow into curb-opening inlets. *Sewage and Industrial Wastes*, 722–738.

Li W. H. (1956). The design of storm-water inlets. John Hopkins University, Baltimore, MD, USA, internal report.

Lopes, P., Leandro, J., Carvalho, R., Russo, B. & Gómez, M. (2010). Assessment of the ability of a volume of fluid model to reproduce the efficiency of a continuous transverse gully with grate. *Journal of Irrigation and Drainage Engineering*, 142, 10.

MacCallan, R. and Hotchkiss, R. (1996). Hydraulic efficiency of highway stormwater inlets: Final report. Technical report, Research Report NE-DOT.

Martins, R., Rubinato, M., Kesserwani, G.,Leandro, J., Djordjević, S., & Shucksmith,J. D. (2018). On the characteristics ofvelocitiesfields in the vicinity ofmanhole inlet grates duringfloodevents.*Water Resources Research*,54,6408–642

McEnroe, B. M., Wade, R. P., McEnroe, B. M., Wade, R. P., et al. (1998). Hydraulic performance of set-back curb inlets. Technical report, Kansas. Dept. of Transportation.

McEnroe, B. M., Wade, R. P., and Smith, A. K. (1999). Hydraulic performance of curb and gutter inlets. Technical report, Citeseer.

Mustaffa, Z. (2003). An experimental investigation of the hydraulics of street inlets. Degree Thesis, University of Alberta.

Mustaffa, Z., Rajaratnam, N. and Zhu, D. Z. (2006). An experimental study of flow into orifices and grating inlets on streets, *Canadian Journal of Civil Engineering,* 33(7), 837–845.

Nikolaos D. Katopodes, 2019. Chapter 12 – Volume of Fluid Method, in Free-Surface Flow, 766-802.

Orta-Ortiz M. S., Geneletti D. (2022). What variables matter when designing nature-based solutions for stormwater management? A review of impacts on ecosystem services. *Environmental Impact Assessment Review*. 95.

Rajaratnam N. (1997). Hydraulics of K-7 gratings. A report of hydraulic tests prepared for the City of Edmonton. University of Alberta.

Rubinato, M., Martins, R., Kesserwani, G., Leandro, J., Djordjević, S., & Shucksmith, J. (2017). Experimental investigation of the influence of manhole grates on drainage flows in urban flooding conditions. Paper presented at 14th IWA/IAHR International Conference on Urban Drainage, Prague, Czech Republic.

Russo, B. and G´omez, M. (2013). Discussion of "hydraulic efficiency of grate and curb inlets for urban storm drainage" by brendan c. comport and christopher i. thornton. *Journal of Hydraulic Engineering,* 140(1):121–122.

Russo, B., Gómez, M. and Tellez, J. (2013). Methodology to estimate the hydraulic efficiency of nontested continuous transverse grates. *Journal of Irrigation and Drainage Engineering,* 139(10), 864–871.

Sabtu, N. (2012). Hydraulic Interaction Between the Above and Below Ground Drainage Systems

via Gully Inlets. PhD Thesis, Department of Civil and Structural Engineering, University of Sheffield, UK. Available from: http://etheses. whiterose.ac.uk/11506/

Schalla, F. E. (2016). Effects of flush slab supports on the hydraulic performance of curb inlets and an analysis of design equations. Master"s thesis, Dept. of Civil Eng., University of Texas at Austin, USA.

Schalla, F. E. et al. (2017). Limitations of traditional capacity equations for long curb inlets", *Transportation Research Record*, 2638(1), 97–103.

Sezenöz, B. (2014). Numerical Modelling of Continuous Transverse Grates for Hydraulic Efficiency. MSc Thesis, Middle East Technical University, Ankara, Turkey. Available from: https://www.flow3d.com/wp-content/uploads/2014/04/Numerical-Modelling-of ContinuousTransverse-Grates-for-Hydraulic-Efficiency.pdf

Sipahi, S., (2006). Calibration of A Grate on A Sloping Channel. MS Thesis, Middle East Technical University, Ankara, Turkey.

Soares, C. E. (1991). Analysis of the efficiency of an alternative South Carolina storm water drainage structure. PhD thesis, Clemson University.

Spaliviero, F., May, R.W.P., and Escarameia, M. (2000). Spacing of road gullies. Final Report: Hydraulic Perfor- mance of BS EN 124 gully gratings and kerb inlets. Final report SR 533. HR Wallingford, UK.

Stepenson, D. (1981). Stormwater hydrology and drainage. Elsevier Scientific Publishing Company, Amsterdam, The Netherlands, 270p.

Tapley, G.S. (1943). Hydrodynamics of model storm sewer inlets applied to design. Transactions, 108, 409-451.

Tellez-Alvarez, J., Gómez, M. and Russo, B. (2020). Quantification of energy loss in two grate inlets under pressure. *Water,* 12(6), 1601

Thorolfsson, S. T. (2001). Specific problems in urban drainage in cold climate (SP-UDCC). *Urban Drainage Modeling,* 2, 888–899.

Thornton, C. I. and Cox, A. L. (2009). Hydraulic Efficiency of Grate and Curb. Prepared for The Urban Drainage and Flood Control District, Colorado.

Ubbink, (1997). Numerical Prediction of Two Fluid Systems with Sharp Interfaces. PhD Thesis. Imperial College of Science, Technology & Medicine, London, UK.

UN. (2018). World urbanisation prospects: the 2018 revision key facts. Available from https://esa.un.org/ unpd/wup/Publications/Files/WUP2018-KeyFacts.pdf

Uyumaz, A. (1992). Discharge capacity for curb-opening inlets. *Journal of Hydraulic Engineering,* 118(7), 1048–1051.

Uyumaz, A. (1994). Highway storm drainage with kerb-opening inlets. *Science of the Total Environment*, The, 146–147(C), 471–478.

Urban Drainage and Flood Control District (UDFCD). (2016). Urban storm drainage: Criteria manual, 1. Denver, USA

Veerappan, R. and Le, J. 2016. Hydraulic efficiency of road drainage inlets for storm drainage system under clogging effect", 165(Friar), 271–281.

Wakif, S. A., Sabtu, N. and Wakif, S. A. (2019). Hydraulic Performance of Vertically Depressed And Non-Depressed Grate Hydraulic Performance of Vertically Depressed And Non-Depressed Grate. *Urban Water Journal.* Taylor & Francis, 16(8), 554–563.

Walsey, R. J.(1960). Hydrodynamic of Flow From Road Surface Into Curb Inlets. Standard Univ., Dept. of Civ. Engrg., Report No. 6.

Walsey, R. J.(1961). Uniform Flow in Shallow, Triangular Open. Proc., ASCE, 87, (HY5), 149-170.

Wasley, R. (1960). Hydrodynamics of Flow into Curb-opening Inlets. PhD thesis, Department of Civil Engineering, Stanford University.

Woo, D. C., and Jones J. Sterling. (1974). Hydraulic Characteristics of Two Bicycle-safe Grate Inlet Designs, Volumes 74-77. United States. Federal Highway Administration Report - Federal Highway Administration ; no. FHWA-RD-74-77

Wu, C. P., J. T. S. Yu, A. S. T. Wong, and C. W. Li. (2015). Hydraulic Interception Efficiency of Gully Gratings on Steep Roads. *HKIE Transactions,* 22 (3) pp. 192–198.

Yakhot, V. & Orszag, S. A. (1986). Renormalization group analysis of turbulence. I. Basic theory. Journal of Scientific Computing 1 (1), 3–51.

Yakhot, V. & Smith, L. M. (1992). The renormalization group, the e- expansion and derivation of turbulence models. *Journal of Scientific Computing,* 7 (1), 35–61.

Yong, K. (1965). Hydraulic Model Investigation of curb-opening Inlets.". University of New South Wales. Water Research Laboratory.

Yucel, O. et al. (1969). Development of Improved Drainage Inlets Phase 1 : Literature Survey.Fritz Engineering Laboratory Report No. 364.2 .

Zaman, A. B. K., Mustaffa, z., and Gelder P. V. (2021). Probabilistic Assessment for the Capacity of Grate- and Curb-Opening Inlets during Floods. *Journal of Irrigation and Drainage Engineering.* 147-11.

Zhu, Y. Jiang, P. Experimental and numerical investigation of the effect of shock wave characteristics on the ejector performance. Int. J. Refrig. 2014, 40, 31–42.

Zhou, Z., Smith, J. A., Baeck, M. L., Wright, D. B., Smith, B. K., and Liu, S.(2021). The impact of the spatiotemporal structure of rainfall on flood frequency over a small urban watershed: an approach coupling stochastic storm transposition and hydrologic modeling, *Hydrol. Earth Syst. Sci.,* 25, 4701–4717

Zwamborn, J. A. (1966). Stormwater inlet design code. National Mechanical Engineering Research Institute, Council for Scientific and Industrial Research.

## Appendix

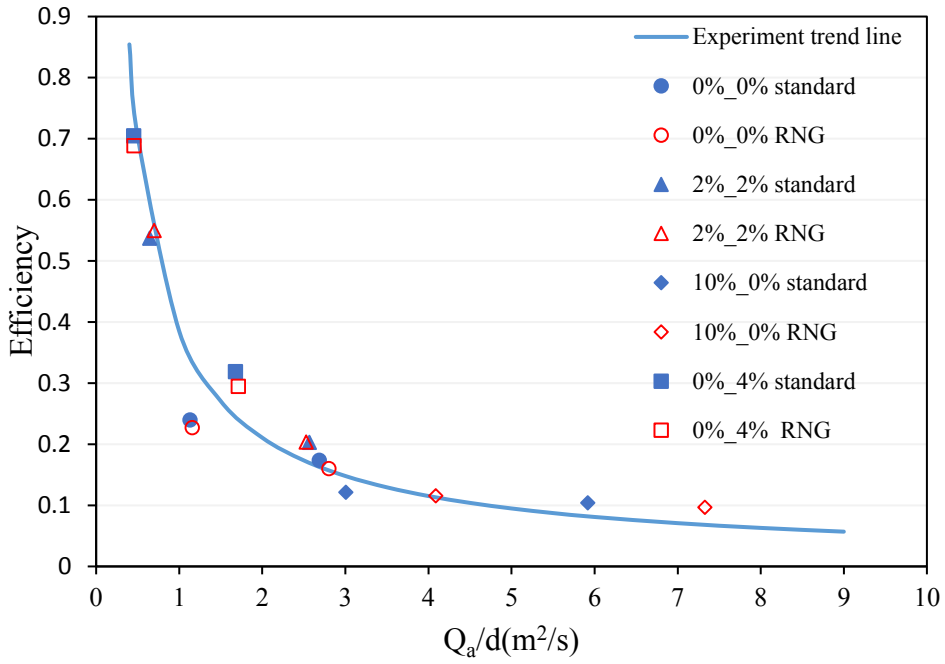


Figure A1 Comparison between the standard and RNG k- ε turbulence models.

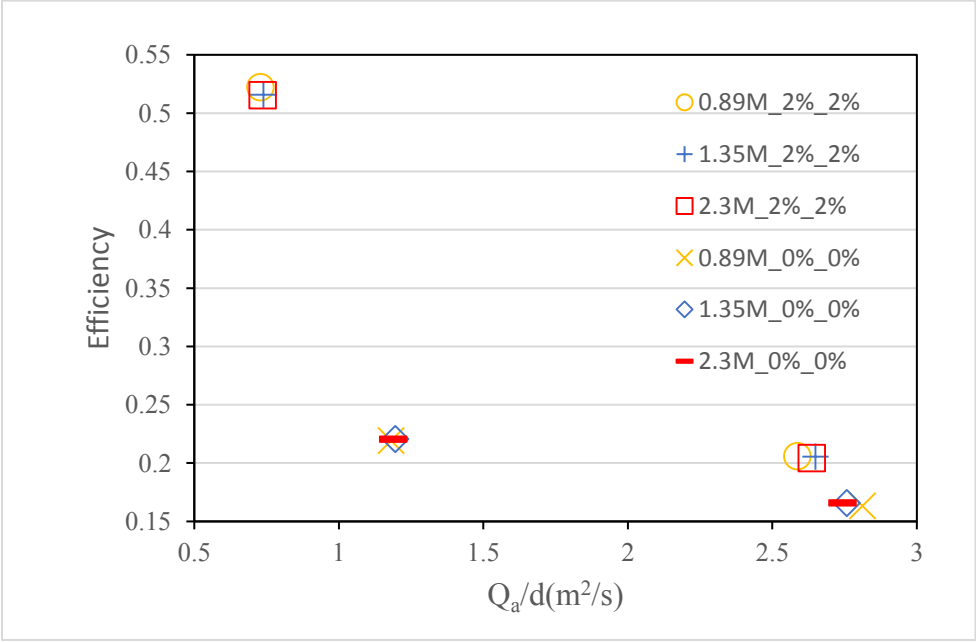


Figure A2 Comparison among three models of 0.89 million, 1.35 million, and 2.3 million cells.

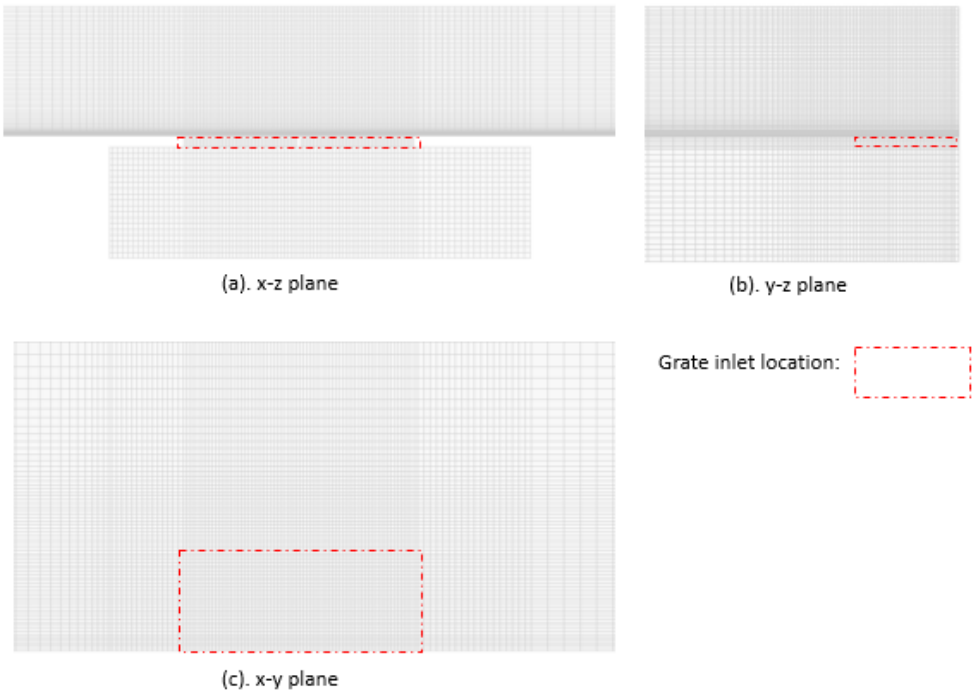


Figure A3 Overview of mesh around the grate inlet.

(a) Clogging pattern 1 (b) Clogging pattern 2 (c) Clogging pattern 3

Figure A4 Clogging patterns defined in the physical experiments (Gómez et al., 2013).

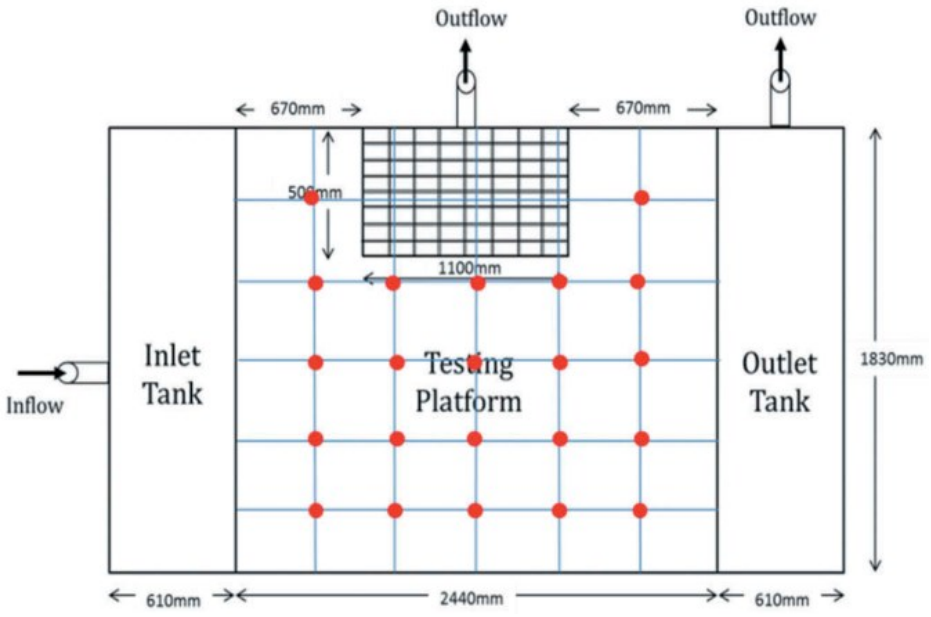


Figure A5 Configuration of testing platform (Wakif et al., 2019).

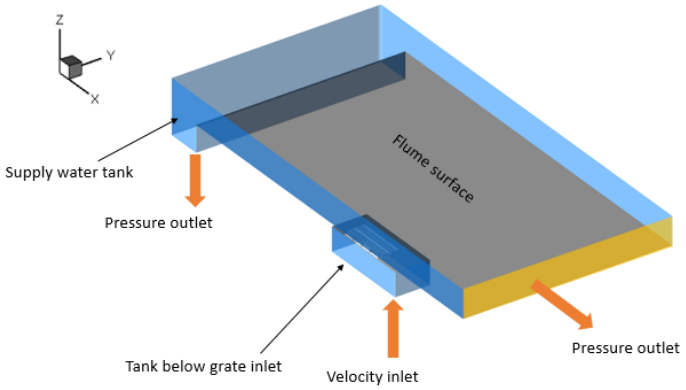


(a)

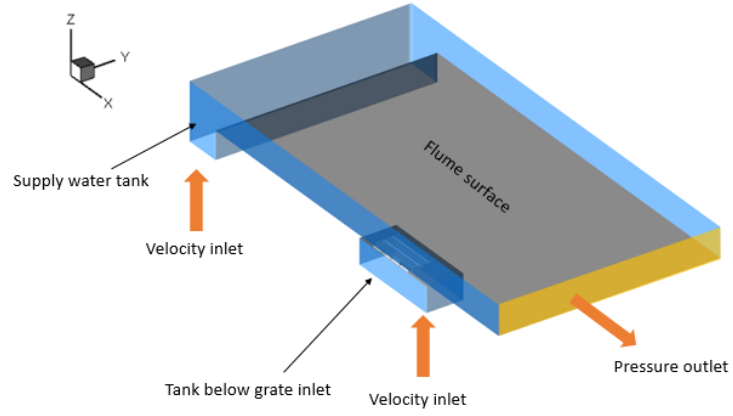


(b)

Figure A6 Sketch of outflow system: (a) Dry floodplain; (b) Wet floodplain

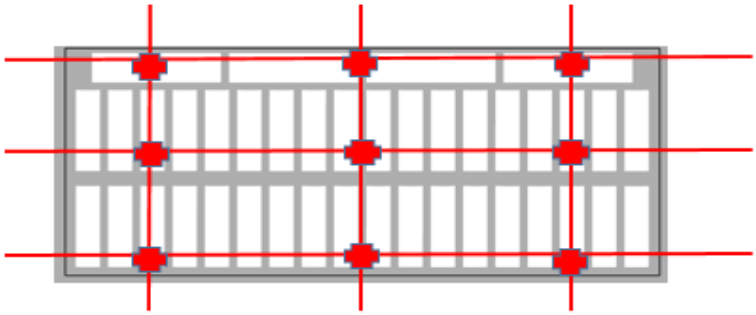

Figure A7 Water level measurement locations